BEHAVIOUR OF TUNNELS WITH DIFFERENT GEOMETRIES UNDER DYNAMIC LOADING CONDITIONS

FARKLI GEOMETRİLERDEKİ TÜNELLERİN DİNAMİK YÜKLER ALTINDAKİ DAVRANIŞLARI

FEVZİ TOSUN

PROF. DR BERNA UNUTMAZ

Supervisor

Submitted to

Graduate School of Science and Engineering of Hacettepe University

as a Partial Fulfillment to the Requirements

for the Award of the Degree of Master of Science

in Civil Engineering

2024

Dedicated to my mother

ABSTRACT

BEHAVIOUR OF TUNNELS WITH DIFFERENT GEOMETRIES UNDER DYNAMIC LOADING CONDITIONS

Fevzi TOSUN

Master of Science, Department of Civil Engineering

Supervisor: Prof. Dr. Berna UNUTMAZ

December 2024, 107 pages

With the rapidly increasing population around the world, issues such as transportation and the use of underground spaces in urban areas have become increasingly significant. Tunnels are being used more and more for the benefit of humanity in both of these areas. Given the high costs associated with tunnel construction and maintenance, these structures are expected to offer substantial safety during earthquakes and require minimal upkeep once operational. Although it is known that underground structures have much higher earthquake performance than above-ground structures, tunnel damages caused by earthquakes, especially in the last century, have caused us to question our knowledge of tunneling and these situations have been reported in detail. In this thesis, the cumulative studies conducted by taking into account the damages reported on this subject were reviewed. In addition to that, tunnel behavior varies with environmental conditions, shape, and depth are assessed using finite element analysis. In general, it is proven that tunnels perform better with increasing depth and circularization of their shape.

Keywords: Tunnels, Horseshoe Tunnels, Box Tunnels, Tunnel Depths, Seismic Analysis

ÖZET

FARKLI GEOMETRİLERDEKİ TÜNELLERİN DİNAMİK YÜKLER ALTINDAKİ DAVRANIŞLARI

Fevzi TOSUN

Yüksek Lisans, İnşaat Mühendisliği Bölümü

Tez Danışmanı: Prof. Dr. Berna UNUTMAZ

Aralık 2024, 107 sayfa

Dünya genelindeki hızlı artan nüfus ile birlikte özellikle ulaşım ve şehir içlerinde yeraltı alanların kullanılması gibi konular önem arz etmeye başlamıştır. Tüneller bu iki konuda da insanlık yararına gün geçtikçe daha da fazla kullanılmaktadır. Tüneller yapım ve bakım maliyetleri yüksek olan yapılar olması nedeniyle genel olarak hem depremlerde can güvenliğini sağlaması hem de çok küçük bakım ve onarımlar ile hizmete açılması beklenen yapılardır. Her ne kadar yeraltı yapılarının yer üstü yapılarına göre çok daha yüksek deprem performanslarının olduğu bilinse de özellikle son yüzyılda meydana gelen depremlerde oluşan tünel hasarları tünelcilik bilgimizi sorgulamaya sebep olmuştur ve bu durumlar detaylıca raporlanmıştır. Tez çalışmasında bu konuda raporlanan hasarlar dikkate alınarak yapılan kümülatif çalışmalar incelenmiş ve tünellerin dinamik davranışının bulunduğu ortama, tünel şekline, tünel derinliklerine göre nasıl davrandığı sonlu elemanlar analizleri yardımıyla incelenmiştir. Genel olarak, tünellerin artan derinlik ve şeklinin daireselleşmesi ile birlikte daha iyi performans gösterdiği kanıtlanmıştır.

Anahtar Kelimeler: Tüneller, Kutu Tüneller, At Nalı Tüneller, Tünel Derinlikleri, Sismik Analiz

ACKNOWLEDGEMENTS

I am profoundly thankful for the support and inspiration offered by all those who have played a role in my M.Sc. study.

I am especially grateful to Prof. Dr. Berna Unutmaz, whose guidance throughout my studies was invaluable. Her limitless energy and enthusiasm for research have been a constant source of motivation for me. Moreover, her accessibility and willingness to help me with my studies made a significant difference. The way she guided me to different experiments related to the study was the most significant factor that kept my vision wide open and stimulated.

I would like to express my deepest gratitude to my mother for her endless support and love throughout my life. I could not have accomplished this thesis without her constant encouragement.

TABLE OF CONTENTS

LIST OF FIGURES

LIST OF TABLES

LIST OF SYMBOLS AND ABBREVATIONS

Symbols

A	Free-field displacement response amplitude of an ideal sinusoidal shear wave
A_c	Cross-sectional area of tunnel lining
a_P	Peak particle acceleration associated with P-wave
a_R	Peak particle acceleration associated with Rayleigh-wave
a_S	Peak particle acceleration associated with S-wave
C_P	Apparent velocity of P-wave propagation
C_R	Apparent velocity of Rayleigh-wave propagation
C_S	Apparent velocity of S-wave propagation
c_{v_s}	Parameter was determined according to the approach described by Numanoğlu et al. (2017)
D, d	Diameter of circular tunnel
Δd/d	Diametral strain
E_l	Elastic modulus of the tunnel lining
E_m	Modulus of the elasticity of the medium
ε^{ab}	Total free-field axial strains
$\varepsilon^{b}{}_{max}$	Maximum bending strain
ε_l	Longitudinal strain
ε_{lm}	Maximum longitudinal strain
ε_n	Normal strain
ε_{nm}	Maximum normal strain

f	Ultimate friction force (per unit length) between the tunnel and surrounding soil
f_{max}	Maximum unfiltered frequency value
G_m	Shear modulus of the medium
$G_{0,ref}$	Reference shear modulus at very small strains
h	Thickness of the soil layer
I	Moment of inertia of the tunnel lining (per unit width) for circular lining
I_c	Moment of inertia of the tunnel section
K	Free-field curvature due to body or surface waves
K_a	Longitudinal spring coefficient of medium
K_m	Maximum curvature
K_t	Transverse spring coefficient of medium
K_0	Soil pressure coefficient at rest
K_1	Lining response coefficient
L	Wavelength of an ideal sinusoidal shear wave
M_{max}	Maximum bending moment
m	Power for stress-level dependency of stiffness
p	Artificial support pressure
p_α	Residual support pressure
p_{ref}	Reference confining pressure
p_s	Defined support pressure
p_0	Initial ground pressure
$\frac{1}{p}$	Curvature
$\frac{1}{P_{max}}$	Maximum curvature

R diametric deflection	The ratio of the lining diameter deflection to the free-field
R	Tunnel contraction
R^n	The lining-soil racking ratio under normal loading
r	Radius of circular tunnel or half height of a rectangular tunnel
T_{max}	Maximum thrust
T	Predominant natural period of the soil deposit
τ	Free-field shear stress
V_{max}	Maximum shear force
V_P	Peak particle velocity associated with P-wave
V_R	Peak particle velocity associated with Rayleigh-wave
V_S	Peak particle velocity associated with S-wave
v_l	Poisson's ratio of tunnel lining material
v_m	Poisson's ratio of the medium
$v_{u,r}$	Poisson's ratio of unloading-reloading case
γ	Shear strain
γ_m, γ_{max}	Maximum shear strain
$\gamma_{0.7}$	Treshold shear strain
σ	Uniaxial compressive strength
σ'_v	Vertical effective stress
ϕ'	Internal friction angle
ϕ	Angle of incidence of wave with respect to tunnel

Abbrevations

A	Amplitude
ASCE	American society of civil engineers
C	Compressibility ratio
c	Cohesion
DSHA	Deterministic seismic hazard analysis
F	Flexibity ratio
FE	Finite element
GSI	Geological strength index
M_L	Richter local magnitude
NATM	New Austrian tunneling method
PSHA	Probabilistic seismic hazard analysis
P wave	Primary or pressure wave
R	Radius of the tunnel lining
S wave	Secondary or shear wave
SSI	Soil structure interaction
t	Thickness of the tunnel lining
TBM	Tunnel boring machine
2D	2 dimensional
3D	3 dimensional

1. INTRODUCTION

1.1 General

In ancient times, people dug tunnels to store food and protect themselves from dangerous enemies. Almost every major civilization in history, such as the Aztec, Inca, Babylonian, Egyptian and Persian, has built tunnels. The tools used in tunneling differed according to their era. For the first human beings, these were bone, horn, flint and wood, while bronze, iron and steel were used in later periods. Today, with the development of technology, tunnels are excavated using advanced equipment powered by motor power or blasting methods. Tunnels are excavated by reinforcement instead of support. With the developing machine technology, it is possible to reach behind the plastic zones with bolting technology. In addition, by means of shotcrete support applied instantaneously after excavation, the relaxation in the rock environment is prevented and the pressure is reduced by spreading over a wider surface. In addition to traditional tunneling, machine tunneling technology is also progressing rapidly. Today, small tunnels with diameters of 2-3 meters can be drilled with the method called pipe-jacking all over the world, while tunnels with higher diameters can be driven with the help of a TBM machine. TBM tunneling is applied not only for circular tunnels but also for variable shaped tunnels. Considering the speed and economy achieved by TBM tunneling, it is estimated that it will become much more prevalent in the near future.

Human understanding of earthquakes is not as old as tunneling. Although we have some evidence of the earthquake in China in 780 BC, the first known earthquake to be scientifically surveyed is the 1755 Lisbon, Portugal earthquake. Since then, earthquakes have become a source of lessons for humanity. Especially in Japan and the United States, studies have begun to investigate the mechanism and consequences of this devastating event. With the studies carried out, it has been observed that the performance of the structure increases when steel is placed in concrete and the regulations have been reviewed and updated in this respect. Earthquakes have delivered a very destructive lesson to humankind and taught the application of very solid rules against it. Similarly, thanks to the developing technology, earthquake records are recorded electronically with advanced measurements, enabling much more advanced research.

Tunneling is a rapidly growing sector all over the world. Tunnels are engineering structures that bring economic benefits to developing economies. For instance, research shows that metro and high-speed rail lines have grown enormously in the last two decades, while conventional lines have not changed much. It is estimated that the length of the high-speed rail network will be completed or under construction by 2050 and that the number of high-speed rail train tracks will double by 2050. It seems that tunneling will continue to develop with the increasing world population.

Although our understanding of tunneling and earthquake engineering has improved a lot with advancing technology, there are still tunnels in the world today that are damaged in earthquakes. Especially for economically growing countries located in the earthquake zone, it is expected that the behavior of underground structures during earthquakes should be predictable in order to keep the damage level of underground structures under control.

1.2 Objective of the Thesis

The major intendment for this work is to investigate how three types of tunnel shapes commonly used in the industry perform under earthquake loading. The tunnel shapes mentioned are horseshoe, circular and box-section tunnels. Each tunnel shape has different objectives according to its intended use. Within the scope of the research, tunnels will be considered using various parameters such as depth, site class, and geological condition. In this way, it aims to look from a wider perspective to evaluate the performances of different shapes better. The study will contribute to ensuring that welfare is damaged as little as possible, both economically and socioculturally, after major earthquakes that may occur, especially in seismically active regions. In this way, it aims to bring benefit both in terms of construction and in case of earthquakes within the scope of economy, which is one of the most important engineering factors. These analyses were performed with the help of Plaxis 2D software and mathematical calculations are presented at the end as a complementary analysis, which satisfies the finite element analysis results.

1.3 Scope of the Thesis

After Section 1, Section 2 presents the research on underground structures in the literature, with a special focus on tunnels. In this context, the tunnels that have been damaged so far are explained in which way they were damaged. Seismicity is summarized

and the empirical formulas used to calculate the effects of tunnels under earthquake loading are presented. In addition, modeling techniques in industry for finite element program are stated.

Section 3 explains the shape, depth, site class, rock strength properties and earthquake records to be used in the analysis. In the same section, details about the dynamic and sensitivity analysis methods are mentioned.

In Section 4, the forces obtained as a result of the dynamic analysis performed as a solution of finite element analysis are given separately in accordance with the categories in the parametric study. Furthermore, mathematical calculations were made, and relevant comparisons were conducted.

Section 5 contains the results obtained. In addition, it includes suggestions for future research.

2. LITERATURE REVIEW

2.1. Tunnels and Seismic Analysis

Structures are usually designed to have sufficient capacity under static conditions. The static capacity usually provides adequate performance for non-major earthquakes, but for major earthquakes or unfavorable soil conditions, it should be checked whether this capacity is adequate (Hashash, 2001).

Essentially, while civil engineering can be defined as the engineering of forces, earthquake engineering can be defined as the engineering of displacements. However, displacements are not the only factor for all structures in earthquake design. Because the inertia forces of the superstructures are dominant in earthquakes, while in buried structures since the inertia forces are negligible compared to the surrounding ground, buried structures will have to follow the displacements of the environment they are located in. The researchers' measurements have confirmed this situation. For this reason, the basic design philosophy in buried structures is the displacements that occur in the free field. At the same time, the flexibility of the underground facilities relative to the environment is another factor (Okamoto, 1973).

Accordingly, it would be the simplest way to determine the displacements of the environment in which the tunnel is located without considering the soil-structure interaction, especially for designs to be made in environments with rigid mediums such as rock. Another simple way to determine the behavior of tunnels under earthquakes is to examine the behavior by applying pseudo-static acceleration to the ground environment where the tunnel is located. However, both methods have shortcomings. The soil-structure interaction is ignored in the effects obtained from free field analysis and the propagation effects of earthquake waves are ignored in the pseudo-static method. As a better method, the dynamic analysis method can be used with the help of numerical tools where the deficiencies mentioned above can be considered (Hashash, 2001).

2.2. Field Observations of Tunnels After Earthquakes

Various researchers, including Owen and School (1981), Sharma and Judd (1991), Power et al. (1998), etc., have examined many case studies. The results of all these studies can be summarized as follows.

1- In case of earthquakes, underground structures are much less damaged than above ground structures.
2- It was observed that the structural damages decreased with increasing burial depth. In addition, in the shake table experiments (Feng, 2015), the maximum impacts are taken around 15 meters and decrease significantly with increasing depth up to about 40 meters, while at depths greater than 40 meters, seismic stresses do not change significantly with depth and are relatively small.
3- Tunnels constructed in rigid rock mass receive less damage compared to the soil environment.
4- Damages occurring in tunnels can be associated with concepts such as maximum ground acceleration and moment magnitude, but the importance of earthquake duration should not be ignored.
5- There is a high probability of damage to the tunnel structure in and around the portal due to unstable slopes.

2.3. Effects of Earthquakes on Tunnels

The effects of earthquakes on buried structures can be generally analyzed in two class: (1) ground shaking (2) ground failure by including liquefaction, movement along faults and slope stability problems.

Firstly, liquefaction is the rapid loss of soil strength under dynamic, repetitive loads such as earthquakes. As a result of sudden loading, the structure of the water-saturated soil is disrupted, the contact force between the grains decreases, the pore water pressure increases and the soil loses its resistance. As a result, the following problems may occur (Hashash, 2001).

a) Rise in lateral soil pressure,

b) Loss in lateral soil passive pressure,

c) Flotation or sinking,

d) Lateral dislocation if the soil is exposed to lateral displacement,

e) Following a decrease in pore pressure and soil consolidation, the result might be permanent settlement, compression, and tension failure.

An example of fault displacement and slope stability problem is the earthquake (M_L 7.3) that occurred in Chi-Chi on September 21, 1999. The damage to the portal areas during

the earthquake is shown in Figure 2.1. Due to a 4-meter fault displacement, a tunnel on the Chelungpu fault has gone out of service during the earthquake.

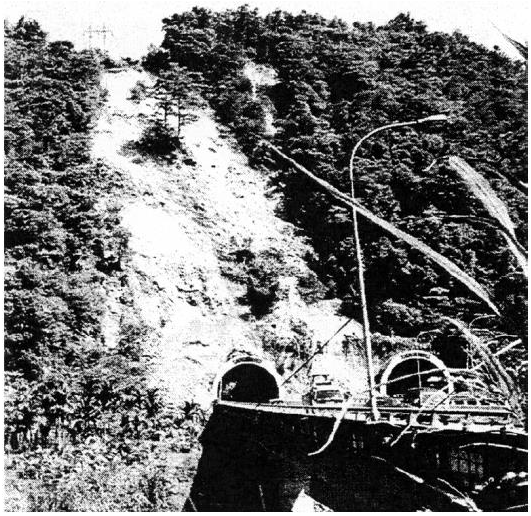

Figure 2.1. Slope failure at portal, Chi-Chi Earthquake (Hashash, 2001)

These problems sit in the category of foreseeable problems. As Penzien (2004), points out in one of his interviews, there are preventive and cure methods in medicine and it is also valid for design point of view. It is more logical to prevent the failures discussed earlier rather than addressing them after they occur. Therefore, when designing, it is crucial to incorporate precautions to avoid such problems in the first place.

Ground shaking is the deformations caused by the propagation of earthquake waves. The factors affecting the damage caused by shaking are (1) the structure's form, size, and deepness; (2) the rock or soil characteristics around it; (3) the characteristics of any support system; and (4) the magnitude of the strong ground motion (St. John and Zahrah, 1987).

Together with these factors, the deformation of tunnels under earthquakes can be found with the phenomenon that the tunnel will follow the displacements of the environment in which it is located (Seismic Deformation Method). Accordingly, considering the tunnel as an elastic beam and applying the free-field displacements onto that beam can be used to see the response of the tunnel. There are generally 3 types of deformation of underground structures (Owen and Scholl, 1981). These are (1) axial compression and extension (Figure 2.2.a, b), (2) longitudinal bending (Figure 2.2.c, d) (3) ovaling/racking (Figure 2.2.e, f). Axial deformation will be accompanied by wave motions parallel to the

tunnel axis. These motions will create compressive or tension movements in the tunnel. Bending moments will be observed in seismic motions perpendicular to the longitudinal direction. These two motions are the forms of deformation that should be considered in the design along the axis of the tunnel. Perpendicular movements will occur when shear waves act perpendicular to the axis. In this case, ovaling/racking deformations will be observed in the tunnel. To understand the general behavior of the tunnel lining, modeling can be performed in plane-strain conditions (Hashash, 2001).

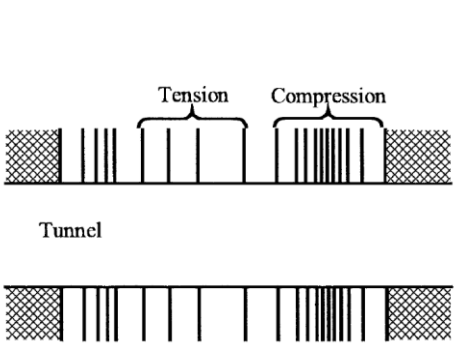

(a) Compression-extension

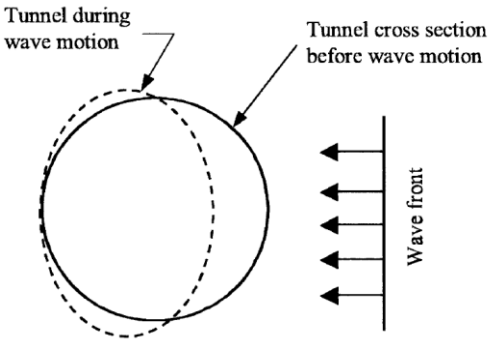

(b) Compression of a tunnel section

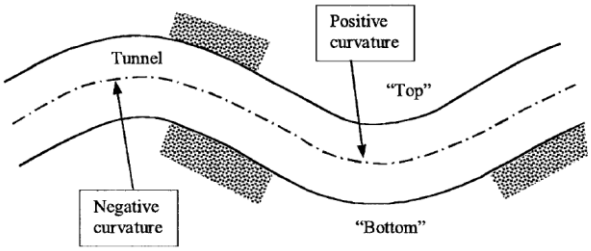

(c) Longitudinal bending

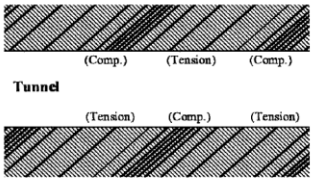

(d) Diagonally propagating wave

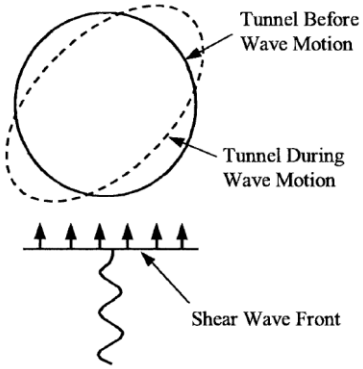

(e) Ovaling of tunnel body

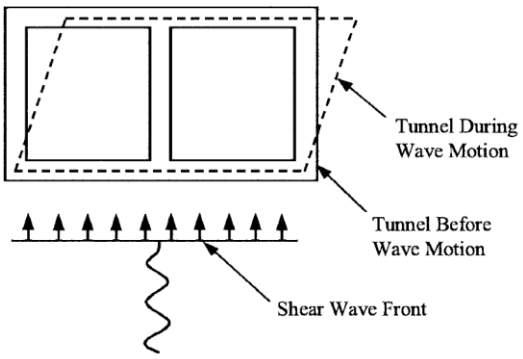

(f) Racking of tunnel body

Figure 2.2. Tunnel deformation mechanisms triggered up by seismic waves (after Owen and Scholl, 1981)

Considering all these considerations, understanding the seismic performance of underground facilities requires first understanding the strong ground shaking, then understanding how this shaking behaves in the ground and how this behavior affects the structures. Table 2.1. provides a summary of these stages. Accordingly, there are 3 basic stages.

Table 2.1. Seismic analysis and design procedure (Hashash, 2001)

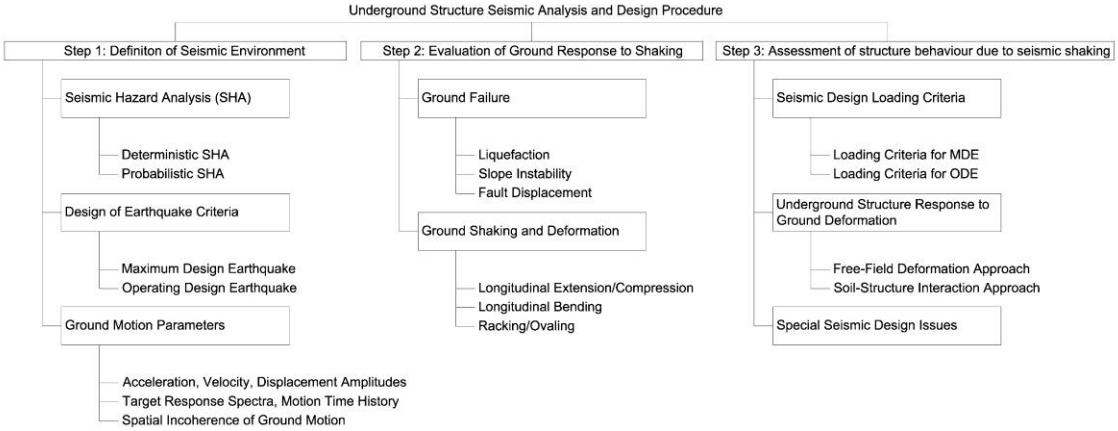

2.4. Identification of Seismic Environment

Maintaining a desired degree of damage under an anticipated earthquake load is the objective of designing an earthquake-resistant underground construction. This level is generally defined as the occurrence of an earthquake of a certain magnitude within a certain period (Kramer, 1996). This information could be provided by conducting seismic hazard analysis.

Seismic hazard analysis is performed by investigating the seismicity of a region by investigating the concepts such as earthquakes that have occurred in that region, recurrence periods and magnitudes of earthquakes, active fault lines, lengths, and types of faults. There are two types of seismic hazard analysis: deterministic and probabilistic. The deterministic approach provides more precise judgments about the site, while the probabilistic approach presents the probability of several earthquakes and their occurrence, considering the uncertainties that may emerge.

2.4.1. Deterministic Seismic Hazard Analysis (DSHA)

DSHA investigates a specific earthquake that is expected to occur at a site. It is essentially a "postulated occurrence" for that site. Reiter (1990) proposed a 4-step process on how to conduct this analysis.

1- Identify all sources that may generate large earthquakes in the area and determine their behavior, such as geometry and earthquake potential.
2- Determining the distances between the site and these sources.
3- Selecting the strongest one among the identified earthquake sources.
4- Expressing the concepts like maximum acceleration, velocity and displacement that determine the characteristics of the strongest earthquake selected.

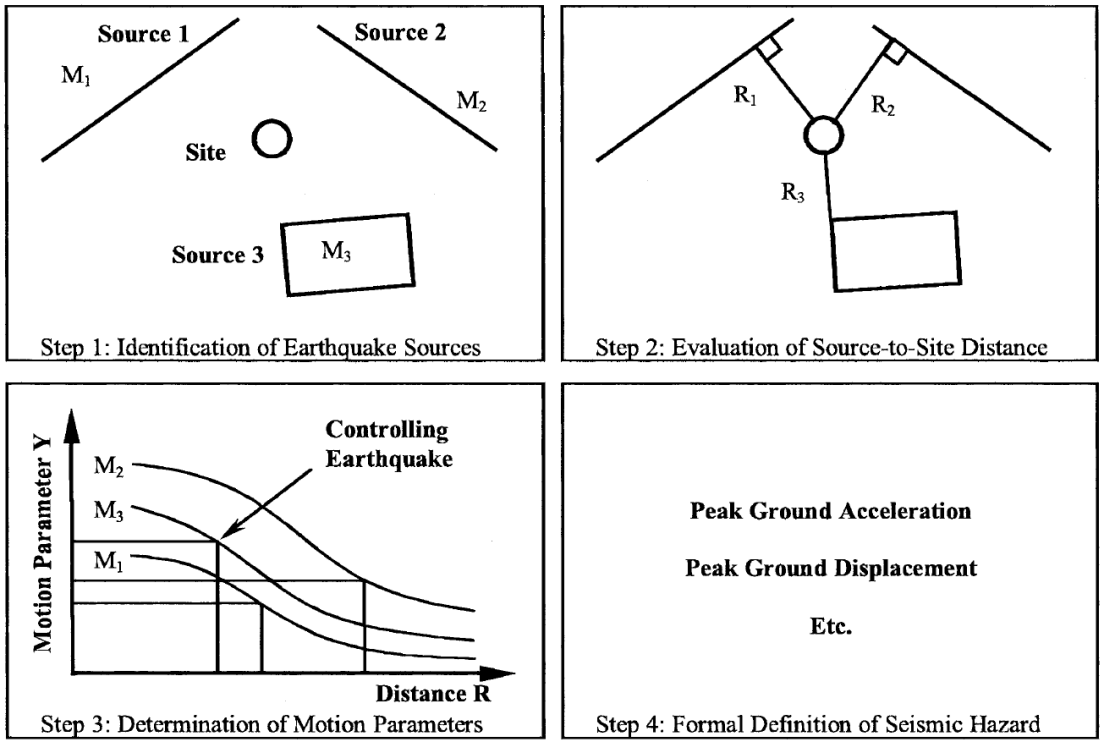

Figure 2.3. Deterministic seismic hazard analysis procedure (after Reiter, 1990)

In these four stages, a data is presented by considering the worst possibilities. It nevertheless doesn't provide details on the likelihood or frequency of an earthquake striking. The probabilistic method should be taken into consideration if such data is required.

2.4.2. Probabilistic Seismic Hazard Analysis (PSHA)

In PSHA, uncertainties about the locations where an earthquake is likely to occur, and its magnitude are evaluated using probabilistic background along with the period of occurrence. This approach provides more comprehensive information about the expected earthquake. Although it is not very accurate, this approach assumes that the earthquakes that may occur at the selected location behave independently of each other. This approach gives quite good results. Reiter (1990) also proposed a 4-step process on how to perform this analysis.

1- Determination of all sources that may generate earthquakes in the field by probabilistic distribution approach and then integrating it with the source geometry to derive the likelihood distribution of the distance from the source to the field.
2- Seismicity recurrence characterization of the site with the help of historical or paleo seismological studies.
3- Identification of any earthquake that may occur at any source by the use of attenuation relationships.
4- Combining these uncertainties to check whether in a certain amount of time, the provided ground motion will be surpassed.

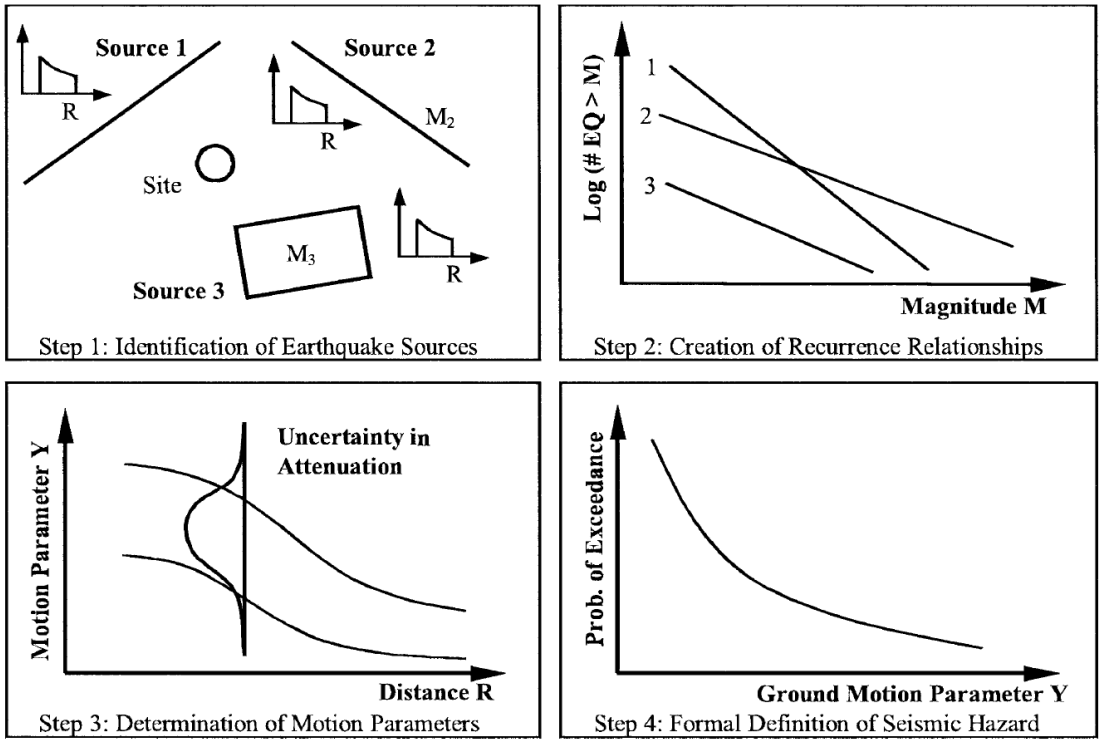

Figure 2.4. Probabilistic seismic hazard analysis procedure (after Reiter, 1990)

More detailed information on occurrence probabilities and uncertainties can be obtained using PSHA.

2.5. Design Earthquakes Criteria

With the seismic characterization of the site, the earthquake level and seismicity design should be defined. In current seismic designs, two capacities are generally checked. The first one is the earthquake corresponding to the collapse stage of the structure against the largest earthquake that can be expected, the aim at this level is to ensure life safety by preventing collapse. This earthquake level is called "maximum design earthquake". The second one is an earthquake that may occur during the life of the structure, at this level, the expectation is to continue the service of the structure without reconstruction or repair costs, the concerns are economic. This earthquake level is defined as "operational design earthquake".

2.5.1. Maximum Design Earthquake

In the deterministic approach, it can be characterized as the largest possible earthquake. In the probabilistic approach, it is characterized as earthquakes with a very low probability of being exceeded during the life of the structure (2% probability of exceeding the spectral magnitudes in 50 years and a corresponding recurrence period of 2475 years). The general purpose of designing for such earthquakes is usually to prevent collapse. Some special structures are designed to continue to operate after the earthquake even in such cases.

2.5.2. Operating Design Earthquake

This kind of earthquake is one that is anticipated over the period of the structure’s existence. It characterizes frequent earthquake ground motion, especially in earthquake codes for structures. At this earthquake level, the main objective for structural design is to keep deformations within elastic limits without exceeding the plastic zone.

2.6. Underground Structure Response to Ground Deformations

In addition to the static loading, the underground structures should also be able to withstand seismic loads in the case of earthquakes. Seismic loads can be defined as the deformations that occur underground in the event of an earthquake and their interaction with the structure (Hashash 2001). In this section, I will discuss how to calculate the displacements and forces in three distortion forms shown in Figure 2.2.

2.6.1. Free Field Deformation Approach

The concept of free-field displacement is the distortions produced by seismic waves in a non-structural environment. These deformations give a good indication of how the structure will behave. It is also possible for designers to apply these deformations directly to the structure, but the results may be too low or too high contingent on the stiffness difference of the structure with the ground (Hashash, 2001).

Newmark (1968) and Kuesel (1969) suggested a straightforward formulation to calculate the free-field soil stresses induced by a harmonically propagating wave at a given angle in a homogeneous, isotropic, elastic medium (Figure 2.5.). In this method, the most critical angle is generally used to eliminate uncertainties in earthquake prediction. Newmark's method requires less input and gives slightly higher results. This makes his method preferred by designers (Wang, 1993).

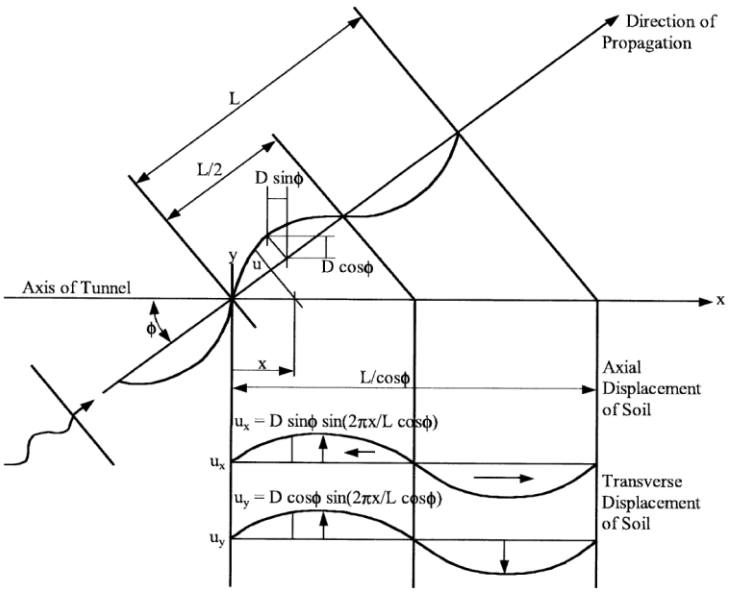

Figure 2.5. Harmonic wave and tunnel (after Wang, 1993)

Using Newmark's approach, John and Zahrah (1987) developed solutions for compressive, tension and shear stresses resulting from free-field axial and bending displacements. While the solutions for each of the wave sorts are detailed in Table 2.2, it is noteworthy that S waves are often linked to the highest particle accelerations and velocities, as noted by Power et al. (1996). Figure 2.6 shows the seismic waves responsible for triggering the stresses. Determining the dominant wave type in a design is often a challenge. As observed by Wang (1993), it is worth noting that stresses generated by Rayleigh waves show a tendency to predominate primarily in structures that are not deep and in regions away from the source of the earthquake. The overall free-field axial strains could be generated by assuming the tunnel lining as an elastic beam, resulting from the combination of longitudinal stresses caused by both axial and curvature displacements (Power et al., 1996).

for P - waves

$$\varepsilon^{ab} = \left[\frac{V_P}{C_P} cos^2\phi + r\frac{a_P}{{C_P}^2} sin\phi cos^2\phi\right] \quad (2.1)$$

for S - waves

$$\varepsilon^{ab} = \left[\frac{V_S}{C_S} sin\phi cos\phi + r\frac{a_S}{{C_S}^2} cos^3\phi\right] \quad (2.2)$$

for Rayleigh – waves

$$\varepsilon^{ab} = \left[\frac{V_R}{C_R} cos^2\phi + r\frac{a_R}{{C_R}^2} sin\phi cos^2\phi\right] \quad (2.3)$$

Where:

r: tunnel radius

a_P: maximum particle acceleration affiliated with Primary wave

a_S: maximum particle acceleration affiliated with Secondary wave

a_R: maximum particle acceleration affiliated with Rayleigh wave

ϕ: angle of incidence of wave

v_l: Poisson's ratio of lining

V_P: maximum particle velocity affiliated with Primary wave

C_P: velocity of Primary wave propagation

V_S: maximum particle velocity affiliated with Secondary wave

C_S: velocity of Secondary wave propagation

V_R: maximum particle velocity affiliated with Rayleigh wave

C_R: velocity of Rayleigh-wave propagation

Table 2.2. Strain and curvature due to body and surface waves (after St. John and Zahrah, 1987)

	Longitudinal strain	Normal strain	Shear strain	Curvature
P-wave	$\varepsilon_l = \frac{V_P}{C_P} cos^2\phi$	$\varepsilon_n = \frac{V_P}{C_P} sin^2\phi$	$\gamma = \frac{V_P}{C_P} sin\phi cos\phi$	$\frac{1}{p} = \frac{a_p}{C_P^2} sin\phi cos^2\phi$
	$\varepsilon_{lm} = \frac{V_P}{C_P} for\ \phi = 0°$	$\varepsilon_{nm} = \frac{V_P}{C_P} for\ \phi = 90°$	$\gamma_m = \frac{V_P}{2C_P} for\ \phi = 45°$	$\frac{1}{P_{max}} = 0.385 \frac{a_p}{C_P^2}\ for\ \phi = 35°16'$
S-wave	$\varepsilon_l = \frac{V_S}{C_S} sin\phi cos\phi$	$\varepsilon_n = \frac{V_S}{C_S} sin\phi cos\phi$	$\gamma = \frac{V_S}{C_S} cos^2\phi$	$K = \frac{a_S}{C_S^2}\ cos^3\phi$
	$\varepsilon_{lm} = \frac{V_S}{2C_S} for\ \phi = 45°$	$\varepsilon_{nm} = \frac{V_S}{2C_S} for\ \phi = 45°$	$\gamma_m = \frac{V_S}{C_S} for\ \phi = 0°$	$K_m = \frac{a_S}{C_S^2}\ for\ \phi = 0°$
Rayleigh wave Compressional componnent	$\varepsilon_l = \frac{V_{RP}}{C_R} cos^2\phi$	$\varepsilon_n = \frac{V_{RP}}{C_R} sin^2\phi$	$\gamma = \frac{V_{RP}}{C_R} sin\phi cos\phi$	$K = \frac{a_{RP}}{C_R^2} sin\phi cos^2\phi$
	$\varepsilon_{lm} = \frac{V_{RP}}{C_R} for\ \phi = 0°$	$\varepsilon_{nm} = \frac{V_{RP}}{C_R} for\ \phi = 90°$	$\gamma_m = \frac{V_P}{C_R} for\ \phi = 45°$	$K_m = 0.385 \frac{a_{RP}}{C_R^2}\ for\ \phi = 35°16'$
Rayleigh wave Shear componnent		$\varepsilon_n = \frac{V_{RS}}{C_R} sin\phi$	$\gamma = \frac{V_{RS}}{C_R} cos\phi$	$K = \frac{a_{RS}}{C_R^2}\ cos^2\phi$
		$\varepsilon_{nm} = \frac{V_{RS}}{C_R} for\ \phi = 90°$	$\gamma_m = \frac{V_{RS}}{C_R} for\ \phi = 0°$	$K_m = \frac{a_{RS}}{C_R^2}\ for\ \phi = 0°$

By using P- and S-wave velocities, Poissons's ratio and dynamic modulus could be obtain: $v_m = \frac{1}{2}\frac{(C_P/C_S)^2-2}{(C_P/C_S)^2-1}$ or $C_P = \sqrt{\frac{2(1-v_m)}{(1-v_m)}} C_S$; $E_{mP} = \rho {C_P}^2 \frac{(1+v_m)(1-2v_m)}{(1-v_m)}$; and $G_m = \rho {C_S}^2$, respectively.

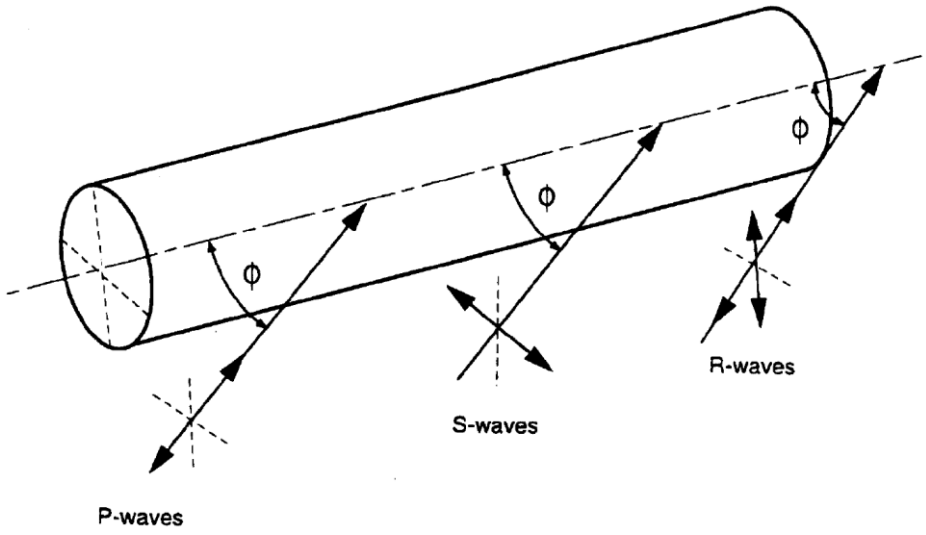

Figure 2.6. Seismic waves lead to longitudinal axial and curvature strains (Power et al., 1996)

While the tunnel's diameter gets bigger, the effect of curvature deformation on the axial stress gets bigger. Despite this, the free field equality presented in Table 2.2 show that the bending component of the stress in tunnels subjected to seismic loading is usually relatively small compared to the axial stress. Also, if we examine the tension cracks under cyclic earthquake loading at this point, it is normal for tension cracks to occur. These cracks will close when the system is reinforced by steel and if they do not reach their limits. Wang (1993) even stated that even non-steel tunnel linings will be sufficient under very small cracks. However, Lu and Hwang (2017) studied the tunnels damaged in the 1999 earthquakes in Chi-Chi and emphasized the importance of reinforcement in the permanent lining, especially in areas with high seismic activity.

2.6.1.1 Deformation of Tunnels

Ovaling deformations are resulted from shear waves perpendicular to the tunnel axis. Shear waves are the prevalent waveform of ovaling, however researches have shown that oblique or horizontal waves can also produce ovaling (Wang, 1993).

Free field displacements can be defined in two ways. These distortions will be determined only depending on the ground environment for soils without openings.

$$\frac{\Delta d}{d} = \pm \frac{\gamma_{max}}{2} \ (free\ field, imperforated) \qquad (2.4)$$

If there is an opening in the soil medium, the Poisson's ratio of the medium will also be included in the equation.

$$\frac{\Delta d}{d} = \pm 2\gamma_{max}(1 - v_m)\ (free\ field, perforated) \qquad (2.5)$$

Where:

Δd/d: diametral strain

γ_{max}: maximum shear strain

v_m: Poisson's ratio of the medium

It is noticeable that there is no factor for the tunnel lining in either of the above equations. These sets of equations were created without considering the soil-structure interaction. In a free field environment, the perforated ground environment will distort 2-3 times more.

By ignoring the tunnel-ground interaction, the amount of lining displacement can be generally divided into three categories. First, if the distortion stiffness of the lining is slightly higher than the stiffness of the surrounding ground environment, it is appropriate to use equation 2.5. In the second case, if the distortion stiffness of the lining is equal to the distortion stiffness of the surrounding ground environment, in other words, if there is no difference in distortion stiffness between the ground we are excavating for tunnel construction and the tunnel lining, it will be necessary to say that the lining will be displaced by equation 2.4 simply. In the third and last case, we will consider the case where the distortion stiffness of the lining is much higher than the distortion stiffness of the ground environment. In this case, the lining will have even less displacement than equation 2.4 (Wang, 1993). It should be noted that the as the tunnel moves less, the more forces it will have on the lining itself.

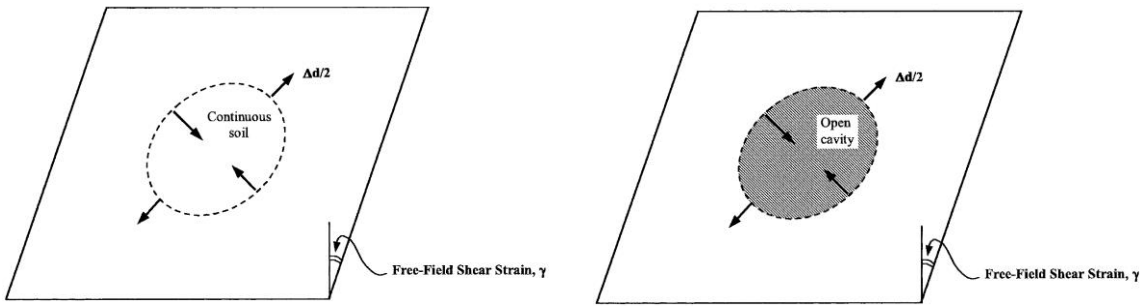

Figure 2.7. Free-field shear displacement of perforated and non-perforated ground, circular shape (after Wang, 1993)

Box sections experience transverse racking deformations when subjected to earthquakes. These quantities can be calculated using the set of equations in Table 2.2.

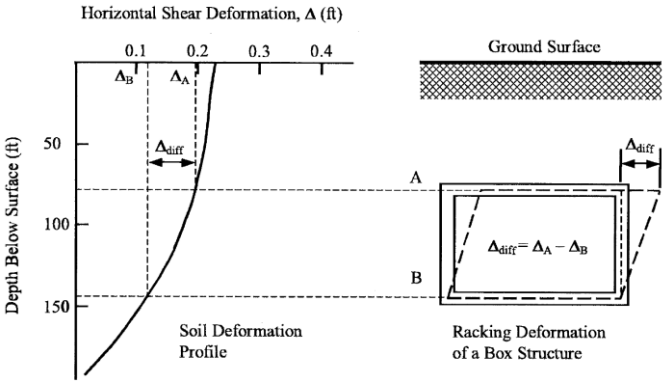

Figure 2.8. Typical free-field racking deflection applied to a buried rectangular structure (after Wang, 1993)

2.6.1.2 Numerical Analysis and Application of Free Field Deformations

In today's world, the use of computers has become prevalent in general, so numerical approaches can be used to obtain free field displacements, especially in soil profiles with multilayer variable field properties. Many softwares such as Deepsoil, Shake, Plaxis are available for this purpose. These programs obtain free field displacements by using one dimensional wave propagation theorems. These results can be used by applying them to the relevant depths (Hashash, 2001). Kuesel (1969) stated that for many cases, designs that can remain in the elastic region at free-field displacements do not require a special seismic investigation.

The free-field approach can be used as a valid design option in cases where the earthquake level is low, such as in a rigid rock environment. However, in soft soil environments, free-field displacements give very conservative results. In such cases, it is necessary to consider the soil-structure interaction (Wang, 1993). A comparison of seismic design is presented in Table 2.3.

Table 2.3. Seismic analysis methods (after Wang, 1993)

Approaches	Advantages	Disadvantages	Applicability
Dynamic earth pressure methods	1. Used with reasonable results in the past 2. Require minimal parameters and computation error 3. Serve as additional safety measures against seismic loading	1. Lack of rigorous theoretical basis 2. Resulting in excessive racking deformations for tunnels with significant burial 3. Use limited to certain types of ground properties	For tunnels with minimal soil cover thickness
Free-field racking deformation method	1. Conservative for tunnel structure stiffer than ground 2. Comparatively easy to formulate 3. Used with reasonable results in the past	1. Non-conservative for tunnel structure more flexible than ground 2. Overly conservative for tunnel structures significantly stiffer than ground 3. Less precision with highly variable ground conditions	For tunnel structures with equal stiffness to ground
Soil–structure interaction finite-element analysis	1. Best representation of soil–structure system 2. Best accuracy in determining structure response 3. Capable of solving problems with complicated tunnel geometry and ground conditions	1. Requires complex and time consuming computer analysis 2. Uncertainty of design seismic input parameters may be several times the uncertainty of the analysis	All conditions
Simplified frame analysis model	1. Good approximation of soil–structure interaction 2. Comparatively easy to formulate 3. Reasonable accuracy in determining structure response	1. Less precision with highly variable ground	All conditions except for compacted subsurface ground profiles

2.6.2. Soil Structure Interaction (SSI) Approach

The free field displacement approach gets modified when buried structures are involved. In this section, the mathematical background of the presence of structures will be discussed.

2.6.2.1 Closed Form Elastic Solutions for Soil Structure Interaction Approach

In this methodology employ a beam-on-elastic foundation model to represent the SSI effects (quasi-static) without considering inertia effects. In the case of seismic loading, the tunnel lining will experience the deformations experienced by the surrounding ground. These maximum structural stresses will occur when the shear wave has 45 degree with horizontal as shown in Figure 2.5.

$$\varepsilon^{a}{}_{max} = \frac{\left(\frac{2\pi}{L}\right)A}{2+\left(\frac{E_l A_c}{K_a}\right)\left(\frac{2\pi}{L}\right)^2} \leq \frac{fL}{4E_l A_c} \qquad (2.6)$$

Where:

L: wavelength of S-wave

K_a: longitudinal spring coefficient of ground

A: displacement amplitude of an S-wave

A_c: Cross-Sectional area of tunnel lining

E_l: lining deformation modulus

f: maximum friction between lining and soil

The effects on tunnel lining arising from seismic waves in the perpendicular or horizontal direction to the tunnel axis are shown in Figure 2.9. The axial stresses in the lining are limited by the frictional forces between the tunnel and the ground. This maximum frictional force was obtained by Sakurai and Takashi by multiplying one-quarter of the wavelength with the maximum frictional force per unit length, as shown in Equation 2.6.

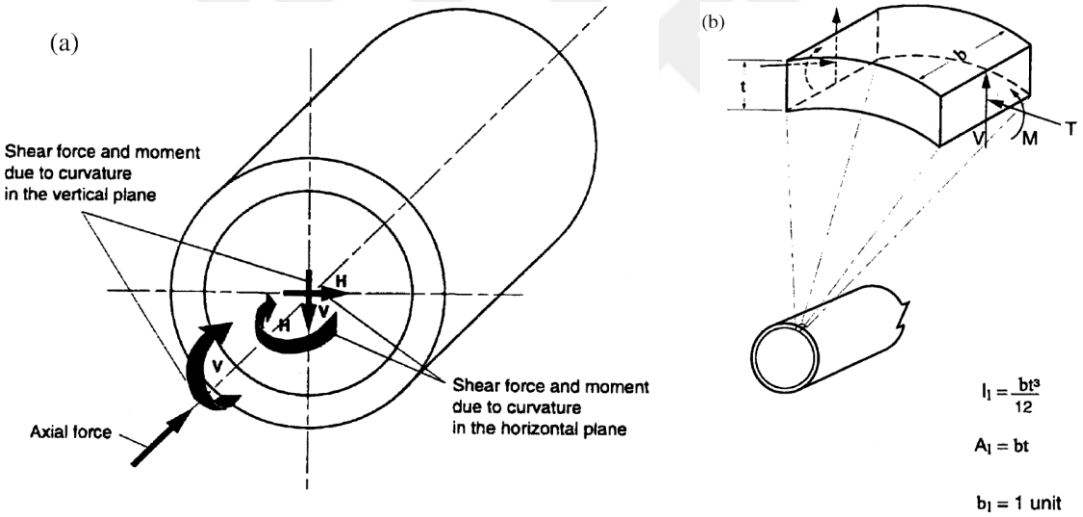

Figure 2.9. Internal effects induced by earthquake waves (Power et al., 1996), (a) Internal effects occur due to waves propagating through the tunnel axis, (b) Internal effects occur due to waves propagating perpendicular the tunnel axis

The highest bending strain at a 0-degree angle can be found by the following formula:

$$\varepsilon^b{}_{max} = \frac{\left(\frac{2\pi}{L}\right)^2 A}{1+\left(\frac{E_l I_c}{K_t}\right)\left(\frac{2\pi}{L}\right)^4} r \qquad (2.7)$$

Where:

I_c: moment of inertia

K_t: transverse spring coefficient of medium

r: radius of tunnel

In these sets of axial and bending strain equations, respectively, these strain values can be superposed since the ground environment and tunnel lining are considered linear elastic materials. However, it should be noted that due to the cyclic nature of the earthquake loading, extreme conditions should be considered both on the positive and negative sides. It is possible to calculate the maximum shear force by using maximum bending strain on the lining.

$$V_{max} = \frac{\left(\frac{2\pi}{L}\right)^3 E_l I_c A}{1+\left(\frac{E_l I_c}{K_t}\right)\left(\frac{2\pi}{L}\right)^4} = \left(\frac{2\pi}{L}\right) \quad M_{max} = \left(\frac{2\pi}{L}\right)\left(\frac{E_l I_c \varepsilon^b{}_{max}}{r}\right) \tag{2.8}$$

The total axial strain can be found by conservatively summing the axial and bending strains (Power et al., 1996).

$$\varepsilon^{ab} = \varepsilon^a{}_{max} + \varepsilon^b{}_{max} \tag{2.9}$$

It should be noted that the calculated values are appropriate for soft ground conditions. In stiff ground conditions, design will be possible with free field displacements. In addition, increasing the stiffness of the structure will cause the structure to get more damage (Hashash, 2001). Instead, it should be kept in mind that a system with less stiffness, but ductile reinforcement will be more effective (Wang, 1993).

The strains calculated in the equation proposed by Power et al. (1996) in Equation 2.9 are calculated with the help of spring coefficients. The spring coefficients for the longitudinal and transverse ground sections are symbolized by K_a and K_t for the incident wavelength, respectively.

$$K_t = K_a = \left(\frac{16\pi G_m(1-v_m)}{(3-4v_m)}\right)\left(\frac{d}{L}\right) \tag{2.10}$$

Where:

G_m: shear modulus

v_m: Poisson's ratio

d: diameter

His seminal work in 1993, Wang stated that derivation of ground springs differs from traditional beams in foundation analysis for two important reasons. First, the spring coefficients must accurately reflect the seismic modulus of the soil, especially under dynamic loads. This deviation emphasizes the need for a more subtle understanding of soil behavior under dynamic conditions. Secondly, the derivations take into account the unique nature of seismic loading and recognize that the soil experiences alternating positive and negative loads because of the presumed sinusoidal earthquake wave. This consideration emphasizes the importance of capturing the cyclic and reversible nature of seismic forces in the analysis of the system.

Some researchers have produced equations for the determination of the incident wavelength (Matsubara et al., 1995):

$$L = T.C_s \tag{2.11}$$

Where:

T: natural period of the soil

C_s: shear wave velocity

$T = \frac{4h}{C_s}$ Idriss and Seed (1968) (2.12)

Where:

h: thickness of the soil layer

C_s: shear wave velocity

The amplitude of ground displacement amplitude, “A”, symbolize the spatial differences of ground motions along a horizontal alignment and must be calculated according to site-specific situation. In general, the displacement magnitude will increase as the wavelength increases (SFBART, 1960). Presuming a sinusoidal wave with displacement amplitude “A” and wavelength “L”. “A” could be computed using the following formulas:

For free-field axial strains

$$\frac{2\pi A}{L} = \left(\frac{V_S}{C_S}\right) sin\phi cos\phi \tag{2.13}$$

For free-field bending strains

$$\frac{4\pi^2 A}{L^2} = \left(\frac{a_S}{C_S}\right) cos^3\phi \quad (2.14)$$

2.6.3. Analysis of Circular Shaped Tunnels Considering Soil-Structure Interactions

The effectiveness of the simplified seismic design approach relies on the use of judgment during the design process. However, the flexibility ratio of the tunnel lining can affect the accuracy of predicting the ovalization effects on the tunnel lining. This variability is due to uncertainties in the tunnel-ground interaction and may be insignificant for many real-world applications. In most cases involving circular tunnels, the flexibility ratio (F) is usually large enough to neglect the effects of tunnel-ground interaction, as suggested by (Peck, 1972). This simplification allows reasonable assumptions that the displacements experienced by the lining are equivalent to those in the surrounding ground.

However, difficulties can occur in practical scenarios involving a very rigid structure in a soft ground environment. An illustrative example is the construction of a rigid buried tunnel in a soft lake or riverbed. In such cases, where the flexibility ratio is very low, it becomes imperative to consider the tunnel-ground interaction for a more efficient and accurate design. This emphasizes the need to take into account the various soil-structure interactions in varying geological environments, highlighting the refined nature of the design process (Wang, 1993).

Merritt et al. (1985) introduced the concept of compressibility and flexibility (C and F) ratios to clarify the rigidity relationship among a tunnel and adjacent ground. The compressibility ratio measures the stiffness in extension by showing how the lining responds to compression or extension relative to the medium. On the other hand, the flexibility ratio measures bending stiffness and gives insight into the resistance of the medium to ovalization as a response to external forces.

$$C = \frac{E_m(1-v_l^2)R}{E_l t(1+v_m)(2-v_m)} \quad (2.15)$$

$$F = \frac{E_m(1-v_l^2)R^3}{6E_l I(1+v_m)} \quad (2.16)$$

Where:

E_m: deformation modulus

I: moment of inertia of lining

$R\ and\ t$: radius and thickness of lining

Various closed form solutions have been proposed by many researchers to predict the soil-structure interaction for circular tunnels. Based on a few fundamental presumptions, these methods are frequently utilized in the static design of tunnel linings. First, the ground is assumed to behave as an infinite, elastic, homogeneous and isotropic medium. Secondly, the circular tube is typically considered as an elastic, thin-lining subjected to plane strain conditions.

Two important assumptions play an important role in the models presented in previous studies and their implications were investigated by Mohraz et al. (1975) and Einstein et al. (1979). The first assumption involves the consideration of full slip or non-slip situations through the interface among the medium and the lining. This differentiation in slip conditions can significantly affect the predicted behavior of the tunnel-ground system.

The second main assumption deals with loading conditions that can be developed as either outer loading (overpressure loading) or excavation loading. The choice between those loading circumstances affects the reaction of the lining according to the applied forces and has been the focus of research conducted by Mohraz et al. (1975) and Einstein et al. (1979). Understanding and accounting for these assumptions is crucial for accurate and reliable predictions in the design and analysis of tunnel structures (Wang, 1993).

As noted by Duddeck and Erdmann (1982), the developments in circular tunnel models during those years focused mainly on excavation loading conditions and provided a more realistic simulation of actual tunnel construction. However, in order to assess the response of dynamic loading, it is important to turn to solutions designed for external loading conditions. Building on the study of Burns and Richard (1964) and Hoeg (1968), Peck, Hendron and Mohraz (1972) proposed closed form solutions that specifically address thrust forces, bending moments and displacements especially for outer loading cases.

The formulations for these lining reactions are complexly linked to the flexibity ratio, the compressibility ratio (as previously presented in Equations 2-15 and 2-16), the in-situ overburden pressure ($\gamma_t h$) and the coefficient of at rest soil pressure (K_0). To adapt these solutions to seismic loading, it is necessary to simulate a simple slip condition on site, replacing the in-situ overburden pressure by the free-field shear stress (τ) and assigning

K_0 to -1. The shear stress (τ) could be denominated as a function of the shear strain (γ). Through algebraic modifications, the descriptions obtained for the maximum thrust (T_{max}), bending moment (M_{max}) and diametral strain ($\Delta d/d$) can be formulated in specific and applicable manners. These modifications are crucial to accurately capture the tunnel responses under seismic shear wave loading conditions (Wang, 1993).

$$\frac{\Delta d}{d} = \mp \frac{1}{3} K_1 F \gamma_{max} \tag{2.17}$$

$$T_{max} = \mp \frac{1}{6} K_1 \frac{E_m}{(1+v_m)} r \gamma_{max} \tag{2.18}$$

$$M_{max} = \mp \frac{1}{6} K_1 \frac{E_m}{(1+v_m)} r^2 \gamma_{max} \tag{2.19}$$

Where:

$$K_1 = \frac{12(1-v_m)}{2F+5-6v_m} \tag{2.19}$$

In this context, K_1 is explicitly defined as the lining response coefficient and serves as a key parameter in characterizing the response of the tunnel lining to seismic loading. The dynamic loading value is indicated by the maximum shear strain, γ_{max}, and this value can be determined either by a simplified expression in the Equation 2.20 or by conducting a site response analysis for a more detailed evaluation.

$$\gamma_{max} = \frac{V_s}{C_s} \tag{2.20}$$

Where:

V_s: maximum particle velocity

C_s: effective shear wave propagation velocity

To assist in the design progress, Figures 2.10. and 2.11. illustrate the lining response coefficient K_1 is dependent both the flexibility ratio and the Poisson's ratio of the soil. It is very important to recognize that the solutions presented in these figures are based on the assumption of a full-slip interface, emphasizing the importance of recognizing the conditions under which the models and coefficients are derived (Wang, 1993).

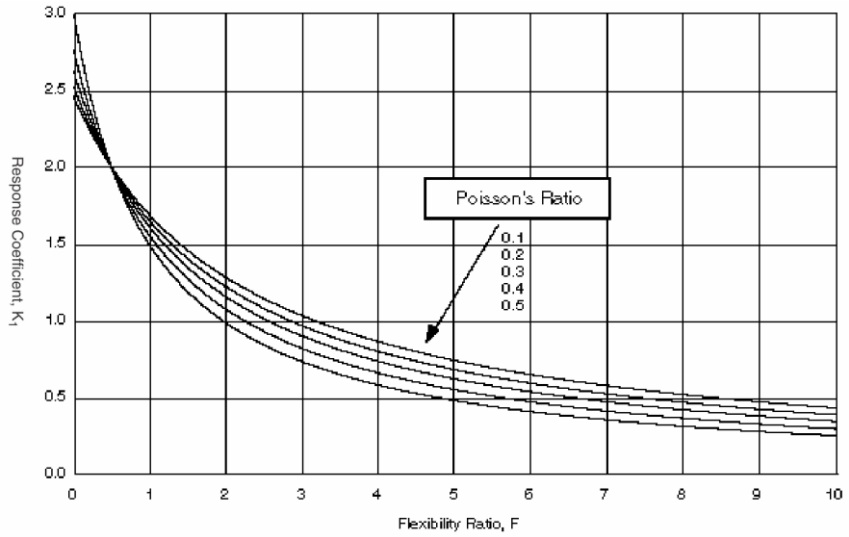

Figure 2.10. Lining response coefficient, K1 (full-slip case), F=0-10 (Wang, 1993)

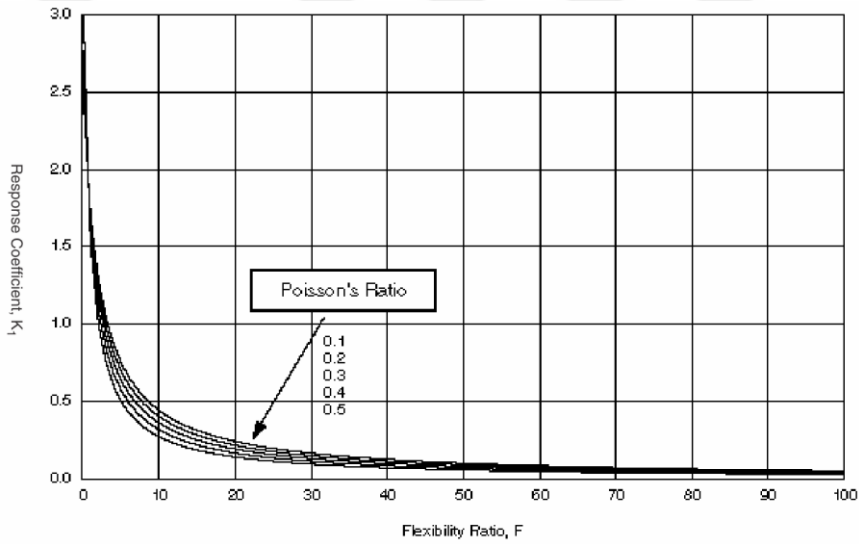

Figure 2.11. Lining response coefficient, K1 (full-slip case), F=0-100 (Wang, 1993)

Figures 2.10. and 2.11. shows the correlation between the K_1 and F under the full slip assumption. Various studies suggest that slip at the interface occurs predominantly in certain types of weak environments or under severe seismic loading intensity conditions. However, it is important to note that for the majority of tunnels, the interface status is somewhere between full slip and no-slip. Therefore, it is recommended that both scenarios be studied to assess critical lining forces and deformations accurately.

Wang (1993) stated that higher values were obtained regarding moments and displacements in the event of full slip and much smaller values were obtained in terms of thrust forces. However, Hashash et al. (2005) showed that this was not the case for

moment and displacements in a parametric study using Wang and Penzien's equations. The results were almost identical for moment and racking in the no-slip and full-slip cases, whereas for thrust, differences were observed in both sets of equations. Consequently, based on Hoge's work (1968), adopting the no-slip assumption, which implies full ground continuity, is recommended to provide a more accurate representation of the tunnel-ground interaction when evaluating the lining thrust response.

$$T_{max} = \mp K_2 \tau_{max} r = \mp K_2 \frac{E_m}{2(1+v_m)} r \gamma_{max} \tag{2.21}$$

Where:

$$K_2 = 1 + \frac{F[(1-2v_m) - C(1-2v_m)] - \frac{1}{2}(1-2v_m)^2 + 2}{F[(3-2v_m) + C(1-2v_m)] + C\left[\frac{5}{2} - 8v_m + 6{v_m}^2\right] + 6 - 8v_m} \tag{2.22}$$

Figure 2.12. and 2.13. shows that seismic-induced thrusts tend to increase as both the compressibility and flexibility ratios decrease, which is particularly noticeable when the Poisson's ratio of the soil is below 0.5. The effect of compressibility becomes more pronounced and leads to an increase in the thrust response under seismic loading conditions.

However, as the Poisson's ratio get closer to 0.5, the thrust response becomes not dependent of compressibility as shown in Figure 2.14., showing the characteristics of saturated undrained clay. In this scenario, the soil is conceived incompressible, as discussed by Wang (1993).

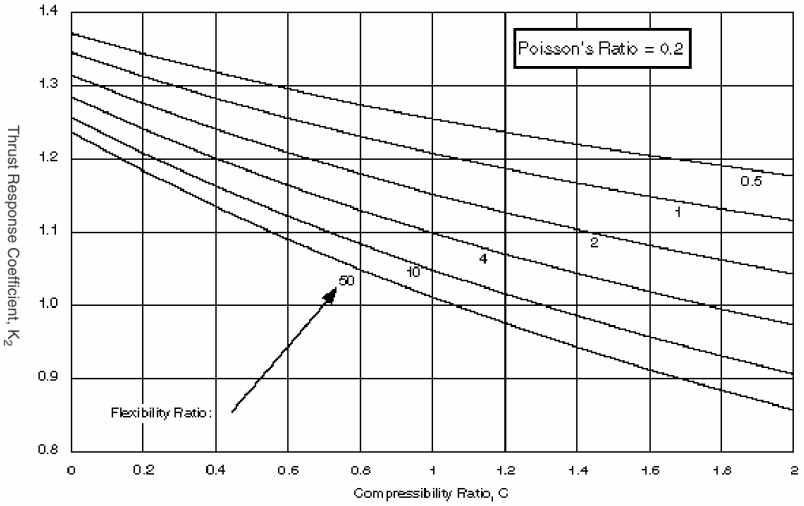

Figure 2.12. Lining response (thrust) coefficient, K2 (no-slip interface), v = 0.20 (Wang, 1993)

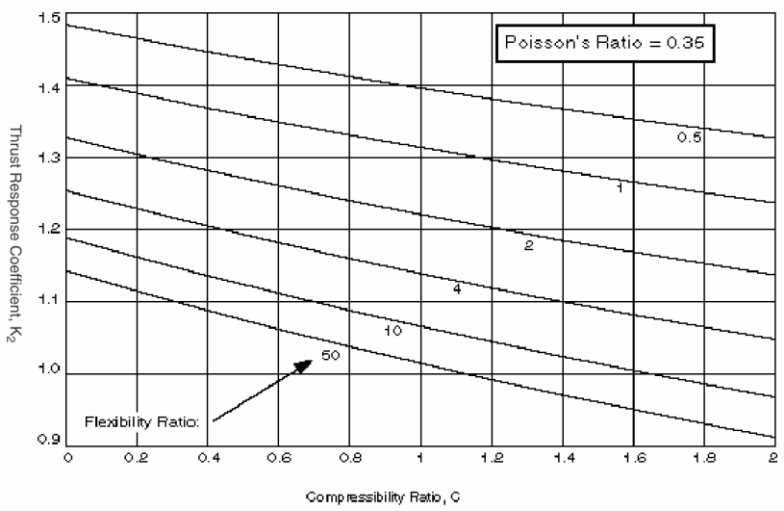

Figure 2.13. Lining response (thrust) coefficient, K2 (no-slip interface), ν = 0.35 (Wang, 1993)

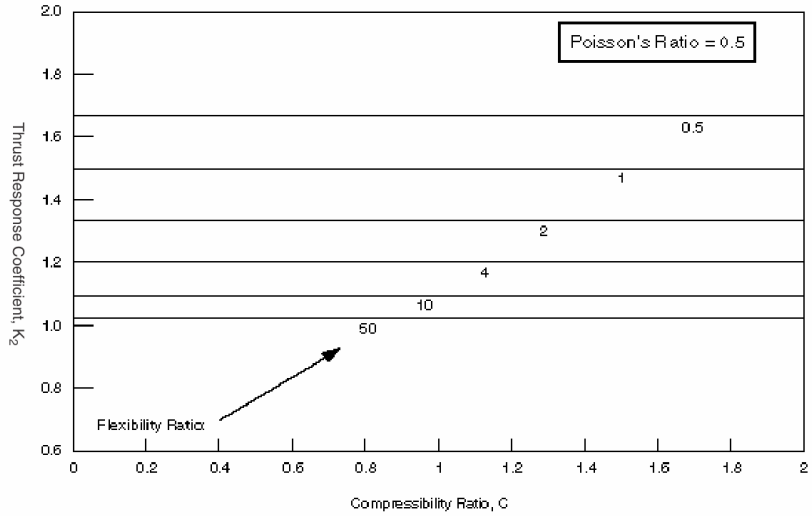

Figure 2.14. Lining response (thrust) coefficient, K2 (no-slip interface), ν = 0.50 (Wang, 1993)

For clarification, an essential piece of information is that the displacement rate among the liner and the free area is expressed as a function of the flexibility ratio, denoted as F. This expression is generated by dividing Equation 2.17 by Equation 2.4 and obtains the following expression.

$$\frac{\Delta d_{lining}}{\Delta d_{free-field}} = \frac{2}{3} K_1 F \qquad (2.23)$$

The normalized lining deflection based on this expression is presented graphically in Figure 2.15. and 2.16, respectively. The findings show that when the flexibility ratio, F, is below about 1, the tunnel tends to resist deformation and displace less than the free field. This can occur when a rigid tunnel is constructed on soft or very soft soils.

When the flexibility ratio gets bigger, the tunnel distorts more according to the free field, potentially reaching a top limit as the flexibility ratio approaches infinity. This more upward-bound displacement corresponds to the perforated soil deflection computed by Equation 2.5 and indicates a perfectly flexible lining scenario.

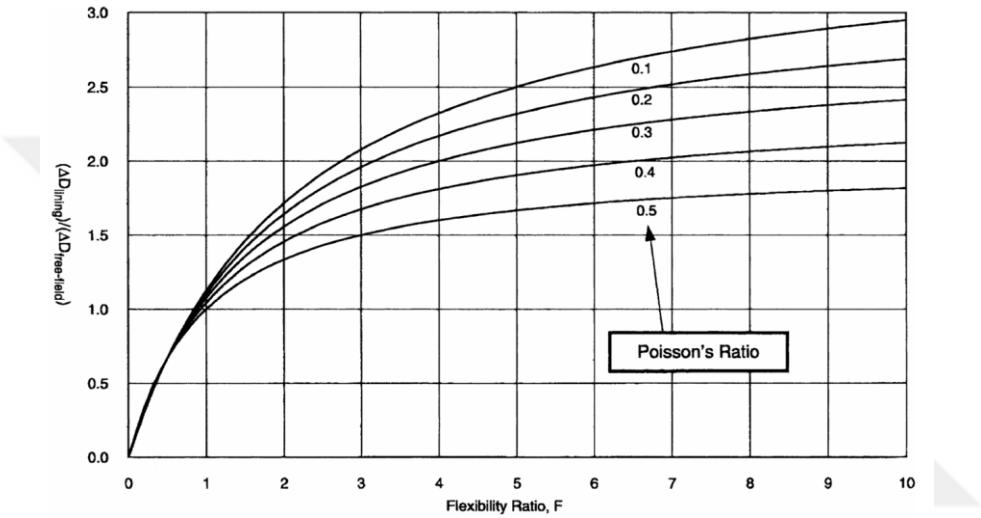

Figure 2.15. Normalized lining deflection (full-slip interface), F=0-10 (Wang, 1993)

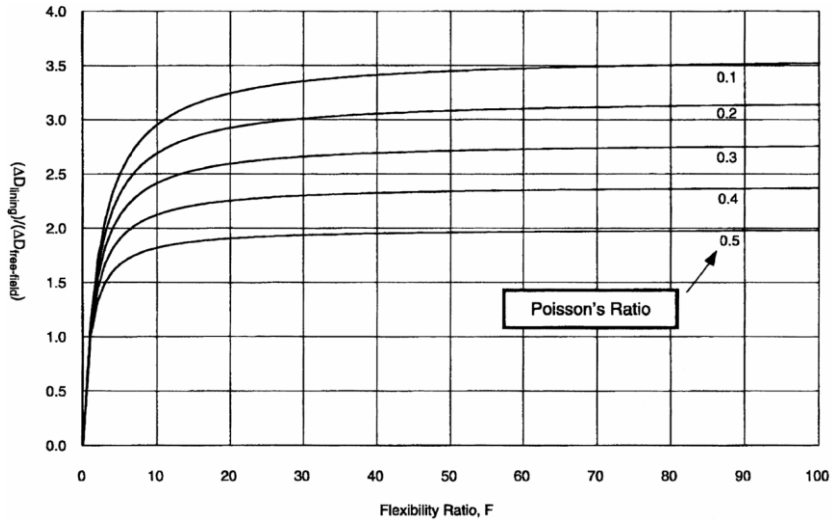

Figure 2.16. Normalized lining deflection (full-slip interface), F=0-100 (Wang, 1993)

In their 1998 study, Penzien and Wu formulated closed-form solutions to address the thrust, shear and moment due to racking deformations in tunnel linings. Building on their previous findings, Penzien extended the analytical framework in 2000 by introducing a procedural approach to evaluate racking deformations in both rectangular and circular tunnel geometries.

A lining-to-soil racking ratio was described to predict the deformation of the structure.

$$\Delta d^n{}_{lining} = R^n \Delta d_{free-field} = R^n \frac{d}{2} \gamma_{max} \tag{2.24}$$

In the event of a circular tunnel, R is the proportion of the lining diameter displacement to the free-field diametric displacement. The equations proposed by Penzien for the maximum thrust, moment and shear that will occur in the lining under an earthquake loading condition in full slip are given below.

$$T_{max} = \mp \frac{12 E_l I \Delta d^n{}_{lining}}{d^3 (1-{v_l}^2)} = \mp \frac{6 E_l I R^n \gamma_{max}}{d^2 (1-{v_l}^2)} \tag{2.25}$$

$$M_{max} = \mp \frac{6 E_l I \Delta d^n{}_{lining}}{d^2 (1-{v_l}^2)} = \mp \frac{3 E_l I R^n \gamma_{max}}{d (1-{v_l}^2)} \tag{2.26}$$

$$V_{max} = \mp \frac{24 E_l I \Delta d^n{}_{lining}}{d^3 (1-{v_l}^2)} = \mp \frac{12 E_l I R^n \gamma_{max}}{d^2 (1-{v_l}^2)} \tag{2.27}$$

The lining-soil racking ratio under normal loading only is described as:

$$R^n = \mp \frac{4(1-v_m)}{(\alpha^n + 1)} \tag{2.28}$$

Where

$$\alpha^n = \frac{12 E_l I (5-6v_m)}{d^3 G_m (1-{v_l}^2)} \tag{2.29}$$

For no slip condition, the equations are presented as:

$$\Delta d_{lining} = R \Delta d_{free-field} = R \frac{d}{2} \gamma_{max} \tag{2.30}$$

$$T_{max} = \mp \frac{24 E_l I \Delta d_{lining}}{d^3 (1-{v_l}^2)} = \mp \frac{12 E_l I R \gamma_{max}}{d^2 (1-{v_l}^2)} \tag{2.31}$$

$$M_{max} = \mp \frac{6 E_l I \Delta d_{lining}}{d^2 (1-{v_l}^2)} = \mp \frac{3 E_l I R \gamma_{max}}{d (1-{v_l}^2)} \tag{2.32}$$

$$V_{max} = \mp \frac{24 E_l I \Delta d_{lining}}{d^3 (1-{v_l}^2)} = \mp \frac{12 E_l I R \gamma_{max}}{d^2 (1-{v_l}^2)} \tag{2.33}$$

Where

$$R = \mp \frac{4(1-v_m)}{(\alpha+1)} \tag{2.34}$$

$$\alpha = \frac{24E_l I(3-4v_m)}{d^3 G_m(1-v_l{}^2)} \tag{2.35}$$

2.6.4. Comparison of Closed-Form Solutions Including Soil-Structure Interaction

Hashash et al. (2005) compared the sets of equations given by Wang and Penzien for full slip and non-slip cases under the material properties given in Table 2.4. and Table 2.5. The equations proposed by Wang and Penzien provide the same results for the full slip case, but the situation is different in the non-slip case. For the thrust force, Penzien's proposed equations for the non-slip case give results almost twice the value of the slip case. If we compare the same case for Wang, the results are almost 16 times higher.

Table 2.4. Soil properties used in the analysis (Hashash, 2005)

Soil parameter	Value	
Case 1	Young's modulus (E_m)	312,000 kN/m^2
	Poisson's ratio (v)	0.3
Case 2	Young's modulus (E_m)	312,000 kN/m^2
	Poisson's ratio (v)	0.49
Case 3	Young's modulus (E_m)	185,400 kN/m^2
	Poisson's ratio (v)	0.49

Table 2.5. Tunnel lining properties used in analysis (Hashash, 2005)

Lining parameter	Value
Young's modulus (E_l)	24,800,000 kN/m^2
Area (per unit width)	0.3 m^2/m
Moment of inertia (I)	0.00225 m^4/m
Lining thickness (t)	0.3 m
Weight	0
Poisson's ratio (v)	0.2

In the comparison of the moment and racking ratio, the equations of Wang and Penzien give approximately the same results for both no-slip and full-slip cases. A summary of their work is presented in Table 2.6.

Table 2.6. Calculated forces and stress using the analytical solutions (Hashash, 2005)

	Wang		Penzien		% Difference	
	Full slip	No slip	Full slip	No slip	Full slip	No slip
Case 1						
Racking ratio	2.58	2.58	2.58	2.55	0	1.2
Maximum thrust (T_{max})	62.94	1045.38	62.94	124.64	0	738.7
Maximum moment (M_{max})	188.81	188.81	188.81	186.95	0	1.0
Maximum shear (V_{max})	–	–	125.87	124.64		
Case 2						
Racking ratio	1.92	1.92	1.92	1.92	0	0.0
T_{max}	46.83	813.59	46.83	93.60	0	769.2
M_{max}	140.48	140.48	140.48	140.40	0	0.8
V_{max}	–	–	46.83	93.60		
Case 3						
Racking ratio	1.84	1.84	1.84	1.84	0	0.0
T_{max}	44.99	507.21	44.99	89.90	0	464.2
M_{max}	134.97	134.97	134.97	134.85	0	41.5
V_{max}	–		44.99	89.90	0	

After the analytical comparison, they made a numerical comparison using the Plaxis software. In their study, they worked in the plane-strain conditions and modeled only the no-slip case. Moment and racking ratios were very similar to the analytical results for case 1 and case 2 but differed by 15% for case 3. Thrust force result is consistent with Wang's solution and differs from Penzien's solution by 700%. Penzien's solution results in an underestimate and is not recommended for calculations for the no-slip case (Hashash, 2005).

2.7. Tunnel Modelling Techniques

Tunneling inherently requires complex three-dimensional stress-strain dynamics, driving engineers to use sophisticated three-dimensional Finite Element (FE) analysis for design purposes. An ongoing controversy in this field revolves around the calculation of structural forces and settlements in tunnel linings, and an important issue is whether a comprehensive 3D analysis is mandatory or whether more basic 2D models will be sufficient. For large tunnel projects of several kilometers in length with different cross-sections, the feasibility of using purely three-dimensional analysis as the primary design tool is impractical. As a result, the agreement in the industry generally tends towards the practical necessity of relying on two-dimensional analyses to address the complexity of such extensive excavations (Möller, 2006).

In analyzing the tunnel excavation with a two-dimensional FE approach, it becomes imperative to accommodate the absence of the third dimension. Figure 2.17 visually illustrates the incorporation of a three-dimensional arch with rotated principal stress directions surrounding the unsupported tunnel face. This structural configuration performs a very important function by efficiently carrying the vertical ground loads in the

context of the two-dimensional model by subtly redirecting them around the unsupported shear stress (Möller, 2006).

As shown in Figure 2.17, the limitations of the two-dimensional analyses become apparent as they fail to capture the three-dimensional arching effect. To overcome this limitation, an artificial support pressure, denoted as p, is introduced. From the literature on two-dimensional approaches for tunnel analysis, it is noticeable that this synthetic counterbalance can be implemented not only with a pressure approach, but also with a displacement approach (Möller, 2006).

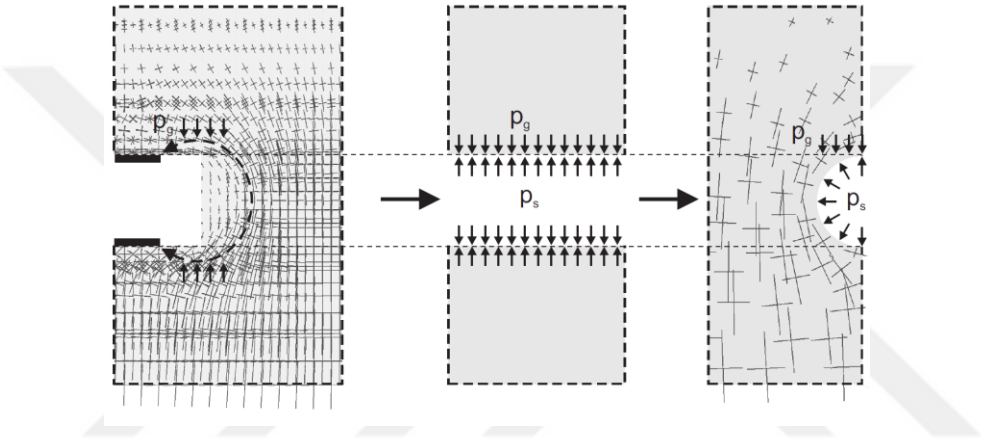

Figure 2.17. 3D arch support and 2D FE-approximation with support pressure

In the context of Figure 2.18, tunneling construction is shown in combination with a ground response curve. This visual representation highlights that the majority of 2D approaches can be categorized into two main methods. The first method uses a stress relaxation approach where the initial ground pressure (p_0) within the tunnel is reduced to a defined support pressure (p_s). The second method uses a displacement/gap approach where the support level is determined by indicating a specified tunnel contraction (R) or ground loss (Möller, 2006). This section will examine these methods in detail.

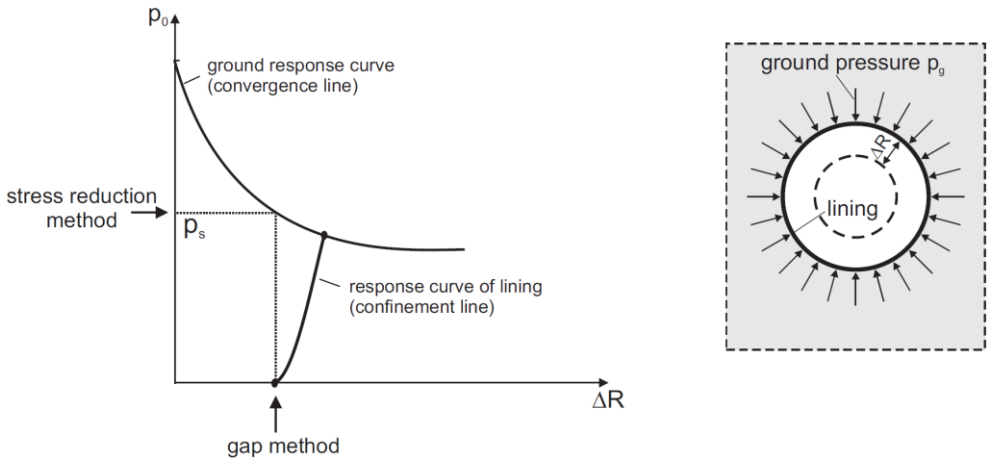

Figure 2.18. 2D FE-approximations: stress reduction and contraction method adopting ground response curve

2.7.1 Core Support Method (α-method)

The core support method, also known as the α method, requires the tunnel core material stiffness to be reduced by a factor α. In the initial calculation stage, where gravity loading is considered, the initial stresses are calculated with the modified core stiffness α × E. This process results in a reduction of the residual support pressure p_α within the tunnel, classifying the method as a stress reduction type approach. In the next calculation phase, the soil inside the tunnel is excavated and the lining is activated. A higher reduction in stiffness tends to result in larger deformations of the surrounding ground, while a lower reduction leads to smaller deformations. Method is often used to model conventional tunneling approaches (Möller, 2006).

Schikora and Fink (1982) provided empirical information, reporting that realistic α values for tunnels with 2 < H/D < 4 are less than 0.2. In cases of partial excavation where the lining ring is not immediately closed, they recommend α values in the range of 0.3 to 0.5.

A commonly adopted reduction amount falls within 40-60% range, a figure often cited as typical according to Mohr and Pierau (2004) and Coulter and Martin (2004). This range is frequently utilized in tunneling analyses (FHWA, 2009).

Sensitivity analyses of the actual reduction value are typically included in the calculations.

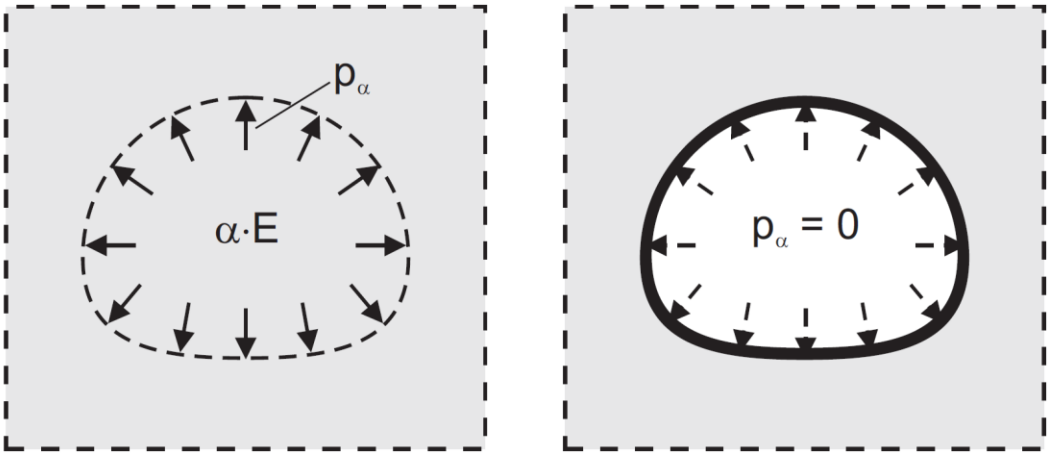

Figure 2.19. The calculation phase of the core support method

2.7.2 Stress Reduction Method (β-method)

The predominant method used to simulate the installation procedures is the stress reduction method, commonly referred to as the β- or λ-method. This approach effectively addresses the stress relaxation that occurs in the ground due to the delayed installation of the shotcrete lining while taking into account the load distribution between the ground and the lining. Consisting of two calculation stages starting from the initial geostatic stresses, Figure 2.20 visually illustrates these stages in conjunction with the ground response curve (Möller, 2006).

In the first calculation stage, the simulation of the tunnel installation involves the deactivation of the ground elements inside the tunnel. The initial ground response acting inside the tunnel is shown as p_0, is then reduced to $\beta . p_0$, where $0 < \beta < 1$. The parameter β, known as the unloading factor, is usually chosen to be around 0.5. This first stage captures the dynamic interaction between the ground and the lining during installation (Möller, 2006).

In the second calculation stage, the lining is installed and the remaining load $\beta . p_0$ is distributed between the lining and the ground. The structural forces within the lining only arise in this second stage. A significant part of the residual load is directed towards the lining for rigid linings. Small β factors are associated with larger round lengths and/or delayed installation of the tunnel lining. In such cases, ground deformations are relatively large, while structural forces within the lining remain relatively low (Möller, 2006).

Conversely, a large β factor results in smaller ground deformations and higher structural forces within the lining. This scenario is particularly relevant for rapid installation of the tunnel lining in the second calculation phase. The interaction between the β factor and the installation sequence plays a critical role in determining the distribution of loads, ground deformations and structural forces within the lining during tunnel simulations (Möller, 2006).

The method is often used to model conventional tunneling approaches. The method has also been proposed for closed shield tunneling but has not been widely adopted. Instead, methods to model ground loss have been adopted.

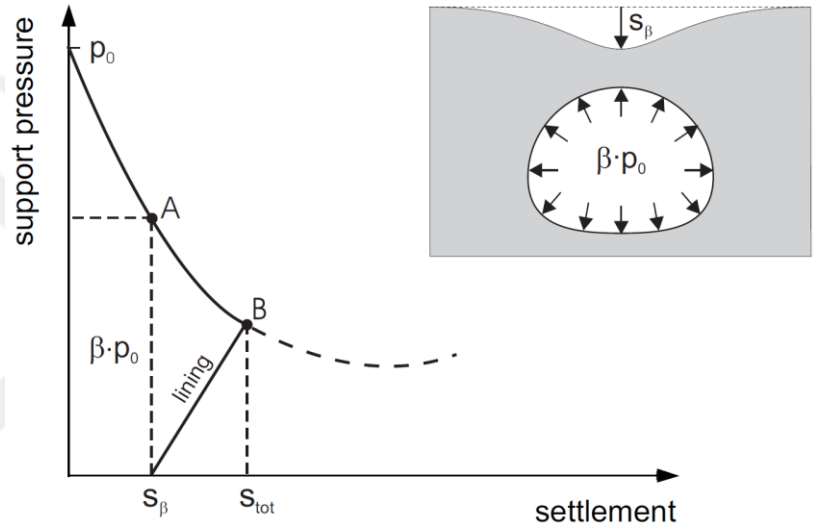

Figure 2.20. Display of stress reduction method adopting ground response curve

In order to incorporate the effects of 3D tunnel installation into this method, assumptions have to be made about the magnitude of the unloading factor.

Several authors have proposed diverse values for unloading factors, drawing upon engineering experience, empirical measurements, theoretical assumptions, or comparisons between 2D and 3D computations. In terms of structural forces, Schikora and Fink (1982) present values of the unloading factor, falling within the range of $0.35 < \beta < 0.6$ for tunnels with $2 < H/D < 4$. In a different approach, Baudendistel (1979) utilized three-dimensional linearly elastic analyses, considering vertical crown displacements of tunnels to derive unloading factors. Unloading factors from Baudendistel's work (1979) are presented in Table 2.7. for a fully excavated horseshoe profile and various round lengths (d), highlighting the appropriateness of linking β to d. The concept of correlating

β with the tunnel round length (d) is recognized as valid in Baudendistel's methodology (Möller, 2006).

Table 2.7. Unloading factors β for full excavation of a horseshoe profile and different round lengths d after Baudendistel (1979)

d	$1.5 \cdot D$	D	$0.5 \cdot D$	$0.25 \cdot D$	$0.125 \cdot D$	0
β	0.0	0.02	0.11	0.23	0.41	0.72

d = round length
β = unloading factor
D = excavation diameter

Laabmayr and Swoboda (1986) derived unloading factors based on the percentage of deformation measured behind the face upon completion of tunneling. For partial excavations, they found unloading factors falling within the range of $0.2 < \beta < 0.5$ for a top heading and $0.4 < \beta < 0.8$ for a wall heading.

Examining existing literature brings to light the considerable variation in unloading factors, underscoring the complexity of establishing precise numerical parameters across a wide range of scenarios. The evaluation of unloading factors constitutes a challenging task as it is influenced not only by tunnel characteristics such as geometry, cross-section and material properties, but also by the complex dynamics of construction techniques (Möller, 2006).

2.7.3 The Gap Method

Rowe et al. (1983) are known for introducing the first void method that focused on accounting for ground loss during tunneling. The approach proposed by Rowe et al. (1983) accounts for ground loss through the concept of a vertical void, as shown in Figure 2.21, where the void represents the vertical distance between the top of the tunnel lining and the original location of the ground cut surface before excavation. In the method outlined by Rowe et al. (1983), the calculation of ground loss involves consideration of the vertical gap between the tunnel top and the initial ground cutting surface, particularly where the tunnel invert is supported by the underlying soil and allows for potential heave.

The tunnel excavation is carried out in a unified computational stage, involving the installation of the tunnel lining along with a predetermined gap at the crown. Throughout this process, the ground is left unsupported, allowing for free displacement until contact with the lining occurs. For values of K_0 less than 1, the initial contact between the ground and the tunnel lining occurs at the crown and bottom of the tunnel, progressively extending to the sides as deformation continues. The deformation monitoring process during tunnel excavation involves observing the tunnel cut surface, and once contact is established with the tunnel lining, the interaction between the ground and the lining is initiated. Rowe et al. (1978) provide a detailed description of the interaction between the ground and the tunnel structure, outlining the dynamics of how the tunnel cut surface engages with the lining during the excavation process (Möller, 2006).

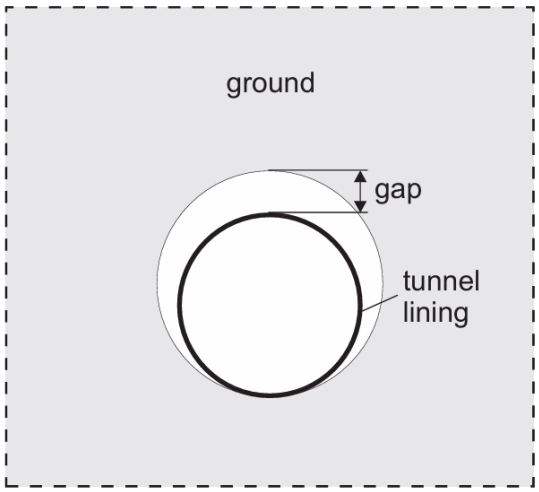

Figure 2.21. Gap method by Rowe et al. (1983)

2.8 Comparison of Response of Different Shapes of Tunnels

Choundary et al. (2018), are studied different tunnel geometries to investigate dynamic tunnel-soil interaction in soft ground conditions. The study was conducted using the finite element software Plaxis 2D and dynamic analysis was carried out using the Kobe 1995 earthquake record. Accordingly, the results for circular, square, square with rounded edges and horseshoe tunnel geometries are obtained for normal force and bending moment.

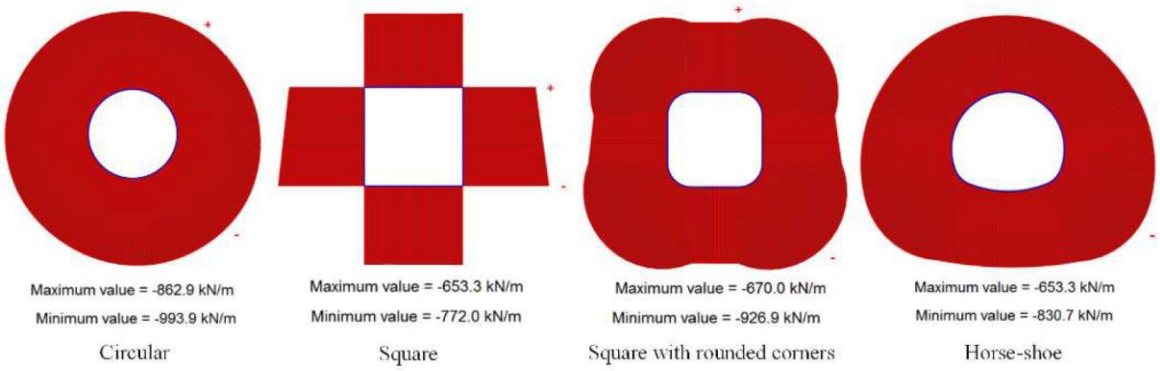

Figure 2.22. Variation in maximum thrust, T_{max} in the tunnel lining with different shapes, Choundary et al. (2018)

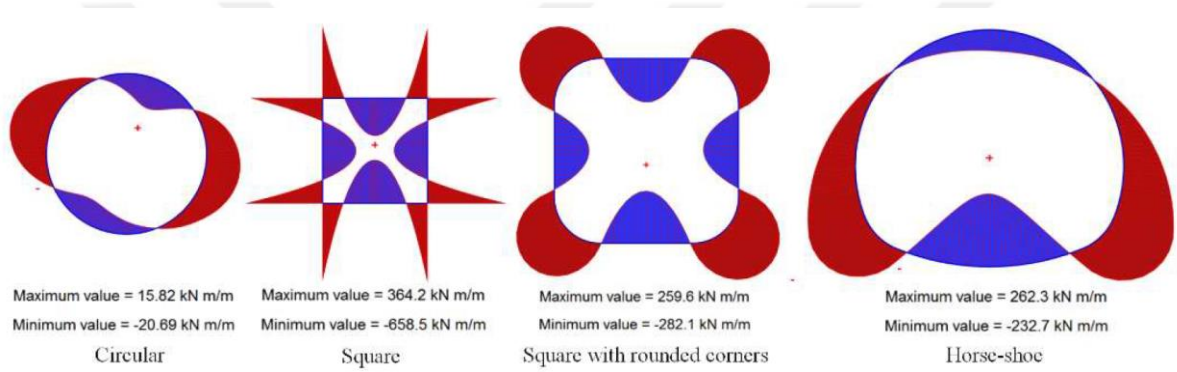

Figure 2.23. Variation in the maximum moment, M_{max} in the tunnel lining with different, shapes Choundary et al. (2018)

Accordingly, as a result of the analysis, it is stated that the maximum thrust force is obtained in the form of circular tunnels. When the bending moment is analyzed, it is stated that the tunnel with square shape has the highest effect and the corners close to the circular shape reduce the bending moment effects. Overall, it was stated that the tunnel with circular shape performed better in the seismic loading case compared to other cases.

3. A PARAMETRIC STUDY WITH DIFFERENT TUNNEL SHAPES

This chapter presents details of the full dynamic numerical modeling of tunnels with 3 different geometries (circular, box and horseshoe) using the finite element software Plaxis 2D. In this context, in order to extend the perspective of the study, parameters such as tunnel shape, depth, class of the site, characteristics of the rock medium, different earthquake records are considered. In summary, the main objective is to evaluate the effects of different tunnel shapes and burial depths on the tunnel lining under dynamic loading conditions.

3.1. Plaxis Model

In this section, the assumptions made for the fully dynamic finite element analyses to be performed with Plaxis will be presented. These studies include the variations in tunnel shape, tunnel depth, site classification, rock strength properties, dynamic analysis method and also sensitivity analysis.

3.1.1 Tunnel Shapes

The most commonly used shapes in practice are circular and horseshoe-shaped tunnels. One of the reasons for the selection of circular or horseshoe shaped tunnels is the operating costs. In general, circular tunnels are driven by TBM machines, and horseshoe tunnels are excavated using NATM methods. When the operating costs of TBM and NATM are compared, after about 6-7 km tunnel length, TBM cost becomes nearly equivalent to the NATM cost by decreasing. For this reason, the tunnelling method also changes depending on the tunnel length. Box sections are generally preferred for cut-and-cover tunnels. In scope of the thesis three different tunnels: circular, box and horseshoe were selected for dynamic analyses. Here, the circular tunnel diameter is determined to be 7 meters, and other tunnel shapes are chosen to have approximately the same excavation area during tunnel construction.

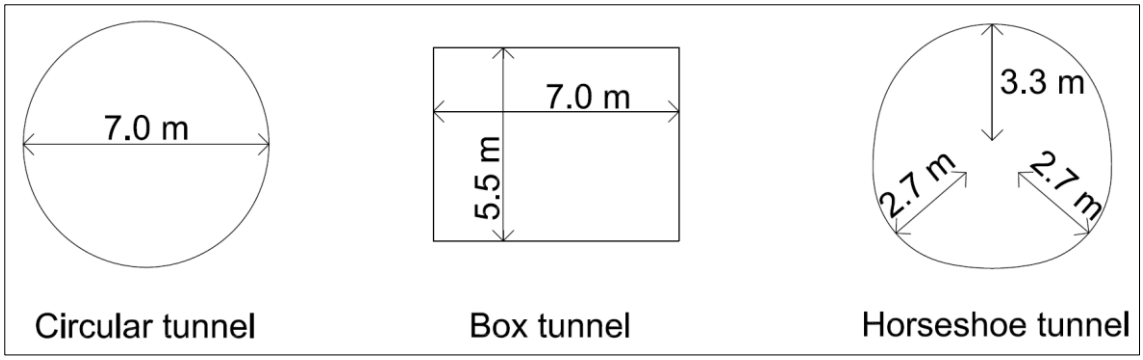

Figure 3.1. Geometric properties of tunnels to be used in analysis

3.1.2 Tunnel Depths

The behavior of three different tunnel shapes with equivalent diameter (D = 7 m) and their relationship with the burial depth will be examined. In this context, different burial depths were selected as 14 meters (2D) and 42 meters (6D), respectively, depending on the tunnel diameters. I have indicated the tunnel depths as shown schematically in Figure 3.2. The boundary conditions of the model geometry are set at a depth of 100 meters. The width will be determined with the help of the ground accelerations obtained at the ground surface in the analyses performed under the section of sensitivity analyses.

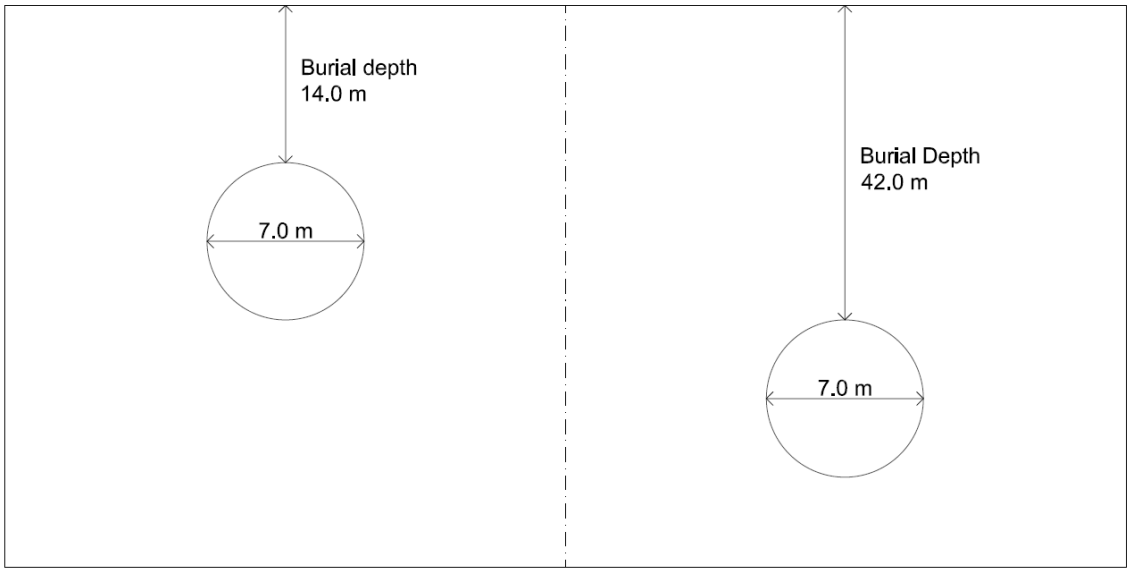

Figure 3.2. Tunnel burial depths to be used in analysis

3.1.3 Site Classification

Investigations carried out in the field show that the behavior and character of the soil/rock is very different from that of many construction materials. While most construction materials can be assumed to demonstrate a homogeneous character, determining the material parameter for the ground can change even every 3-5 meters, depending on the geology. There are situations where even two drillings in the same neighborhood can lead to different results. In this sense, one of the important tests to be performed while studying seismicity, which is the subject of the thesis, will be the tests that determine shear wave velocities. These test results can be a very good indicator of the seismicity behavior of the site and can be useful.

Since a parametric study is carried out within the scope of the thesis, instead of performing a site-specific test or using a test that has already been performed, the site classification of the models has determined according to ASCE 7-16, Table 3.1. site classification table which is given below.

Table 3.1. ASCE7-16 site classification table

Table 20.3-1 Site Classification

Site Class	$\bar{v}_s$	$\bar{N}$ or $\bar{N}_{ch}$	$\bar{s}_u$
A. Hard rock	>5,000 ft/s	NA	NA
B. Rock	2,500 to 5,000 ft/s	NA	NA
C. Very dense soil and soft rock	1,200 to 2,500 ft/s	>50 blows/ft	>2,000 lb/ft^2
D. Stiff soil	600 to 1,200 ft/s	15 to 50 blows/ft	1,000 to 2,000 lb/ft^2
E. Soft clay soil	<600 ft/s	<15 blows/ft	<1,000 lb/ft^2
	Any profile with more than 10 ft of soil that has the following characteristics: — Plasticity index $PI > 20$, — Moisture content $w \geq 40\%$, — Undrained shear strength $\bar{s}_u < 500$ lb/ft^2		
F. Soils requiring site response analysis in accordance with Section 21.1	See Section 20.3.1		

Note: For SI: 1 ft = 0.3048 m; 1 ft/s = 0.3048 m/s; 1 lb/ft^2 = 0.0479 kN/m^2.

In order to extend the comparison of the thesis study, 2 different site classes have been selected for 3 different tunnel geometries and 2 different depths, which have been mentioned in previous sections. These site classes were chosen as B and C.

Shear wave velocity for site class B is approximately 760-1500 m/s. This class is defined between soft rock and hard rock. This covers a wide range and will be taken into account in the selection of strength parameters.

For class C site, the shear wave velocity is approximately 360-760 m/s. This range covers a controversial range, such as where the weathering level of the rock is high or in a very dense soil class. For this range, soft rock will be accepted within the scope of this thesis and the strength parameter will be selected within the scope of rock mechanics.

3.1.4 Rock Strength Properties

Field studies may show different results when we go deeper into the ground. In general, strength parameters are expected to increase depending on the depth of the research work, but there are also contrary situations. The best thing would be to conduct a sufficient number of research studies in the relevant areas of the project site and analyze the necessary data in a laboratory environment. Since this study is parametric, two different situations will be compared. The first is that the material stiffnesses increase as depths go deeper, which can be expected as a normal situation, and the second is that the material parameters remain same with depth, which can be expected as an extreme situation for 100 meter depth.

To clarify the part so far, in order to carry out the parametric study in the scope of thesis, 3 different tunnel shapes at 2 different depths in 2 different site classes for 2 different rock strength properties depending on depth will be created and a total of 24 different models will be examined.

Parameter selection will be made in accordance with the site class and material properties accepted so far. The material property selection will be made for the situation that increases and remains constant with depth for field classes B and C, respectively.

The notion of K, which is the ratio of vertical to horizontal ground pressures, depends only on the Poisson's ratio in terms of rock mechanics has been proven to be incorrect before. While rock behaves anisotropically at shallow depths due to its structure, it starts to behave isotropically with increasing depth. In his study, Sheory (1994) utilized Hoek and Brown and stated that the K value can increase to high values (according to soil mechanics conceptions) such as 1.5-3.0 at shallow depths and converges to around 0.8-1.0 at increasing depths as a result of studies on different works. He also stated that the reason why K is high at shallow depths is the curvature structure of the earth.

Additionally, Hoek and Diederichs (2006) proposed an equation for intact rock deformation moduli (E_i) by using modulus reduction (MR) and uniaxial compressive strength of rock (σ_{ci}).

$$E_i = MR.\sigma_{ci}$$

The intact moduli would be expected to increase with increasing uniaxial compressive strength, if a constant MR is selected for the rock type.

Since this is a parametric study which investigates behavior of different tunnel geometries under dynamic loading condition, all tunnels will experience the same ground conditions during the analysis. For this reason, Jaky's formula (1944) for the coefficient K mentioned above was adopted. In addition, the intact rock moduli (E_i) is taken as a constant for the selection of strength parameters.

3.1.4.1 Rock Properties Increasing with Depth

As mentioned in the previous sections, to achieve more precise results, many different situations will be evaluated, such as the shape of a tunnel, the depth of the tunnel, the site class where the tunnel is located, and the rock material parameters, which increases and remains constant as the model go deeper. Many assumptions have been made in the previous sections and further assumptions will be made in this section. Accordingly, in the assumed 100-meters deep model, the model will be divided into 5 sublayers, and it is assumed that the material parameter and shear wave velocity increase every 20 meters. The selection of material parameters will be done with the help of RocLab (version 1.032) program. As suggested by Hoek (2002), the parameter selection will be made separately for 2D (14 meters) and 6D (42) depths to take into account the changing strength parameters depending on the depth of tunnel burial. This selection is designed to coincide with the appropriate strength parameters of the tunnel site class as B and C.

3.1.4.1.1 Rock Parameters for 2D (14 meters) Depth for Site Class B

The following table and figures presents the summary table of parameters and RocLab analysis of the rock parameters for the tunnel at 2D depth for site class B, respectively. The parameters in the table provide a database for the Plaxis software in the material constitutive models to be used within the scope of dynamic analysis.

Table 3.2. Rock parameters for 2D (14 meters) depth for site class B

Layer No	Depth (m)		V_s (Adopted)	γ (Adopted)	σ (uniaxial compressive strength)	GSI (Adopted)	c (RocLab)	ϕ (RocLab)	$G_{0,ref}$ ($\rho x V_s^2$)	E (RocLab)	E (Adopted)
	Start	End	(m/s)	(kN/m^3)	(MPa)	-	(kPa)	(°)	(MPa)	(MPa)	(MPa)
1	0	20	600	21	12	28	51	41	771	861	600
2	20	40	800	22	14	30	61	43	1435	977	970
3	40	60	1000	23	16	32	73	44	2345	1113	1110
4	60	80	1200	24	18	34	87	45	3523	1272	1270
5	80	100	1400	25	20	36	103	46	4995	1457	1450

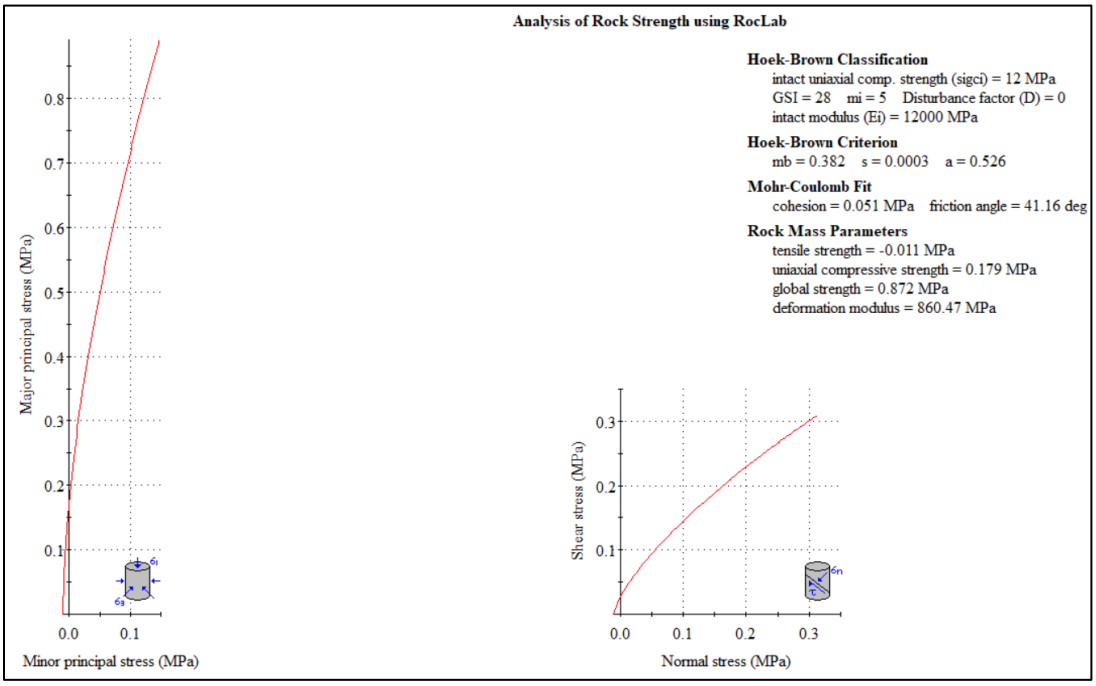

Figure 3.3. 2D (14 meters) tunnel depth/site class B/material between 0-20 meter depth

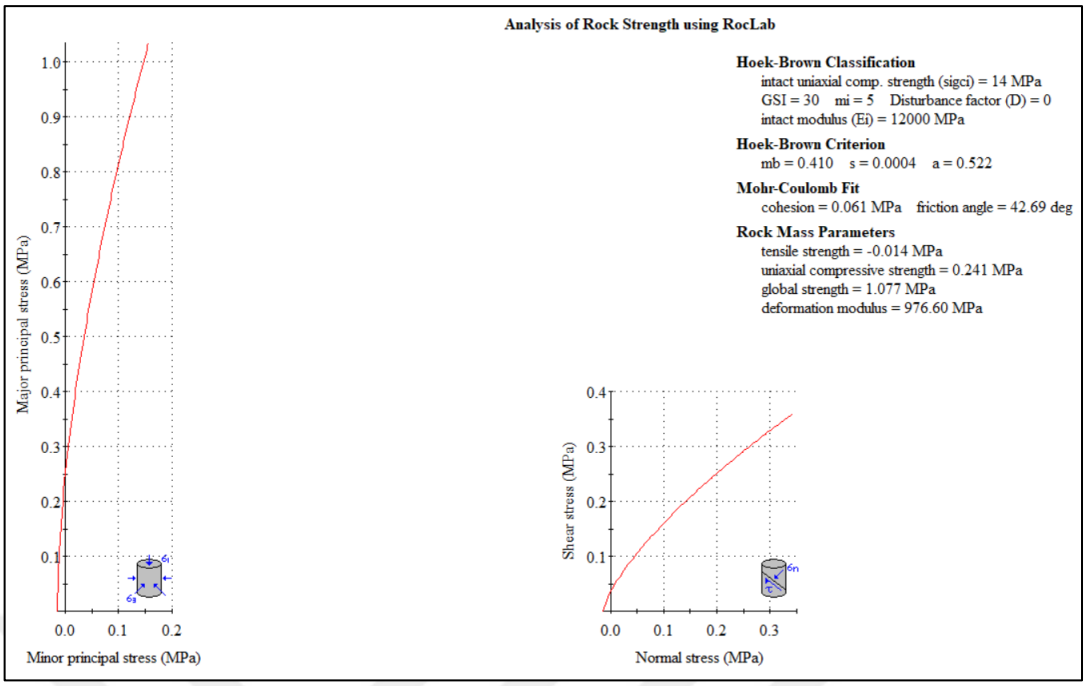

Figure 3.4. 2D (14 meters) tunnel depth/site class B/material between 20-40 meter depth

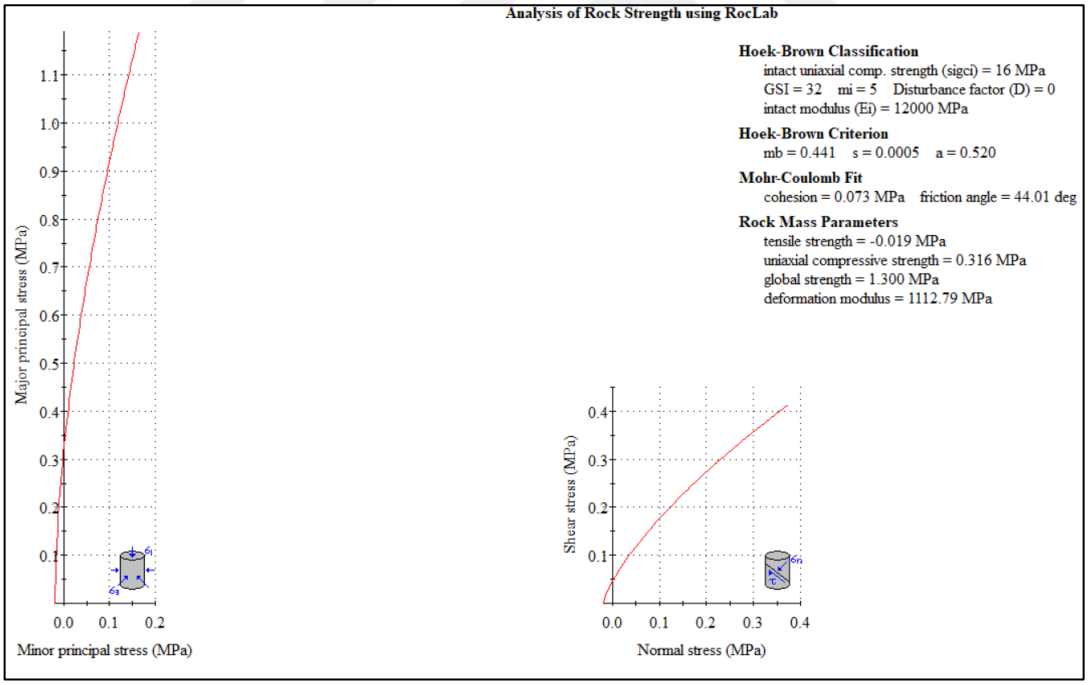

Figure 3.5. 2D (14 meters) tunnel depth/site class B/material between 40-60 meter depth

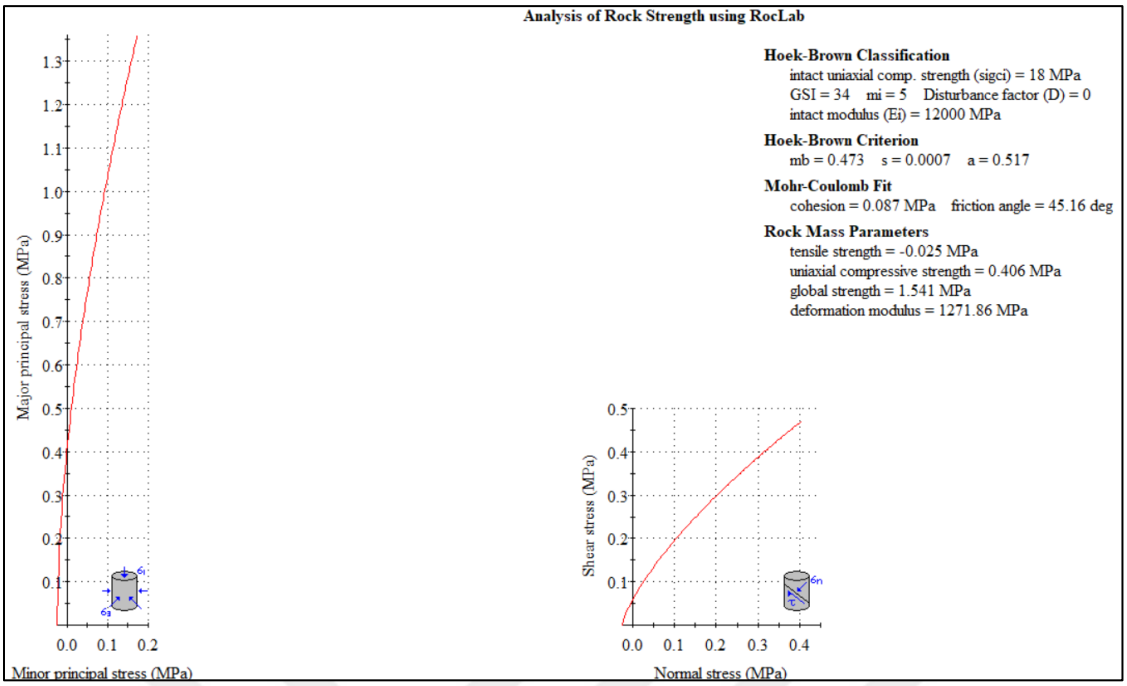

Figure 3.6. 2D (14 meters) tunnel depth/site class B/material between 60-80 meter depth

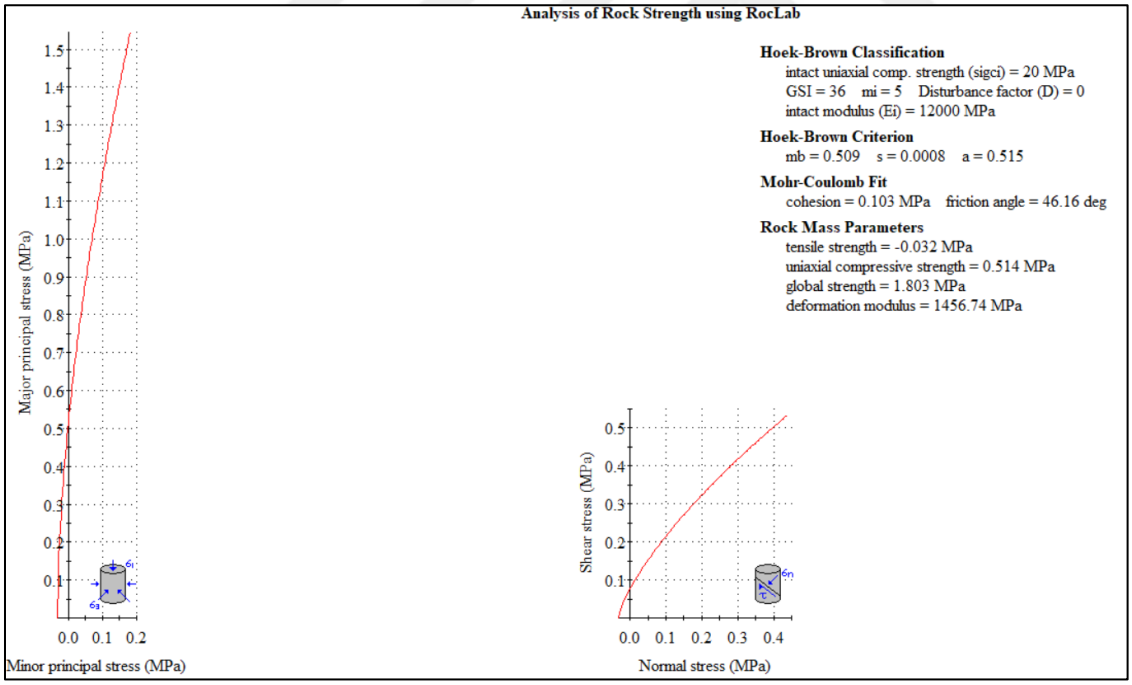

Figure 3.7. 2D (14 meters) tunnel depth/site class B/material between 80-100 meter depth

The site class was selected according to $(V_S)_{30}$, considering the Turkish Seismic Code (2018). Accordingly, when Table 3.2 is observed since the base elevation of this tunnel

is 21 meters, the $(V_S)_{30}$ value is 863 m/s according to the V_S values accepted for rock layers. This corresponds to site class B.

3.1.4.1.2 Rock Parameters for 6D (42 meters) Depth for Site Class B

The following table and figures present the summary table of parameters and RocLab analysis of the rock parameters for the tunnel at 6D depth for site class B, respectively. The parameters in the table provide a database for the Plaxis software in the material constitutive models to be used within the scope of dynamic analysis.

Table 3.3. Rock parameters for 6D (42 meters) depth for site class B

Layer No	Depth (m)		V_s (Adopted)	γ (Adopted)	σ (uniaxial compressive strength)	GSI (Adopted)	c (RocLab)	ϕ (RocLab)	$G_{0,ref}$ ($\rho x V_s^2$)	E (RocLab)	E (Adopted)
	Start	End	(m/s)	(kN/m^3)	(MPa)		(kPa)	(°)	(MPa)	(MPa)	(MPa)
1	0	20	600	21	12	28	90	33	771	861	600
2	20	40	800	22	14	30	105	35	1435	977	970
3	40	60	1000	23	16	32	122	36	2345	1113	1110
4	60	80	1200	24	18	34	140	37	3523	1272	1270
5	80	100	1400	25	20	36	161	38	4995	1457	1450

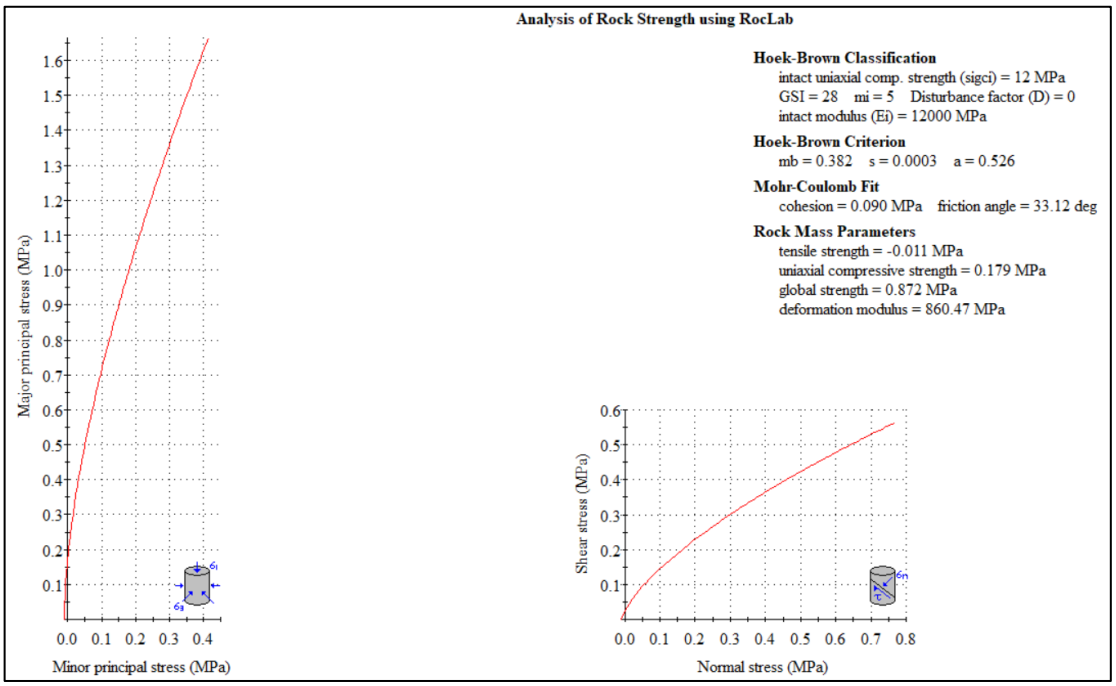

Figure 3.8. 6D (42 meters) tunnel depth/site class B/material between 0-20 meter depth

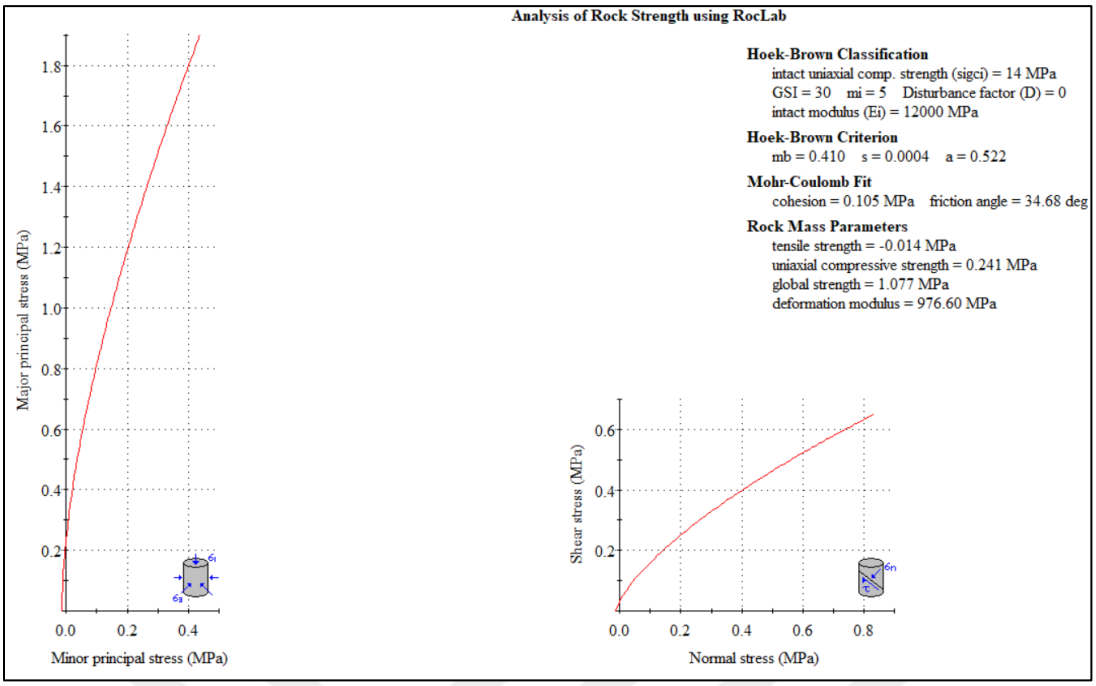

Figure 3.9. 6D (42 meters) tunnel depth/site class B/material between 20-40 meter depth

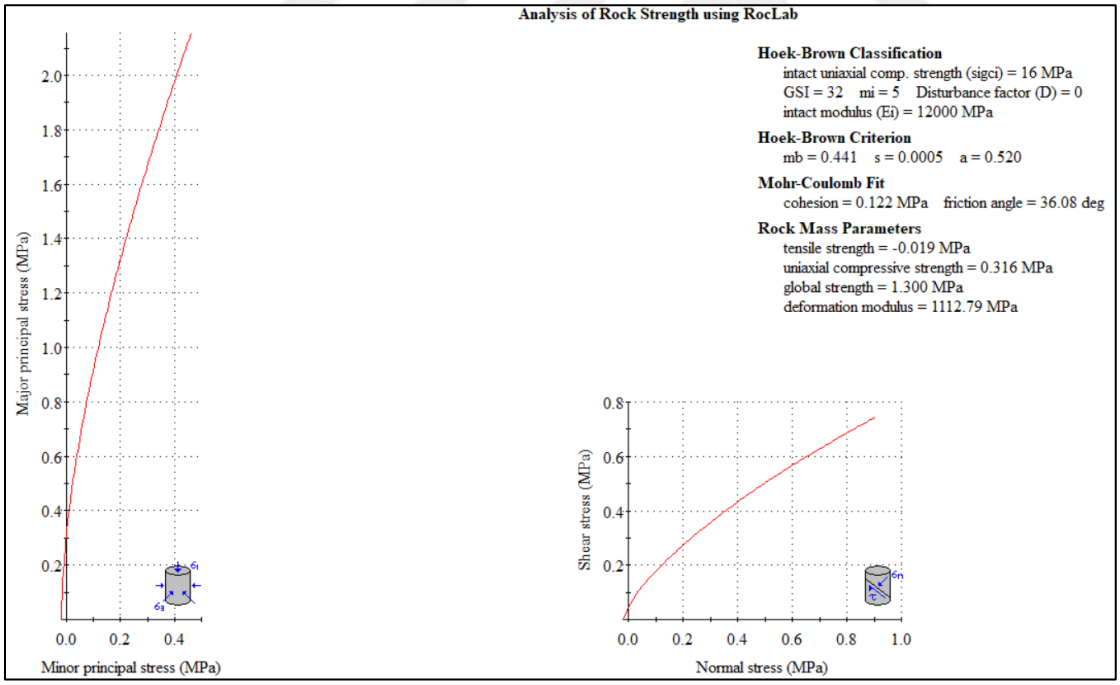

Figure 3.10. 6D (42 meters) tunnel depth/site class B/material between 40-60 meter depth

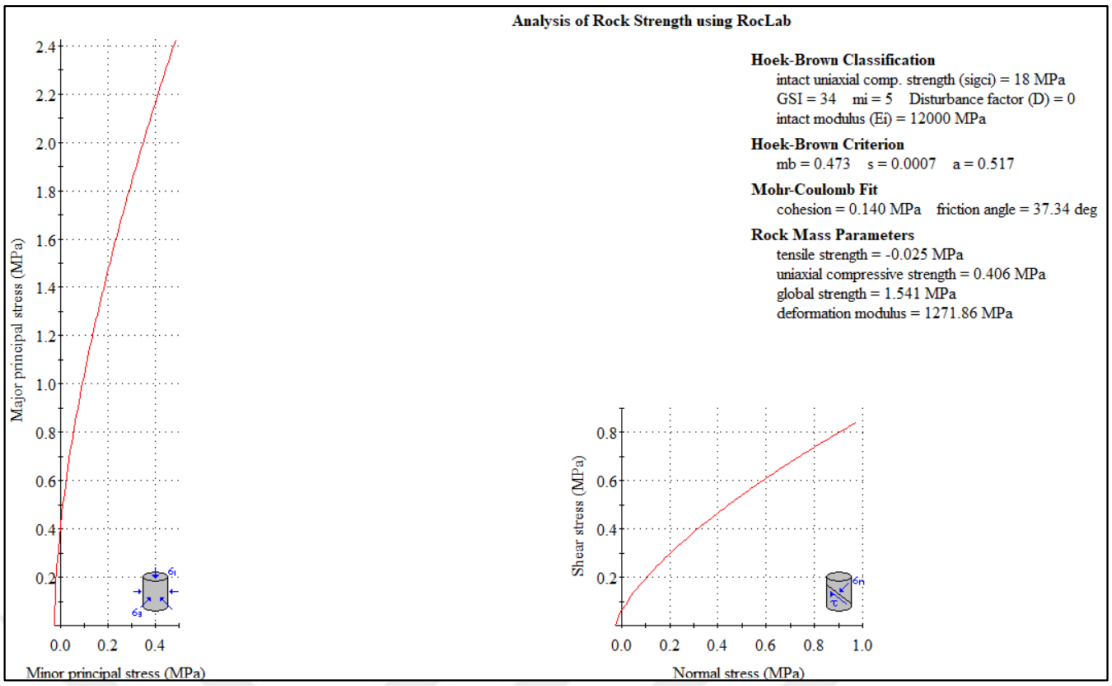

Figure 3.11. 6D (42 meters) tunnel depth/site class B/material between 60-80 meter depth

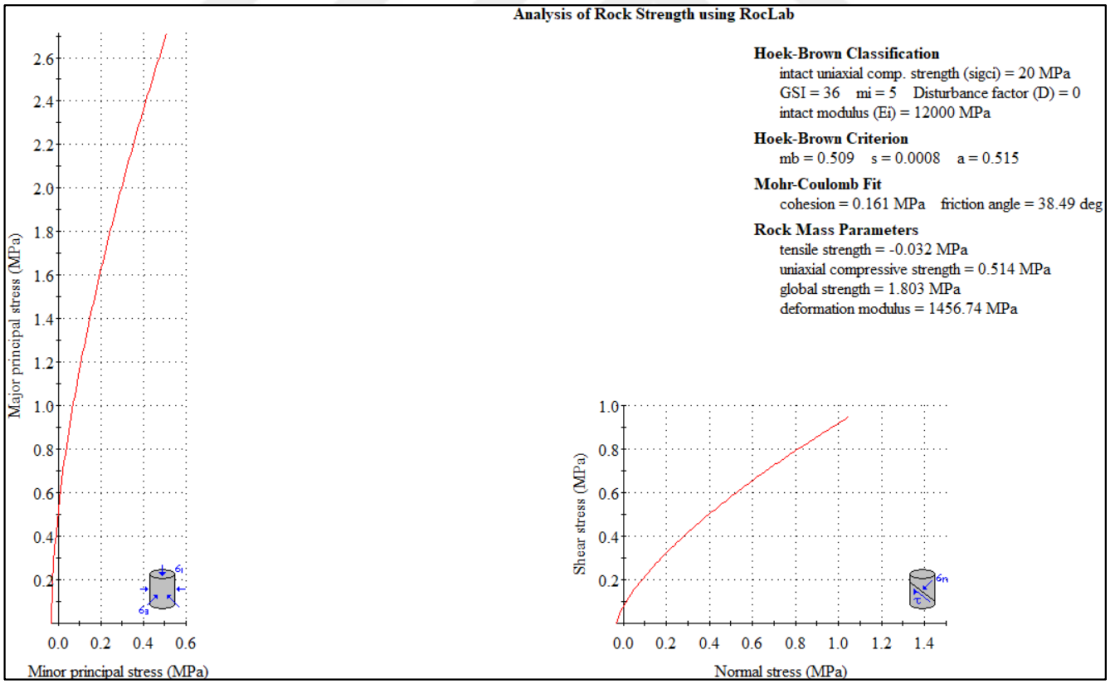

Figure 3.12. 6D (42 meters) tunnel depth/site class B/material between 80-100 meter depth

The site class was selected according to $(V_S)_{30}$, considering the Turkish Seismic Code (2018). Accordingly, when Table 3.3 is observed since the base elevation of this tunnel

is 49 meters, the $(V_S)_{30}$ value is 1118 m/s according to the V_S values accepted for rock layers. This corresponds to site class B.

3.1.4.1.3 Rock Parameters for 2D (14 meters) Depth for Site Class C

The following table and figures present the summary table of parameters and RocLab analysis of the rock parameters for the tunnel at 2D depth for site class C, respectively. The parameters in the table provide a database for the Plaxis software in the material constitutive models to be used within the scope of dynamic analysis.

Table 3.4. Rock parameters for 2D (14 meters) depth for site class C

Layer No	Depth (m)		V_s (Adopted)	γ (Adopted)	σ (uniaxial compressive strength)	GSI (Adopted)	c (RocLab)	ϕ (RocLab)	$G_{0,ref}$ ($\rho x V_s^2$)	E (RocLab)	E (Adopted)
	Start	End	(m/s)	(kN/m^3)	(MPa)	-	(kPa)	(°)	(MPa)	(MPa)	(MPa)
1	0	20	200	19	1	28	19	28	77	143	40
2	20	40	400	20	2	30	27	33	326	163	150
3	40	60	600	21	3	32	34	37	771	186	185
4	60	80	800	22	4	34	41	39	1435	212	210
5	80	100	1000	23	5	36	49	41	2345	243	240

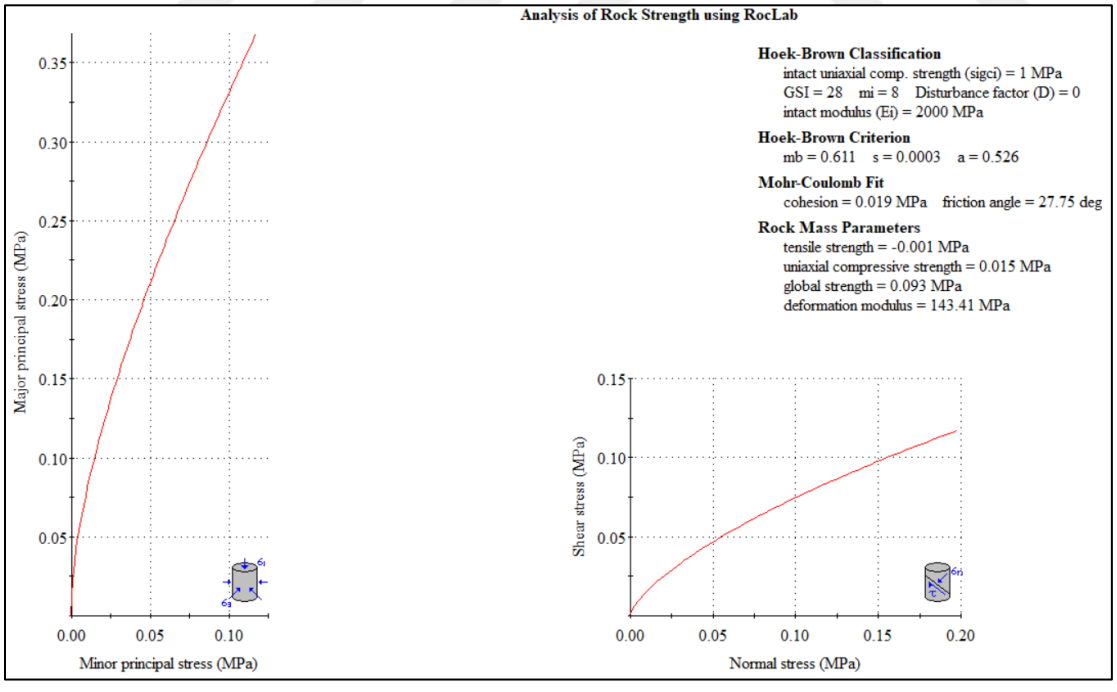

Figure 3.13. 2D (14 meters) tunnel depth/site class C/material between 0-20 meter depth

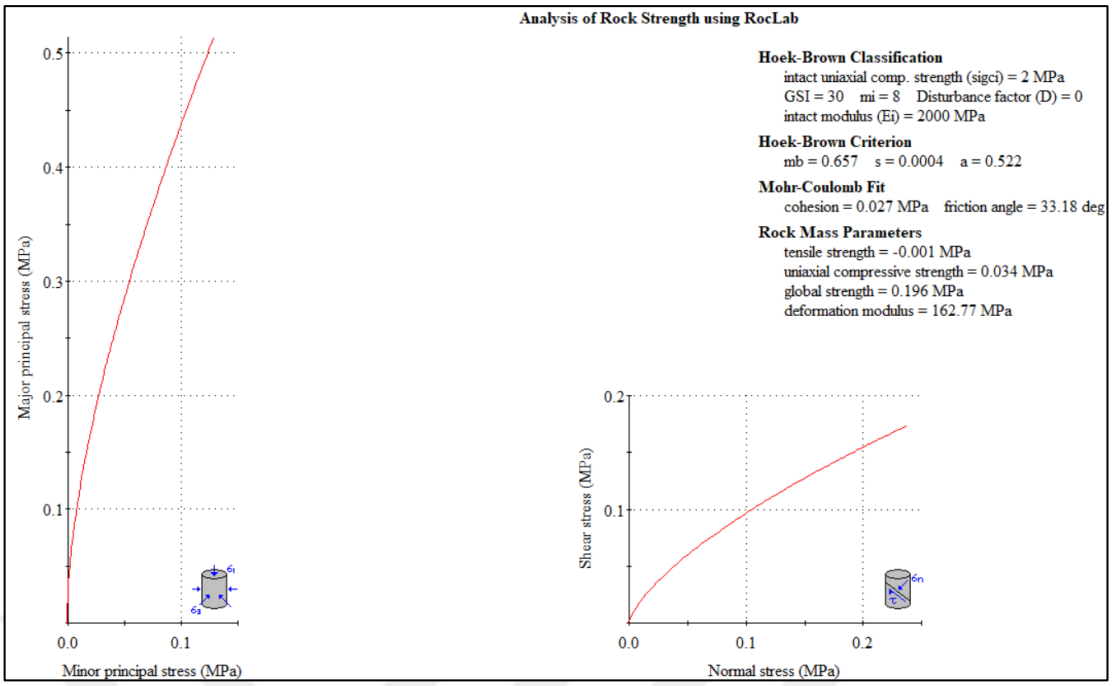

Figure 3.14. 2D (14 meters) tunnel depth/site class C/material between 20-40 meter depth

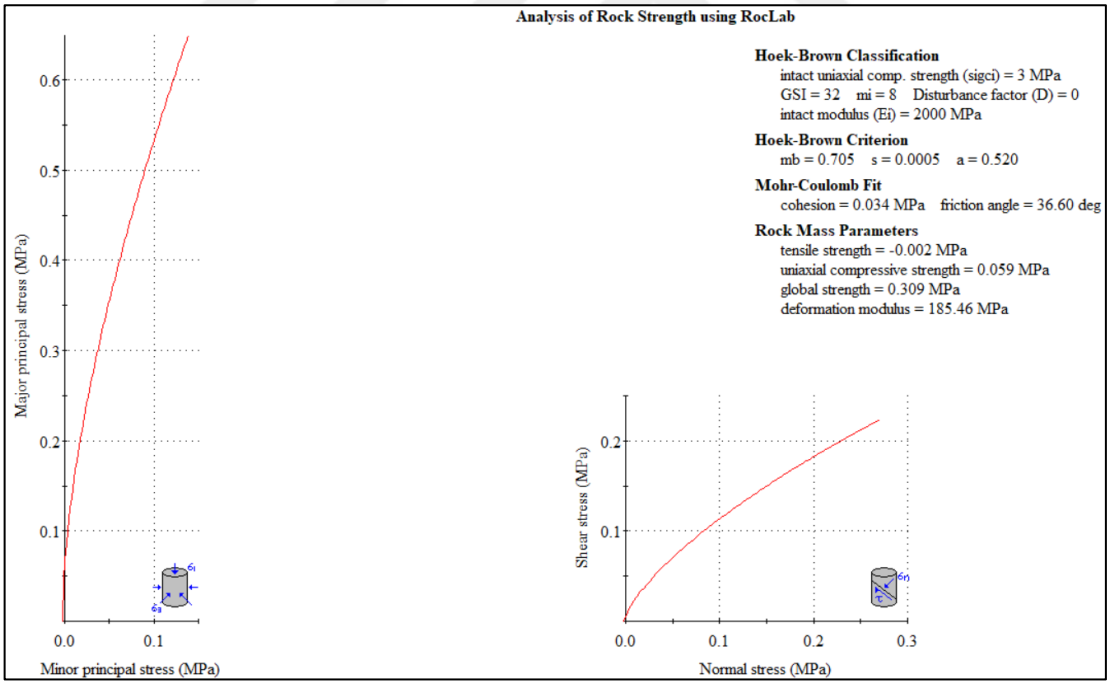

Figure 3.15. 2D (14 meters) tunnel depth/site class C/material between 40-60 meter depth

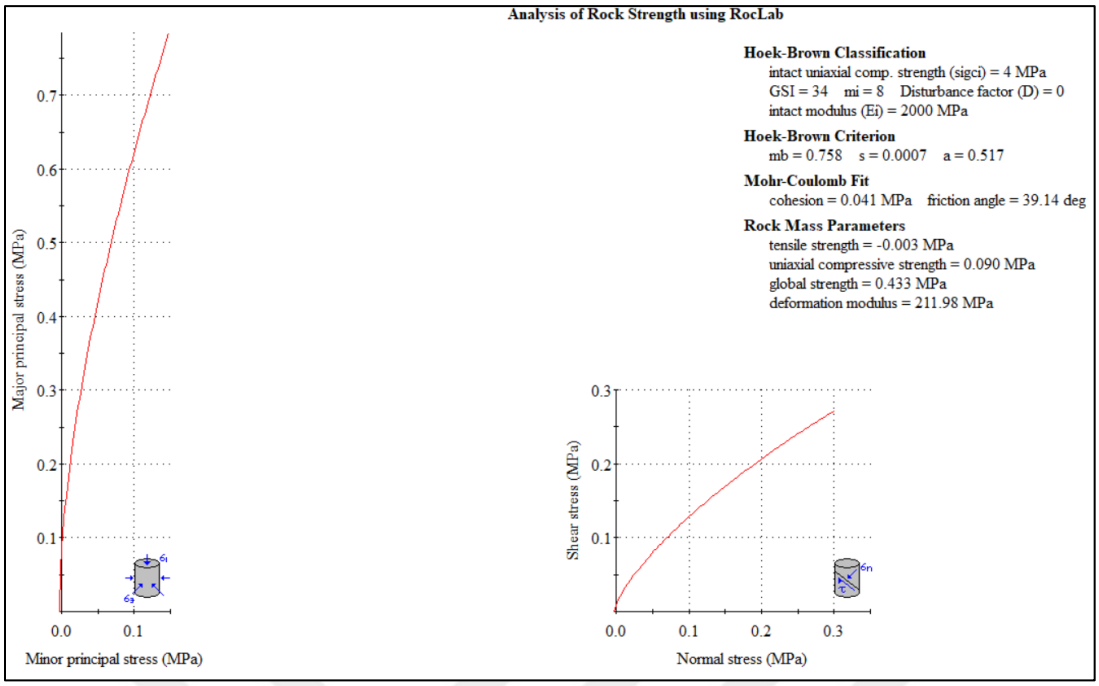

Figure 3.16. 2D (14 meters) tunnel depth/site class C/material between 60-80 meter depth

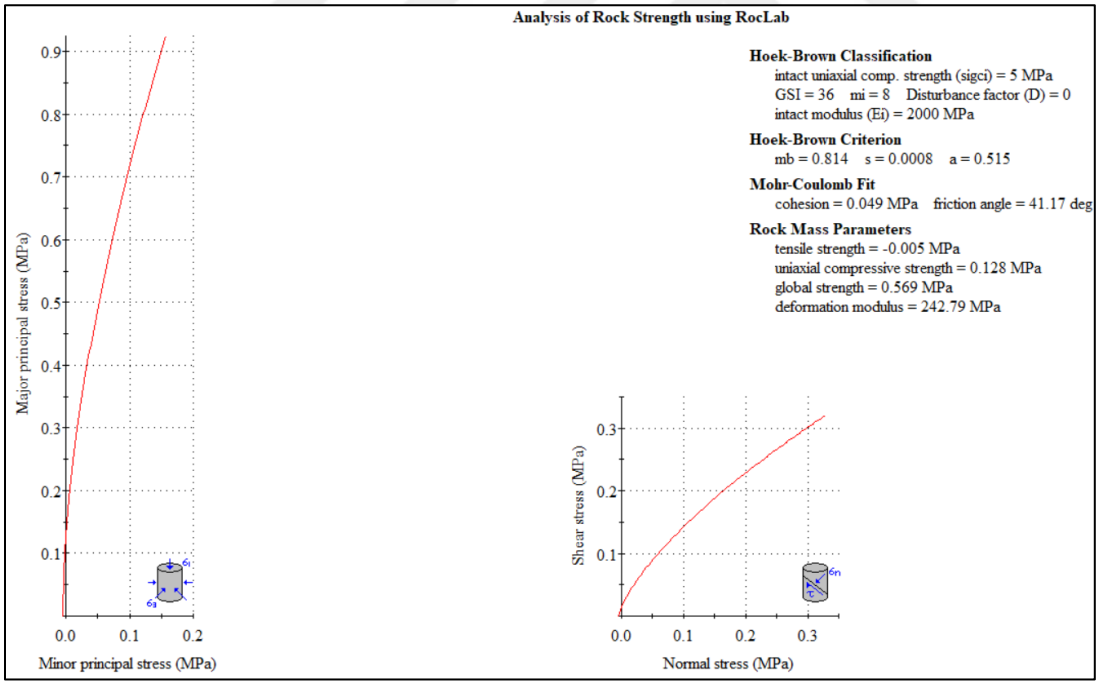

Figure 3.17. 2D (14 meters) tunnel depth/site class C/material between 80-100 meter depth

The site class was selected according to $(V_S)_{30}$ considering the Turkish Seismic Code (2018). Accordingly, when Table 3.4 is observed, since the base elevation of this tunnel

is 21 meters, the $(V_S)_{30}$ value is 456 m/s according to the V_S values accepted for rock layers. This corresponds to site class C.

3.1.4.1.4 Rock Parameters for 6D (42 meters) Depth for Site Class C

The following table and figures presents the summary table of parameters and RocLab analysis of the rock parameters for the tunnel at 6D depth for site class C, respectively. The parameters in the table provide a database for the Plaxis software in the material constitutive models to be used within the scope of dynamic analysis.

Table 3.5. Rock parameters for 6D (42 meters) depth for site class C

Layer No	Depth (m)		V_s (Adopted)	γ (Adopted)	σ (uniaxial compressive strength)	GSI (Adopted)	c (RocLab)	ϕ (RocLab)	$G_{0,ref}$ ($\rho x V_s^2$)	E (RocLab)	E (Adopted)
	Start	End	(m/s)	(kN/m^3)	(MPa)	-	(kPa)	(°)	(MPa)	(MPa)	(MPa)
1	0	20	200	19	1	28	37	20	77	143	40
2	20	40	400	20	2	30	53	25	326	163	150
3	40	60	600	21	3	32	66	28	771	186	185
4	60	80	800	22	4	34	80	31	1435	212	210
5	80	100	1000	23	5	36	93	33	2345	243	240

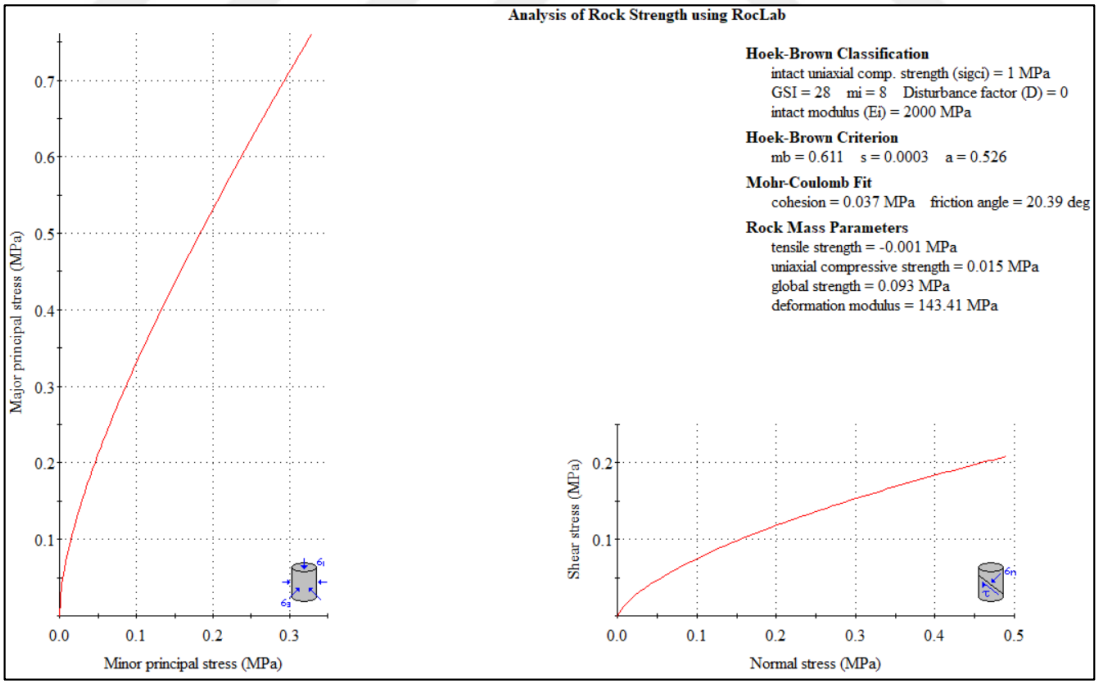

Figure 3.18. 6D (42 meters) tunnel depth/site class C/material between 0-20 meter depth

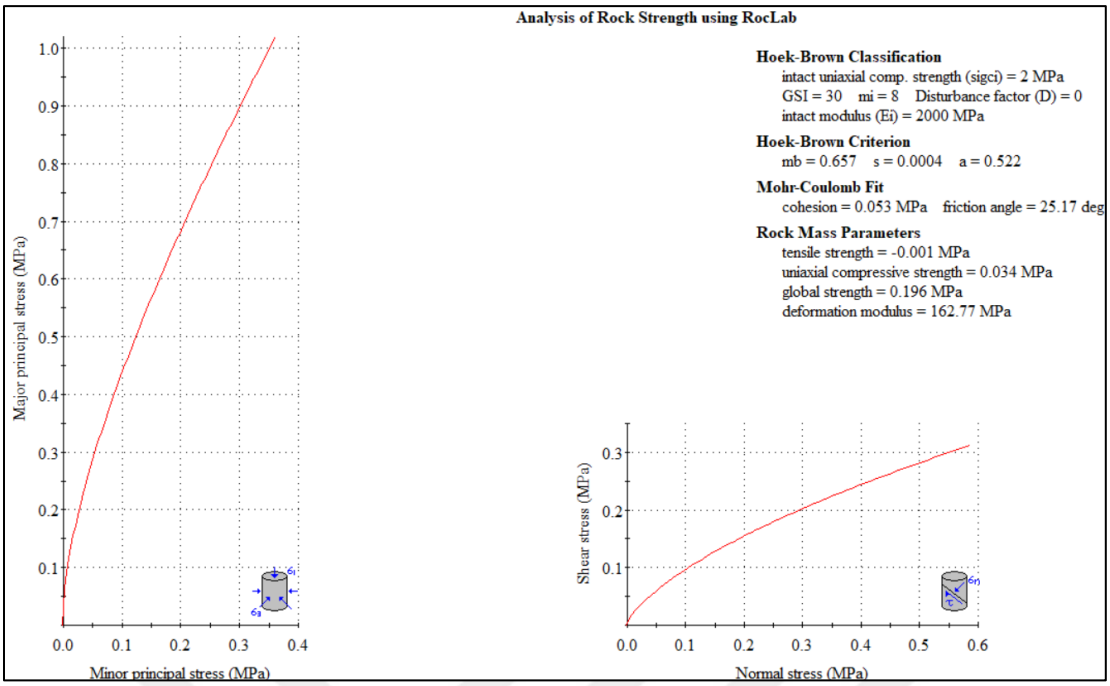

Figure 3.19. 6D (42 meters) tunnel depth/site class C/material between 20-40 meter depth

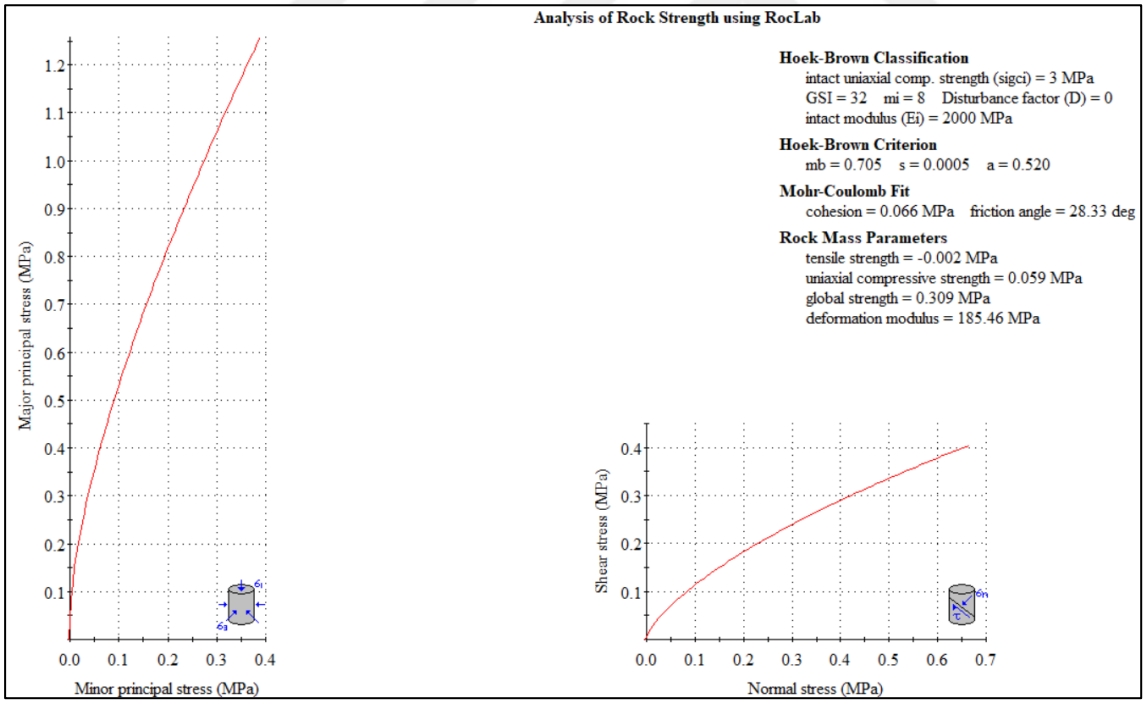

Figure 3.20. 6D (42 meters) tunnel depth/site class C/material between 40-60 meter depth

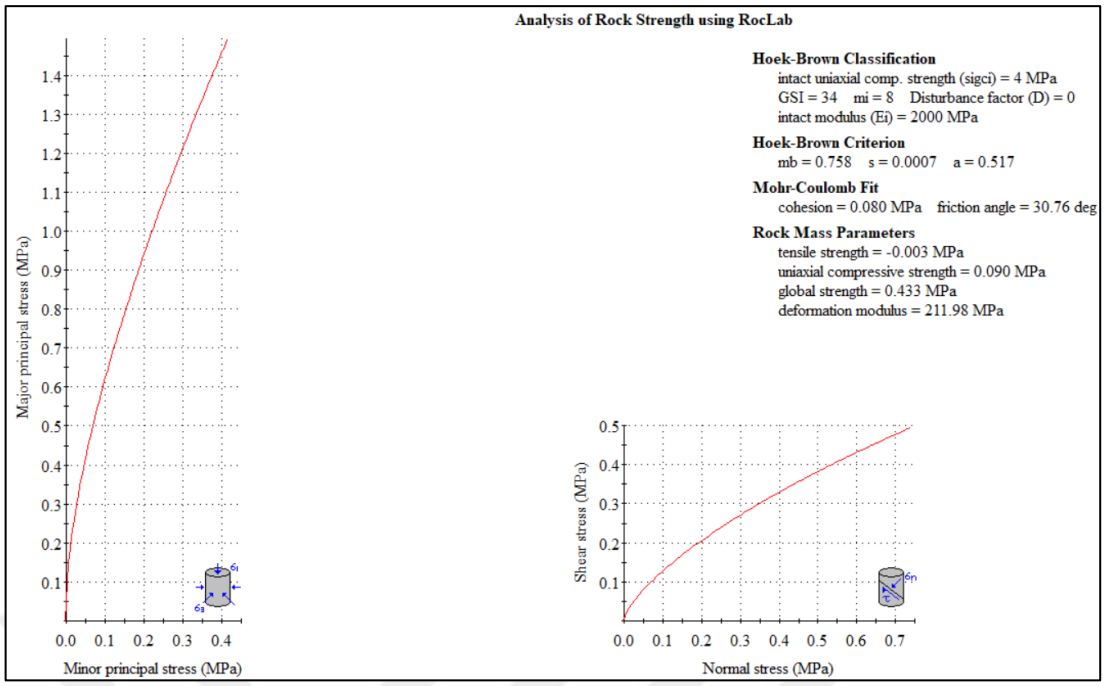

Figure 3.21. 6D (42 meters) tunnel depth/site class C/material between 60-80 meter depth

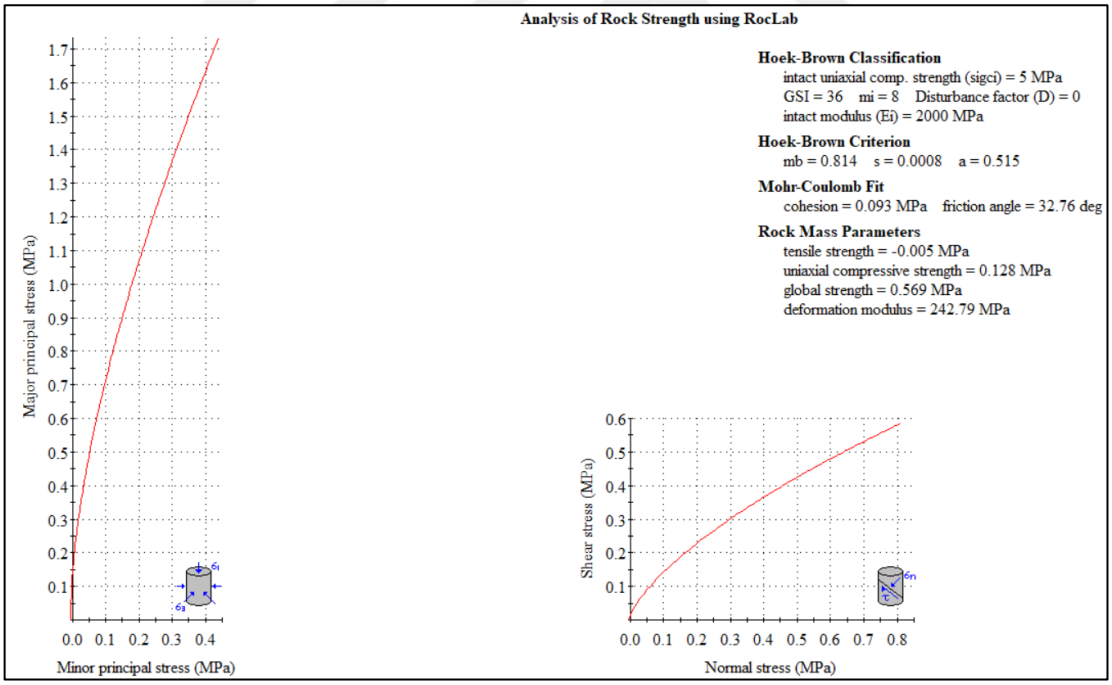

Figure 3.22. 6D (42 meters) tunnel depth/site class C/material between 80-100 meter depth

The site class was selected according to $(V_S)_{30}$, considering the Turkish Seismic Code (2018). Accordingly, when Table 3.5 is observed since the base elevation of this tunnel

is 49 meters, the $(V_S)_{30}$ value is 713 m/s according to the V_S values accepted for rock layers. This corresponds to site class C.

3.1.4.2 Rock Properties Constant with Depth

As mentioned in the previous sections, for the case where rock parameters remain constant with depth, parameters will be selected in consistent with Section 3.1.4.1. Accordingly, the parameters in the profile model determined as the middle of the profile between 40-60 meters will be directly used for the entire profile.

3.1.4.2.1 Rock Parameters for 2D (14 meters) Depth for Site Class B

The following table and figures present the summary table of parameters and RocLab analysis of the rock parameters for the tunnel at 2D depth for site class B, respectively. The parameters in the table provide a database for the Plaxis software in the material constitutive models to be used within the scope of dynamic analysis.

Table 3.6. Rock parameters for 2D (14 meters) depth for site class B

Layer No	Depth (m)		V_s (Adopted)	γ (Adopted)	σ (uniaxial compressive strength)	GSI (Adopted)	c (RocLab)	ϕ (RocLab)	$G_{0,ref}$ ($\rho x V_s^2$)	E (RocLab)	E (Adopted)
	Start	End	(m/s)	(kN/m^3)	(MPa)	-	(kPa)	(°)	(MPa)	(MPa)	(MPa)
1	0	100	1000	23	16	32	73	44	2345	1113	1110

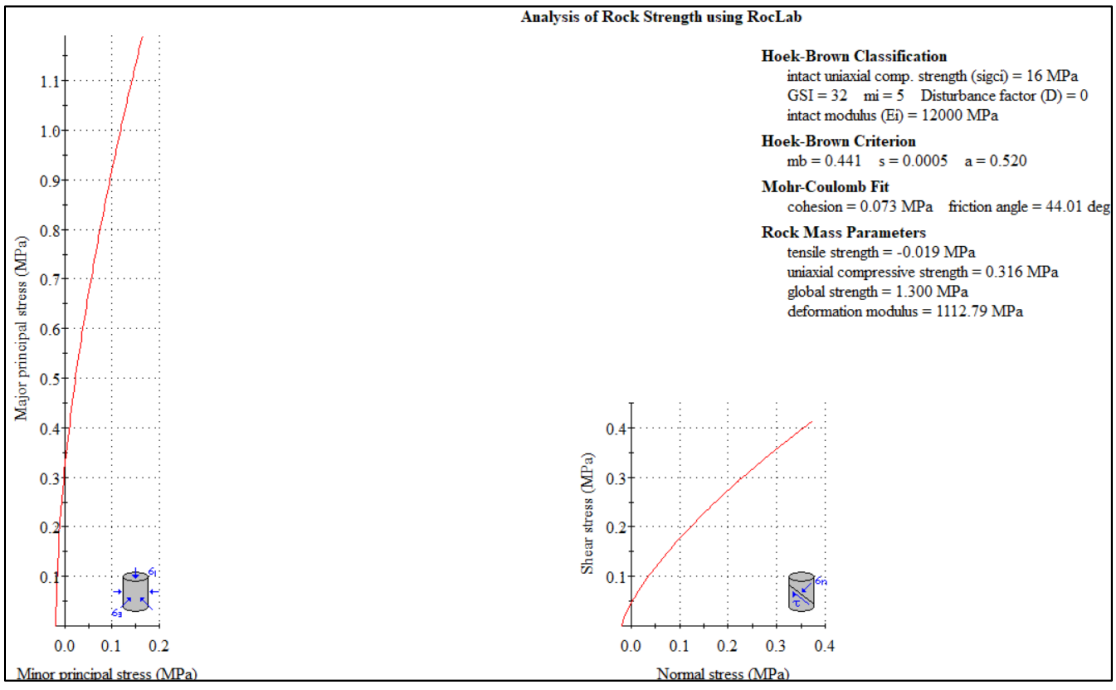

Figure 3.23. 2D (14 meters) tunnel depth/site class B/material between 0-100 meter depth

The site class was selected according to $(V_S)_{30}$, considering the Turkish Seismic Code (2018). Accordingly, when Table 3.6 is observed since the base elevation of this tunnel is 21 meters, the $(V_S)_{30}$ value is 1000 m/s according to the V_S values accepted for rock layers. This corresponds to site class B.

3.1.4.2.2 Rock Parameters for 6D (42 meters) Depth for Site Class B

The following table and figures present the summary table of parameters and RocLab analysis of the rock parameters for the tunnel at 6D depth for site class B, respectively. The parameters in the table provide a database for the Plaxis software in the material constitutive models to be used within the scope of dynamic analysis.

Table 3.7. Rock parameters for 6D (42 meters) depth for site class B

Layer No	Depth (m)		V_s (Adopted)	γ (Adopted)	σ (uniaxial compressive strength)	GSI (Adopted)	c (RocLab)	ϕ (RocLab)	$G_{0,ref}$ ($\rho x V_s^2$)	E (RocLab)	E (Adopted)
	Start	End	(m/s)	(kN/m^3)	(MPa)	-	(kPa)	(°)	(MPa)	(MPa)	(MPa)
1	0	100	1000	23	16	32	122	36	2345	1113	1110

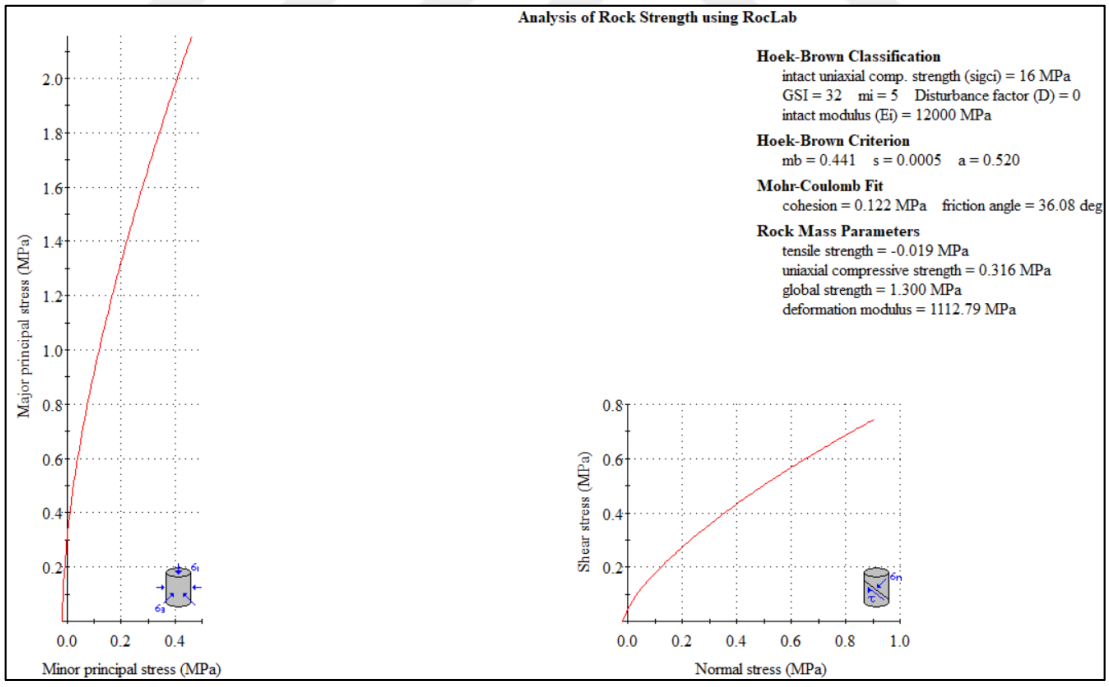

Figure 3.24. 6D (42 meters) tunnel depth/site class B/material between 0-100 meter depth

The site class was selected according to $(V_S)_{30}$ considering the Turkish Seismic Code (2018). Accordingly, when Table 3.7 is observed, since the base elevation of this tunnel

is 49 meters, the $(V_S)_{30}$ value is 1000 m/s according to the V_S values accepted for rock layers. This corresponds to site class B.

3.1.4.2.3 Rock Parameters for 2D (14 meters) Depth for Site Class C

The following table and figures presents the summary table of parameters and RocLab analysis of the rock parameters for the tunnel at 2D depth for site class C, respectively. The parameters in the table provide a database for the Plaxis software in the material constitutive models to be used within the scope of dynamic analysis.

Table 3.8. Rock parameters for 2D (14 meters) depth for site class C

Layer No	Depth (m)		V_s (Adopted)	γ (Adopted)	σ (uniaxial compressive strength)	GSI (Adopted)	c (RocLab)	ϕ (RocLab)	$G_{0,ref}$ ($\rho x V_s^2$)	E (RocLab)	E (Adopted)
	Start	End	(m/s)	(kN/m^3)	(MPa)	-	(kPa)	(°)	(MPa)	(MPa)	(MPa)
1	0	100	600	21	3	32	34	37	771	186	185

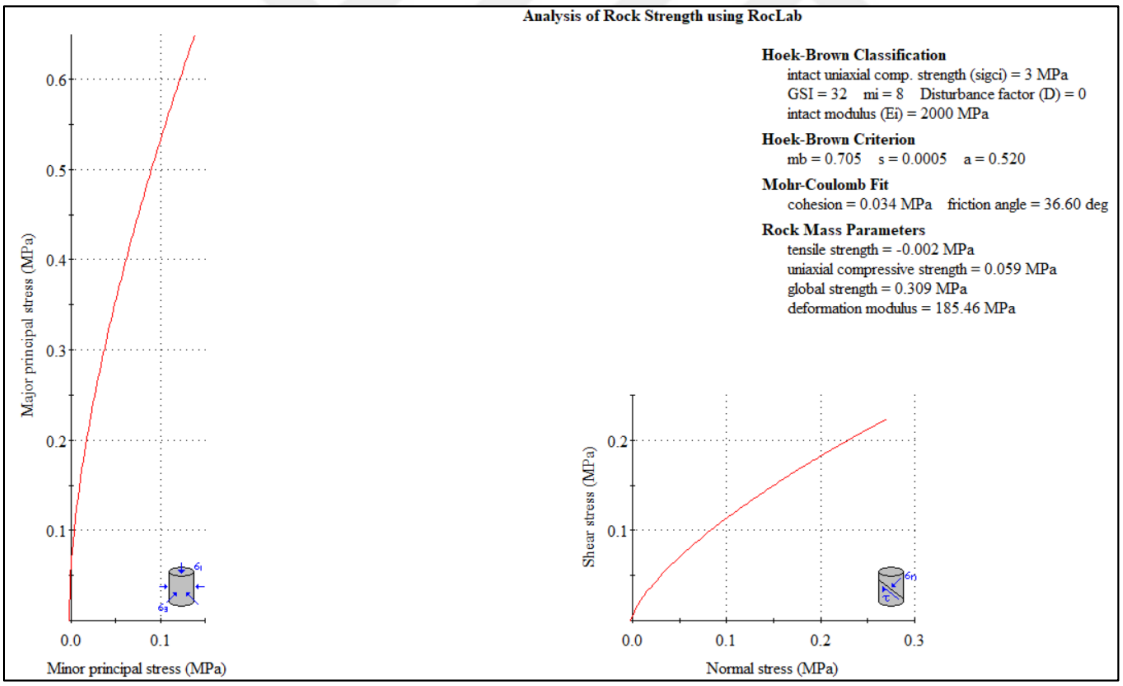

Figure 3.25. 2D (14 meters) tunnel depth/site class C/material between 0-100 meter depth

The site class was selected according to $(V_S)_{30}$, considering the Turkish Seismic Code (2018). Accordingly, when Table 3.8 is observed since the base elevation of this tunnel is 21 meters, the $(V_S)_{30}$ value is 600 m/s according to the V_S values accepted for rock layers. This corresponds to site class C.

3.1.4.2.4 Rock Parameters for 6D (42 meters) Depth for Site Class C

The following table and figures presents the summary table of parameters and RocLab analysis of the rock parameters for the tunnel at 6D depth for site class C, respectively. The parameters in the table provide a database for the Plaxis software in the material constitutive models to be used within the scope of dynamic analysis.

Table 3.9. Rock parameters for 6D (42 meters) depth for site class C

Layer No	Depth (m)		V_s (Adopted)	γ (Adopted)	σ (uniaxial compressive strength)	GSI (Adopted)	c (RocLab)	ϕ (RocLab)	$G_{0,ref}$ ($\rho x V_s^2$)	E (RocLab)	E (Adopted)
	Start	End	(m/s)	(kN/m^3)	(MPa)	-	(kPa)	(°)	(MPa)	(MPa)	(MPa)
1	0	100	600	21	3	32	66	28	771	186	185

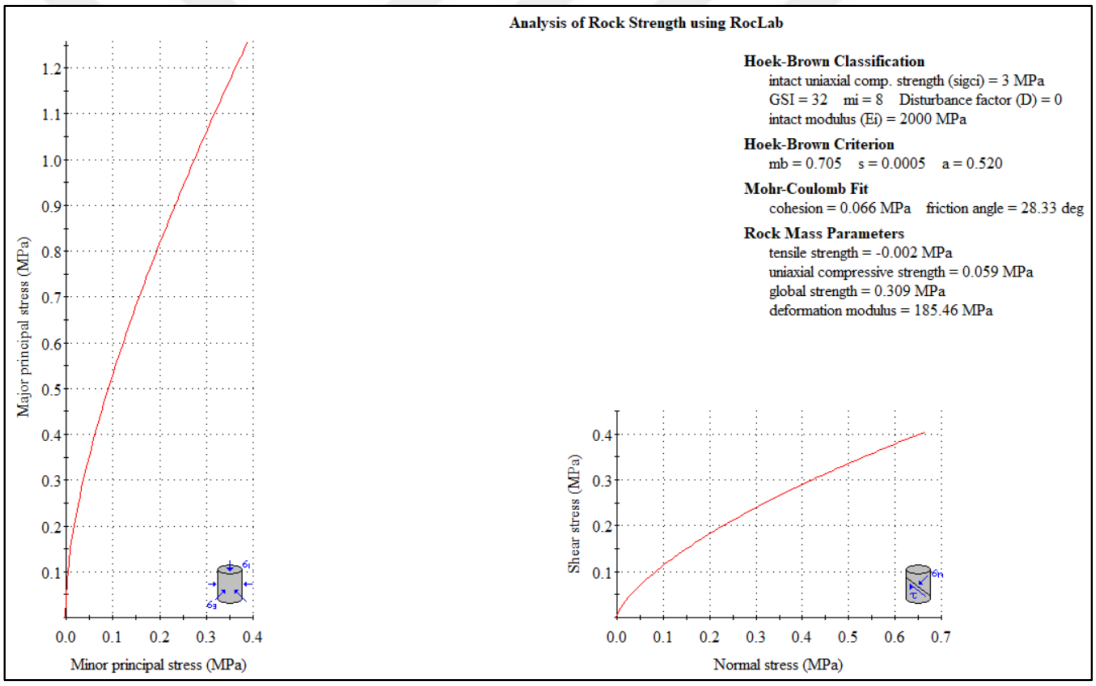

Figure 3.26. 6D (42 meters) tunnel depth/site class C/material between 0-100 meter depth

The site class was selected according to $(V_S)_{30}$ considering the Turkish Seismic Code (2018). Accordingly, when Table 3.9 is observed, since the base elevation of this tunnel is 49 meters, the $(V_S)_{30}$ value is 600 m/s according to the V_S values accepted for rock layers. This corresponds to site class C.

The parameters of the study outlined in detail above are summarized in Table 3.10.

Table 3.10. Analyses to be conducted within the scope of the thesis study

ANALYSES TO BE CONDUCTED WITHIN THE SCOPE OF THE THESIS STUDY					
STRENGTH PARAMETERS INCREASE WITH DEPTH					
SITE CLASS			SITE CLASS		
B			C		
TUNNEL SHAPES			TUNNEL SHAPES		
CIRCULAR	RECTANGULAR	HORSE-SHOE	CIRCULAR	RECTANGULAR	HORSE-SHOE
TUNNEL DEPTHS			TUNNEL DEPTHS		
14 meters (2D)	42 meters (6D)		14 meters (2D)	42 meters (6D)	
STRENGTH PARAMETERS REMAIN CONSTANT WITH DEPTH					
SITE CLASS			SITE CLASS		
B			C		
TUNNEL SHAPES			TUNNEL SHAPES		
CIRCULAR	RECTANGULAR	HORSE-SHOE	CIRCULAR	RECTANGULAR	HORSE-SHOE
TUNNEL DEPTHS			TUNNEL DEPTHS		
14 meters (2D)	42 meters (6D)		14 meters (2D)	42 meters (6D)	

3.1.5 Earthquake Records

Earthquake records to be applied from the bedrock within the scope of the analyses will be explained in this section. In the models, the bedrock has V_S=1400 m/s and V_S=1000 m/s shear wave velocities, respectively. For this reason, the records suitable for the B bedrock class were selected and their properties are presented below for RSN_1111, RSN_285, RSN_1165 records, respectively.

The selected records are scaled to infrequent earthquake ground motion. The probability of exceeding the spectral magnitudes determined for site class B is 2% in 50 years (4% in 100 years) and the corresponding recurrence period is 2475 years.

Characteristic values such as maximum acceleration, maximum velocity and maximum displacement of the scaled RSN_1111, RSN_285 and RSN_1165 records and their graphs are given below, respectively

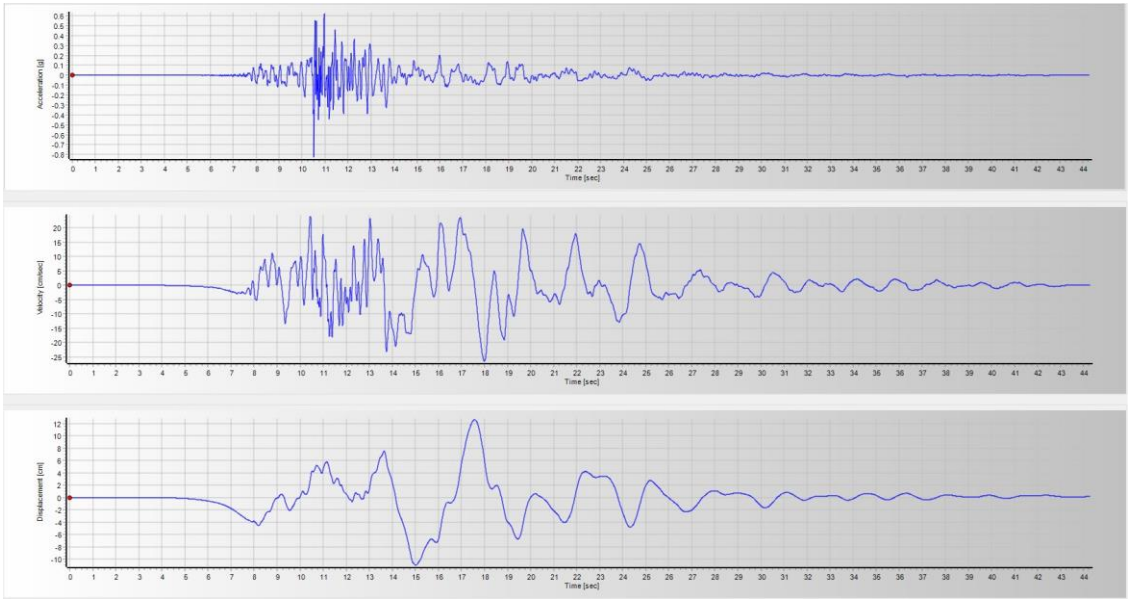

Figure 3.27. Acceleration-velocity-displacement time histories for RSN_1111

Table 3.11. RSN_1111 maximum characteristic values

Parameter	Corrected Accelogram
Maximum Accelaration (g)	0.82471
Time of Maximum Accelaration (sec)	10.52000
Maximum Velocity (cm/sec)	26.40276
Time of Maximum Velocity (sec)	18.00000
Maximum Displacement (cm)	12.64732
Time of Maximum Displacement (sec)	17.58000

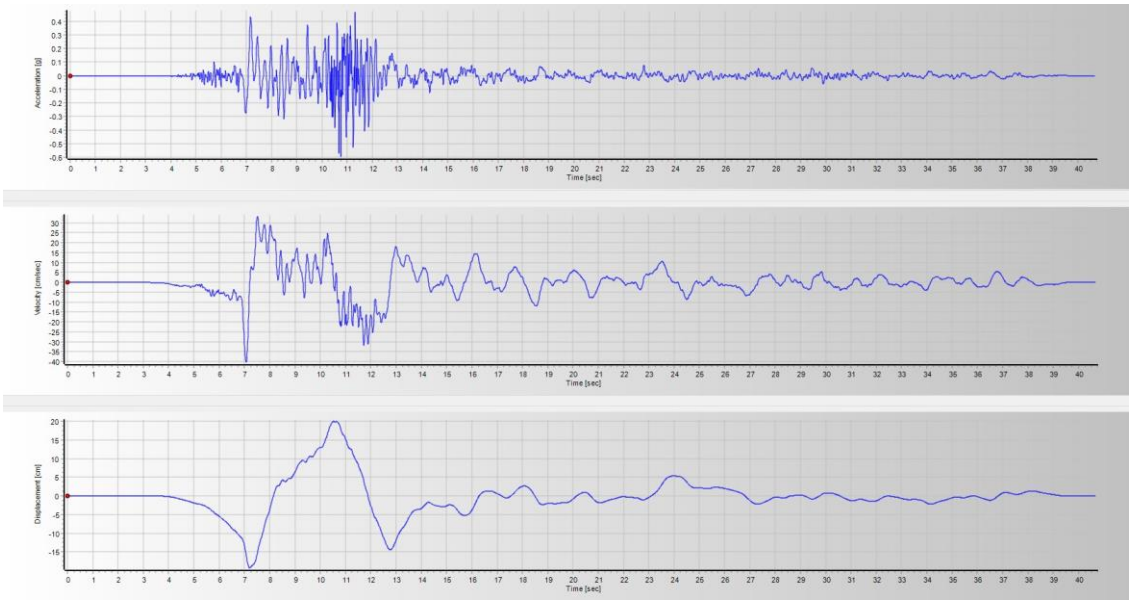

Figure 3.28. Acceleration-velocity-displacement time histories of RSN_285

Table 3.12. RSN_285 maximum characteristic values

Parameter	Corrected Accelogram
Maximum Accelaration (g)	0.59465
Time of Maximum Accelaration (sec)	10.75000
Maximum Velocity (cm/sec)	40.31569
Time of Maximum Velocity (sec)	7.07000
Maximum Displacement (cm)	20.03892
Time of Maximum Displacement (sec)	10.52000

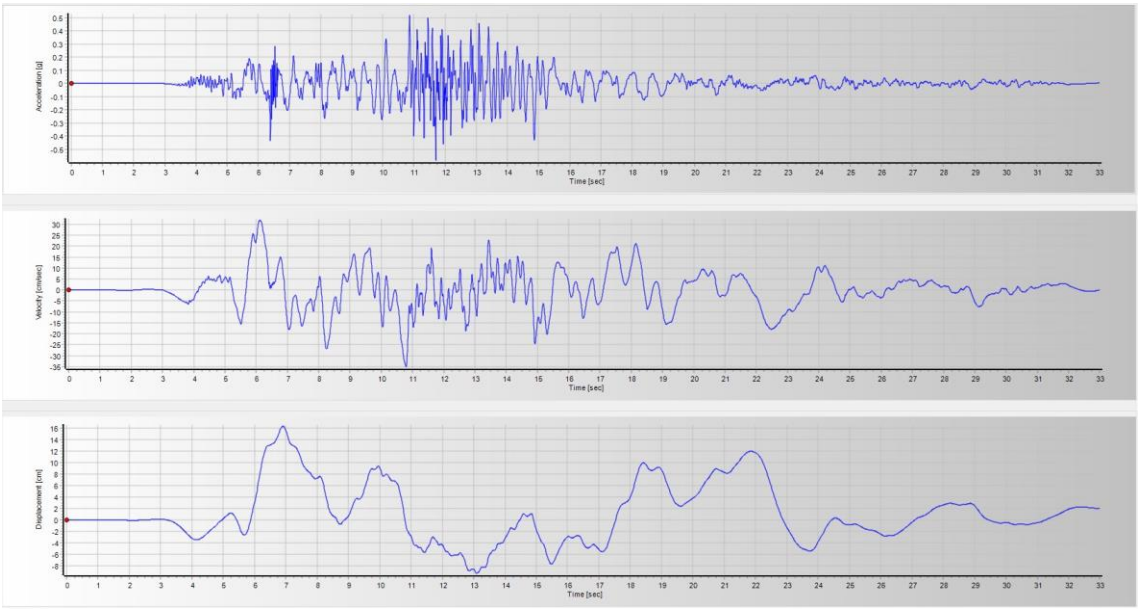

Figure 3.29. Acceleration-velocity-displacement time histories of RSN_1165

Table 3.13. RSN_1165 maximum characteristic values

Parameter	Corrected Accelogram
Maximum Accelaration (g)	0.58392
Time of Maximum Accelaration (sec)	11.70000
Maximum Velocity (cm/sec)	35.08728
Time of Maximum Velocity (sec)	10.80000
Maximum Displacement (cm)	16.35840
Time of Maximum Displacement (sec)	6.91000

3.1.6 Dynamic Analysis Method

The above sections describe the material and geometric properties of the site for the dynamic analysis. This section will indicate the steps and necessary selections for the dynamic analysis to be carried out in Plaxis. In this process, one of the 24 models of the

parametric study will be selected, in which all the steps are the same as in the others, and the model will be described in all its steps.

3.1.6.1 Initial Phase

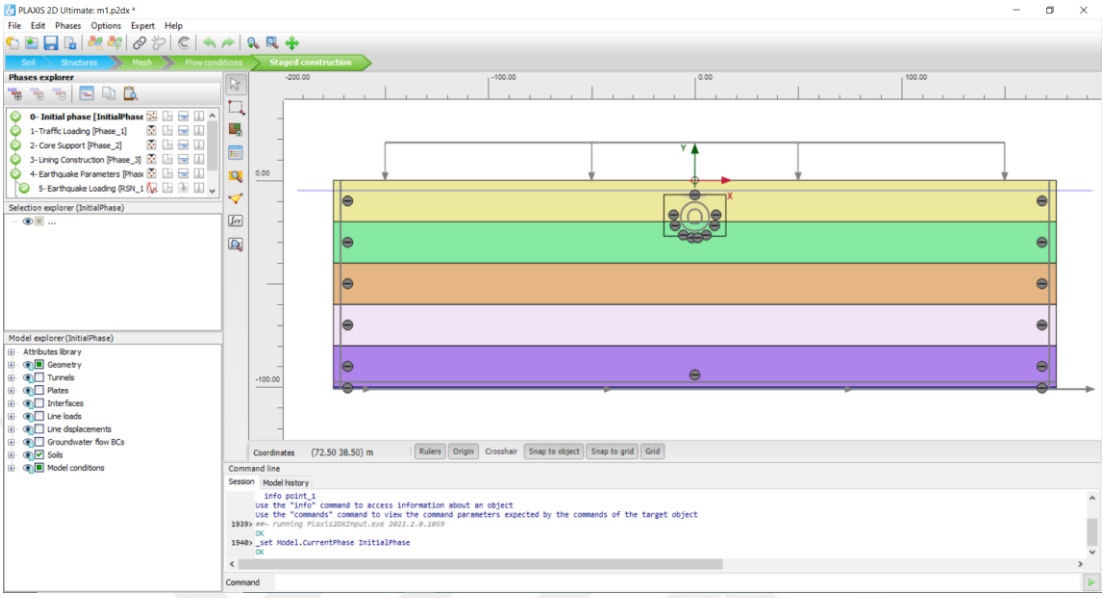

Figure 3.30. Plaxis model initial phase

The initial stage is defined as the initial state of the selected material parameters and geometric properties. Initial stresses are allowed to occur. The Hardening Soil model was selected as the material constitutive model. Gravity loading was selected as the loading condition based on several suggestions offered by Plaxis which gives slightly higher results according to K0 procudure in the background comparison analysis. The groundwater level is assumed to be 5 meters deep in all models. In context of analysis ν_{ur}=0.2, p_{ref}=100 kPa, and m=0.5 values adopted for constitutive model.

3.1.6.2 Phase 1

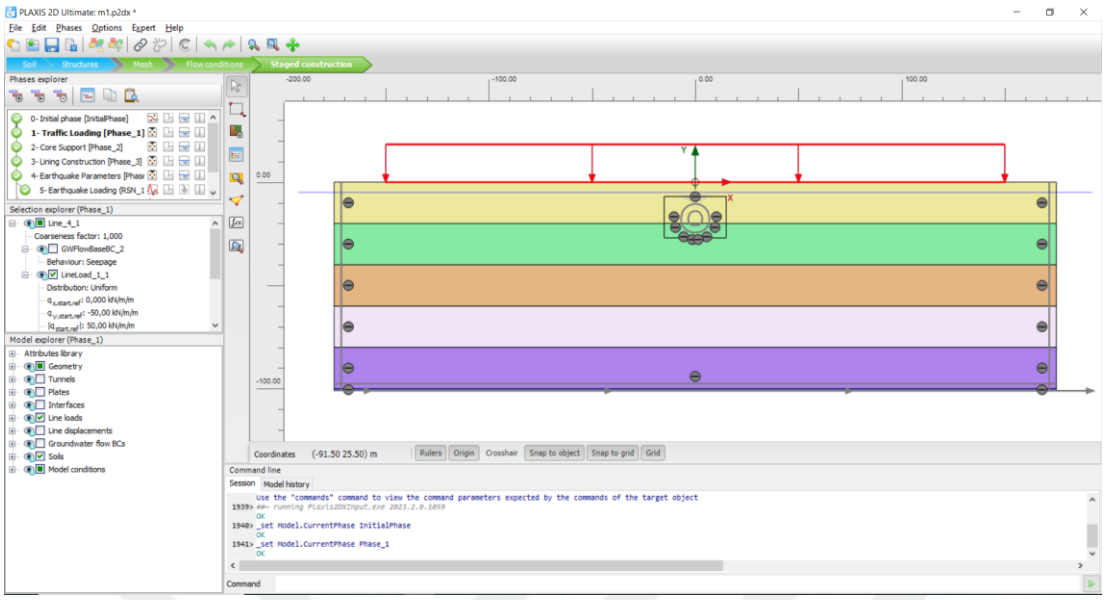

Figure 3.31. Plaxis model phase 1

Phase 1 is the stage where a live load value of 50 kPa is activated to represent the traffic or existing structure loads that may occur in the surrounding area. Displacements are reset to zero for this and backward stages.

3.1.6.3 Phase 2

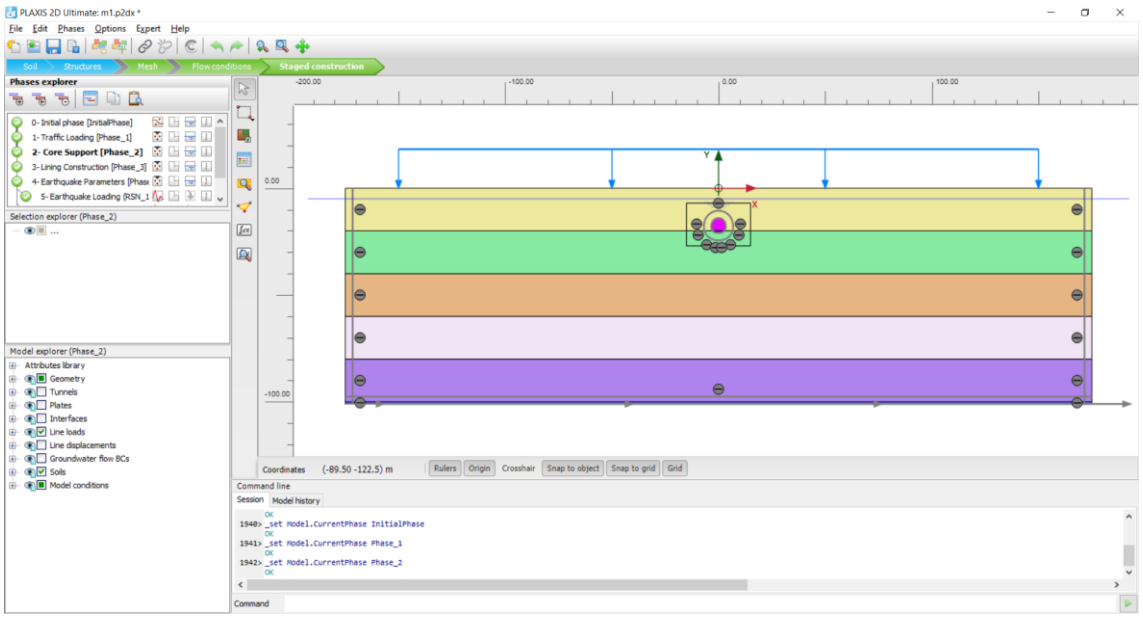

Figure 3.32. Plaxis model phase 2

In phase 2, the "Core Support" method described in section 2.7.1 was adopted to represent the excavation and displacements in the tunnel, and the constitutive model of the material remaining in the tunnel excavation area was converted to "Mohr-Coulomb" and modeled by reducing the modulus of elasticity determined for the material to its 50% percent.

3.1.6.4 Phase 3

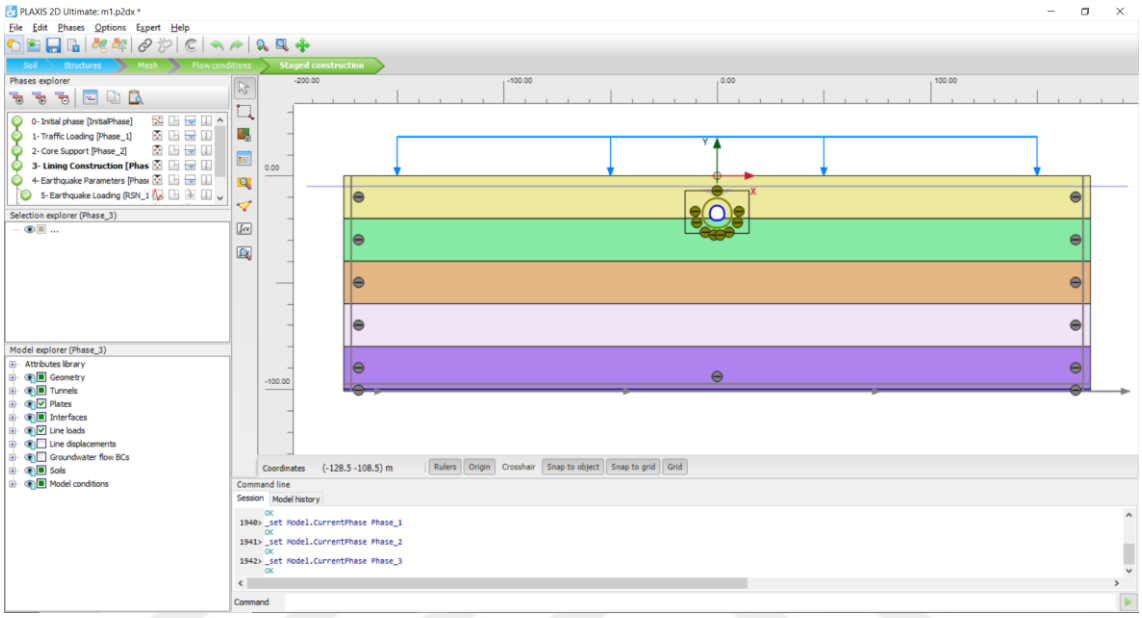

Figure 3.33. Plaxis model phase 3

In phase 3, the material inside the tunnel was removed, and the tunnel lining was activated. In this way, the stage where the lining is loaded for the first time for the static case was created. For all models, the tunnel lining was created with a thickness of 30 cm by assigning stiffness parameters.

3.1.6.5 Phase 4

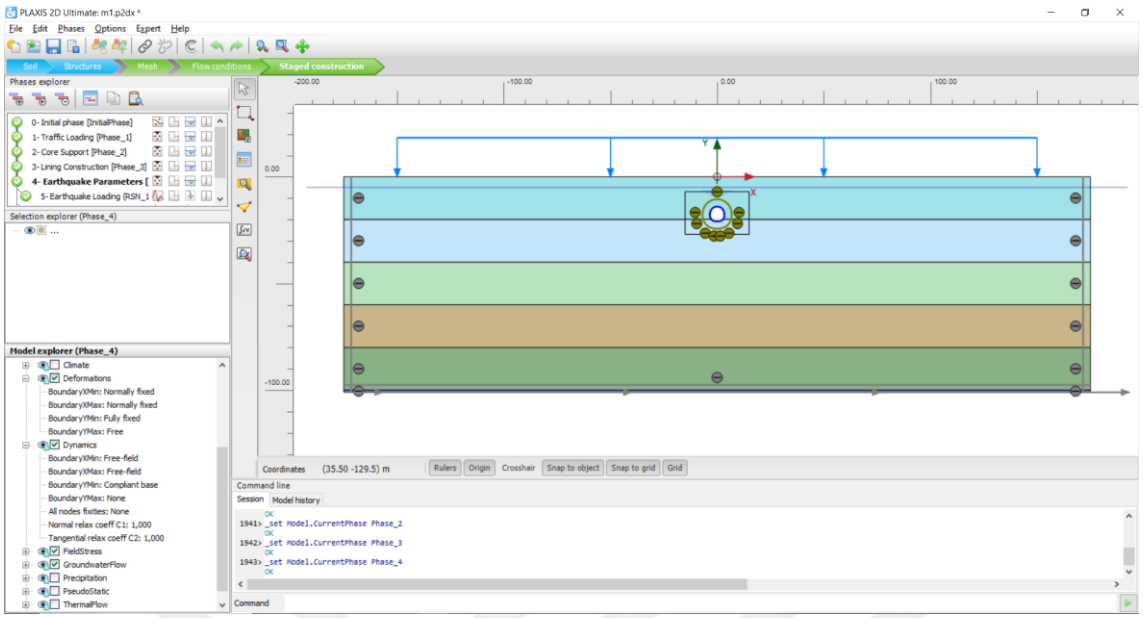

Figure 3.34. Plaxis model phase 4

In phase 4, all constitutive models were converted to the constitutive model HSsmall, which shows the most realistic behavior in case of earthquake. HSsmall model is a modified version of the equation sets proposed by Hardin & Drnevich (1972) for the Hardening Soil model by using smaller threshold shear strain by Santos & Correia (2001). The main difference of this model from the Hardening Soil model is that it enables hysteretic damping by allowing cycles to occur instead of elastic behavior in material for unloading-reloading situations. At this point, it is worth noting that the model conditions, a requirement of 2D dynamic analysis, should be as indicated in the bottom left of the figure above, allowing earthquake waves to behave more realistically at the boundaries. In context of analysis ν_{ur}=0.2, p_{ref}=100 kPa, m=0.5, and $\gamma_{0.7}$=1.00E-3 values adopted for constitutive model.

3.1.6.6 Phases 5, 6, 7

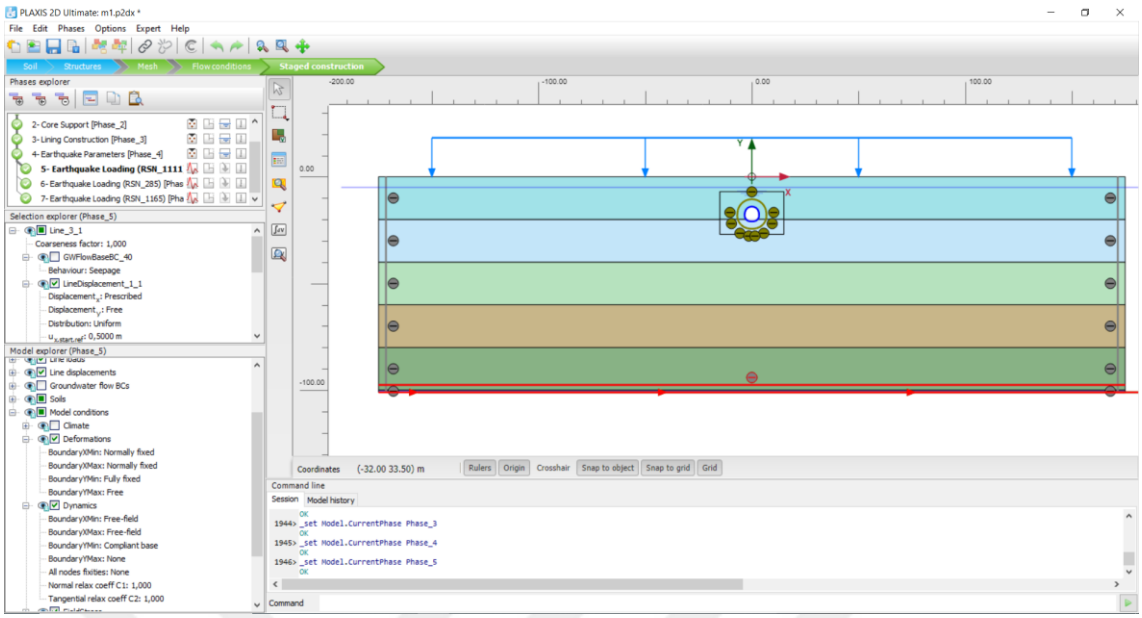

Figure 3.35. Plaxis model phases 5, 6, 7

In Stages 5, 6 and 7, RSN_1111, RSN_285, RSN_1165 records previously mentioned in section 3.1.5 were activated, respectively. Earthquake records were activated as line displacement at the bottom of the models where linear elastic bedrock is defined at the base, which has a thickness of 1 meter.

3.1.7 Sensitivity Analysis

The main objective of sensitivity analyses is to determine whether the model width is sufficient. Accordingly, model widths of 200, 250, 300, 350 and 400 meters were tested, respectively, and positive and negative acceleration values were determined as +4.177; -4.108, 4.488;-3.780, 4.391;-3.788, 4.417;-3.622 and 4.438;-3.785 for a_x (m/sec^2), respectively, from a node to the surface of the model and this point is the same on all of the testing models. a_x refers to accelerations in the x direction with respect to the coordinate axis. The screenshot of the model and outputs of the 200-meter-wide model are presented below as an example.

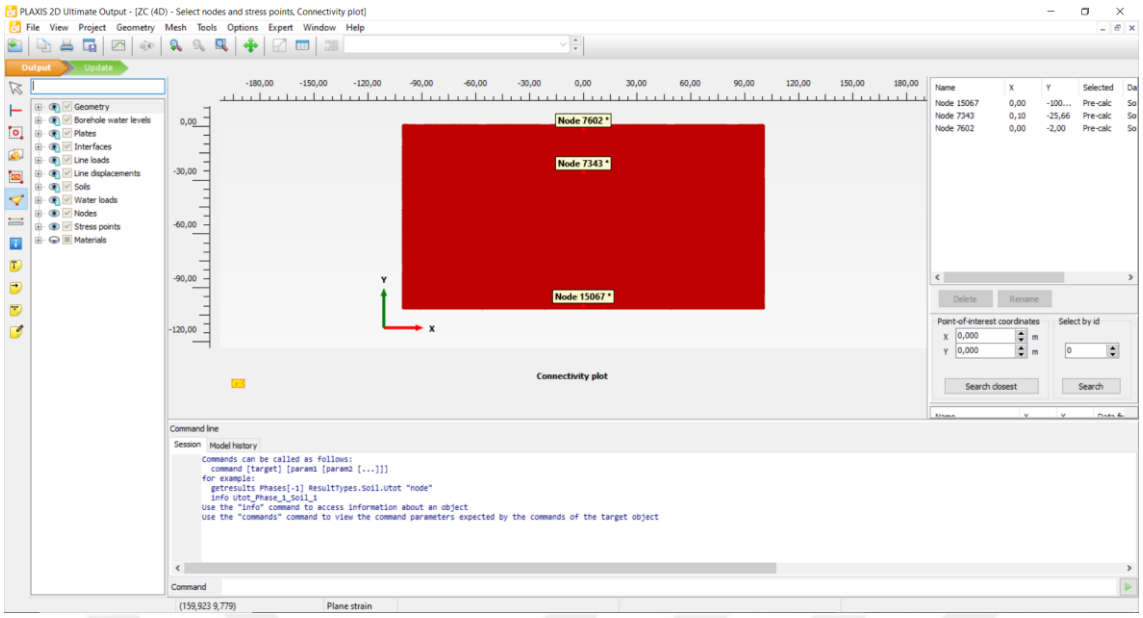

Figure 3.36. Plaxis model sensitivity analysis for 200-meter width

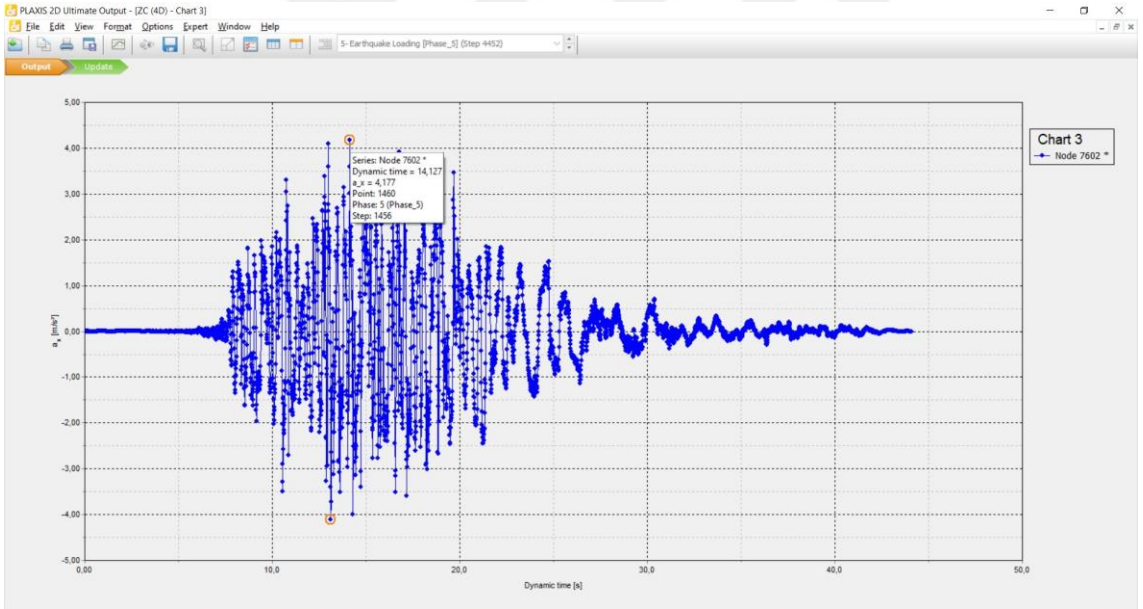

Figure 3.37. Plaxis model sensitivity analysis result for 200-meter width

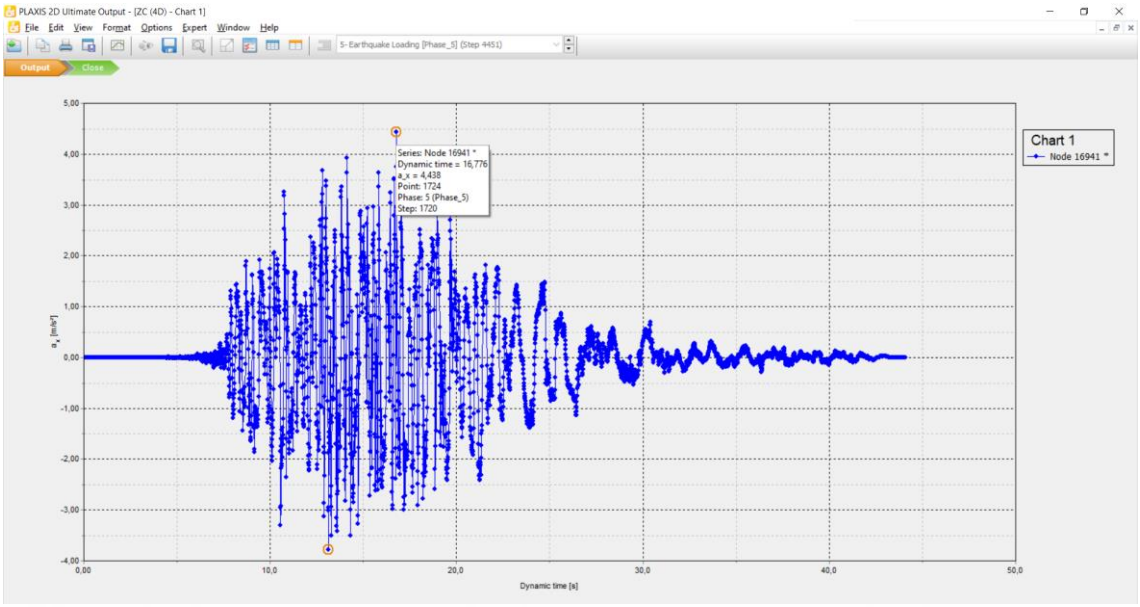

Figure 3.38. Plaxis model sensitivity analysis result for 400-meter width

After evaluating the results, it was decided that the model width of 350 meters would be adequate.

3.1.7.1 Sufficient Element Sizes for Dynamic Finite Element Analysis

Kuhlemeyer and Lysmer (1973) criterion is considered to decide the element size. According to this criterion, for a simple finite element with two nodes, the following inequality must be satisfied for the length of the element (L), the wave speed (C), and the frequency of the harmonic wave (f):

$$L < C/(10 \times f)$$

Since the earthquake accelerations are considered as uniform horizontal motion in the model base, it is concluded that the S-wave is prominent; therefore, the wave velocity (C) should be equal to the S-wave velocity (V_S). For f, the upper limit of the frequency band containing significant amplitudes in the spectrum should be considered. Figures 3.36, 3.37, and 3.38 show the power spectra of the ground motion acceleration records used in the analysis. As the figure shows, the most prominent frequencies are around 12 Hz.

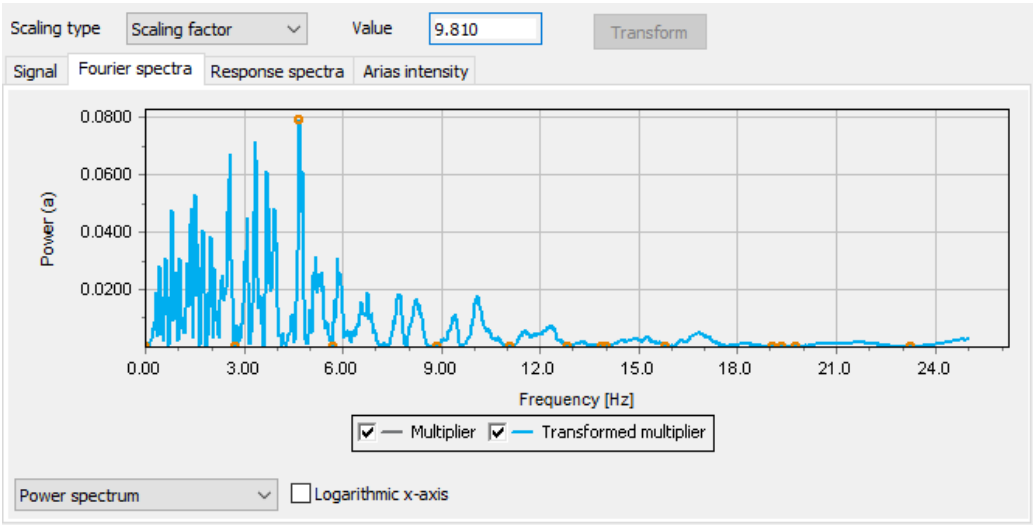

Figure 3.39. RSN_1111 earthquake record power spectrum

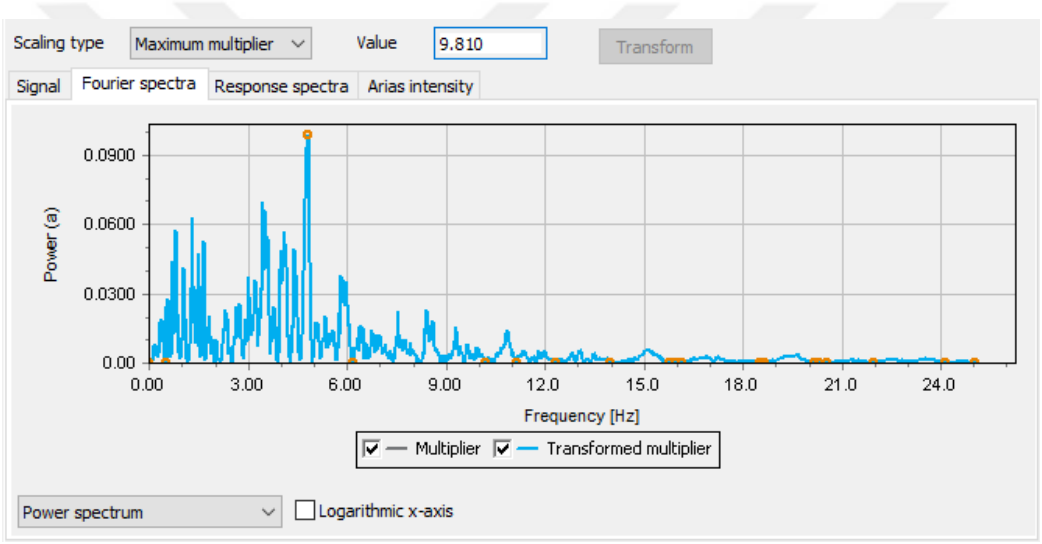

Figure 3.40. RSN_285 earthquake record power spectrum

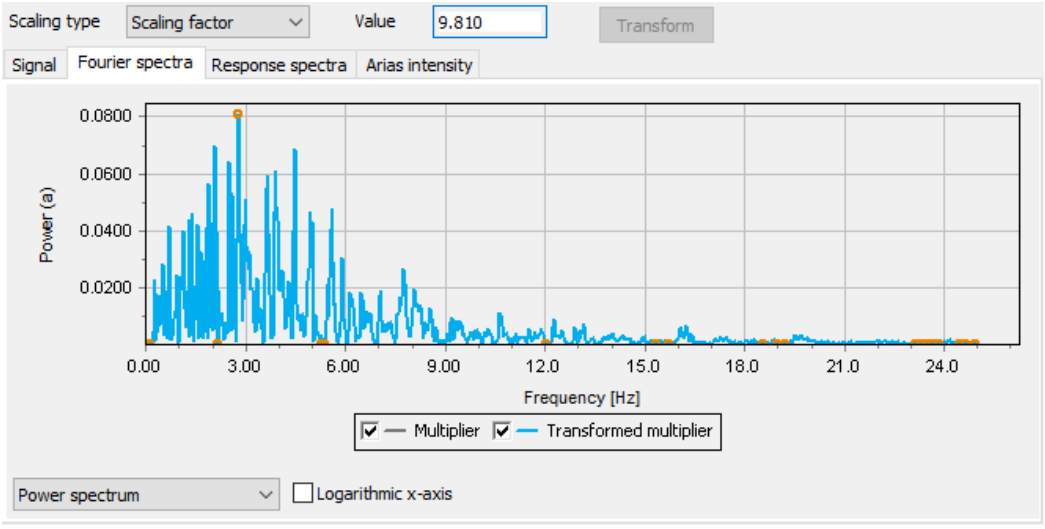

Figure 3.41. RSN_1165 earthquake record power spectrum

In the Plaxis program, triangular elements with 6 nodes were used. Each element has 3 elements on each edge and therefore 2 intervals between the nodes. Therefore, the boundary value for L given by Kuhlemer and Lysmer (1973) is increased by a factor of 2. As a result,

$$L < V_s/(60\ \text{Hz})$$

the relationship is obtained. Table 3.14 calculates the boundary element length with the specified V_S value for each layer. Table 3.14 also gives the largest element edge length available in each layer for each geologic unit in the finite element mesh shown in Figure 3.42. The mesh network was created so that the element length in all the models was ~2.5 meters at minimum and ~6 meters at maximum. The mesh sizes in the area where the tunnel is located have been reduced to obtain more precise results for the lining.

Table 3.14. V_S-L relationship

V_S (m/s)	L
200	3.3
400	6.7
600	10.0
800	13.3
1000	16.7
1200	20.0
1400	23.3

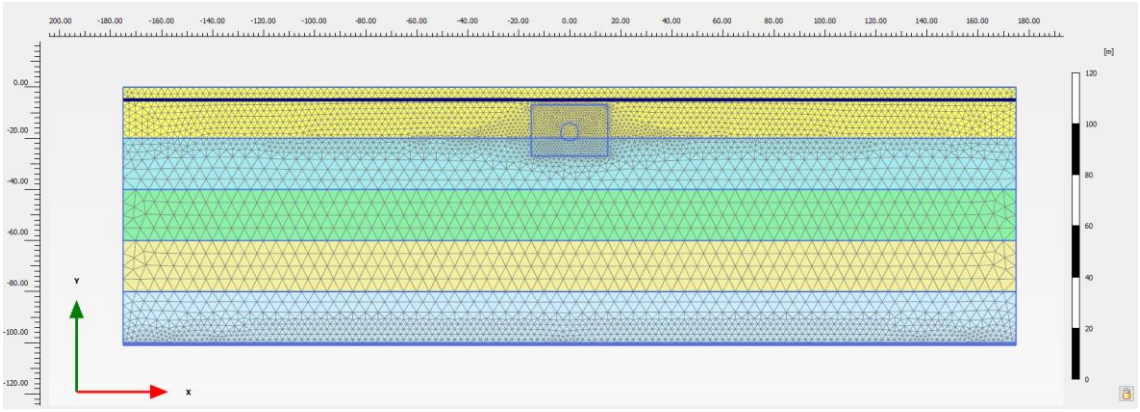

Figure 3.42. Plaxis model mesh

4. EVALUATION OF PARAMETRIC STUDY

In this section, the detailed results of the analyses will be presented in general and case-specific terms for the purposes of comprehensibility. In this context, following the sequence in Chapter 3, the cases where rock parameters increase and remain constant with depth will be evaluated for different tunnel shapes, respectively. The unit of moment is kN.m/m, unit of shear and normal forces will be presented in kN/m in this section.

4.1. Analysis of Rock Properties Increasing with Depth for Plaxis

The table of the results of the analysis performed with the assumption that the rock parameters increase with increasing depth is presented below.

Table 4.1. Analysis results of rock properties increasing with depth

LOADING CONDITIONS	CIRCULAR											
	SITE CLASS C						SITE CLASS B					
	2D			6D			2D			6D		
	MOMENT	SHEAR	AXIAL	MOMENT	SHEAR	AXIAL	MOMENT	SHEAR	AXIAL	MOMENT	SHEAR	AXIAL
STATIC	58	39	1154	47	33	2793	15	11	986	19	12	2258
RSN_1111	214	173	1534	100	108	3297	84	103	1721	79	137	3458
RSN_285	243	186	1572	96	109	3304	91	145	1739	101	127	3709
RSN_1165	243	188	1589	94	97	3258	136	154	1739	89	149	3498

	HORSE-SHOE											
	SITE CLASS C						SITE CLASS B					
	2D			6D			2D			6D		
	MOMENT	SHEAR	AXIAL	MOMENT	SHEAR	AXIAL	MOMENT	SHEAR	AXIAL	MOMENT	SHEAR	AXIAL
STATIC	70	94	1142	125	183	2773	39	55	987	100	167	2316
RSN_1111	382	368	1579	259	365	3343	171	277	1787	171	296	3574
RSN_285	375	368	1605	253	352	3328	173	298	1748	179	326	3819
RSN_1165	397	395	1623	269	375	3314	237	351	1809	179	286	3648

	BOX											
	SITE CLASS C						SITE CLASS B					
	2D			6D			2D			6D		
	MOMENT	SHEAR	AXIAL	MOMENT	SHEAR	AXIAL	MOMENT	SHEAR	AXIAL	MOMENT	SHEAR	AXIAL
STATIC	676	826	874	1577	1826	1976	514	688	736	1590	2189	1852
RSN_1111	1299	1311	1297	2614	3068	3003	1136	1382	1627	2169	3118	3359
RSN_285	1326	1309	1292	2447	2901	2872	1164	1368	1565	2194	3193	3371
RSN_1165	1365	1350	1351	2614	3038	2985	1247	1441	1674	2286	3153	3525

This table will be evaluated in detail, starting from the static case. Afterward, comparisons will be made for the earthquake case using the average values obtained as a result of the 3 earthquake records used. But before then, we will assess the forces of the different tunnel linings under dynamic loads as given in Table 4.2.

In Table 4.2 below, the results for the RSN_1111 record are presented for depth 6D in site class C and the sum of the static and dynamic loads is shown in the lining. The analysis described below is very similar to the static case because the system returns to equilibrium at the end of the dynamic analysis and reaches another static condition. However, during dynamic analysis, it will be possible for the maximum of the internal forces to appear in other parts of the lining due to wave propagation effects.

For circular tunnel, the normal forces are perpendicular to the lining. Moments in circular tunnels occur due to the difference between the horizontal and vertical earth pressures on the lining for static cases. Since the horizontal earth pressure is multiplied by K, it will generally be lower than the vertical earth pressure except for anomalies. As can be seen in the table below, dynamic loads are added to the static loads, causing the effects to increase. The shear force was formed in such a way as to cut the ground environment and the lining in which the tunnel is located.

For the horseshoe tunnel, the normal forces are perpendicular to the lining. These tunnels have variable diameters within themselves. There is a change in diameter between the invert and the walls, and the moments generally accumulate in these areas. For the larger area of horseshoe tunnels, moments can also accumulate on the shoulders of the tunnel. As shown in Table 4.2, the total maximum moments (static and dynamic) occurred at the invert and wall transition. The shear force was formed in such a way as to cut the ground environment in which the tunnel is located and the lining as similar to the circular tunnel.

For box tunnels, the normal forces are perpendicular to the lining. Moment values tend to accumulate at the corner points due to the sharp transition. As will be examined in the following sections, this type of tunnel will already be subjected to excessive loading in the static phase. Similar to the moment, the shear force accumulates at the corner points.

Overall, it is also observed that the homogeneous distribution of internal forces decreases as the tunnel shape changes from circular to box shape.

Table 4.2. Internal forces of different tunnel shapes after dynamic case

Force/ Tunnel shape	Axial Force N diagram	Bending moment M diagram	Shear force V diagram
Circular	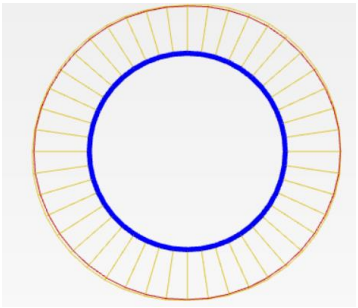	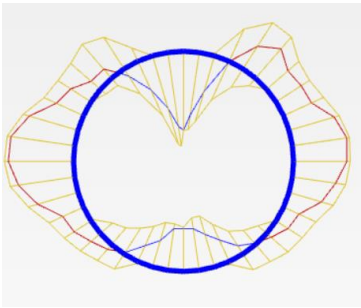	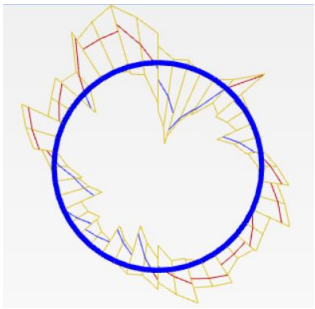
Horse-shoe	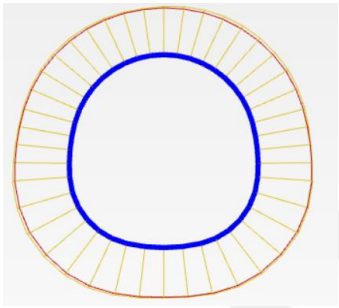	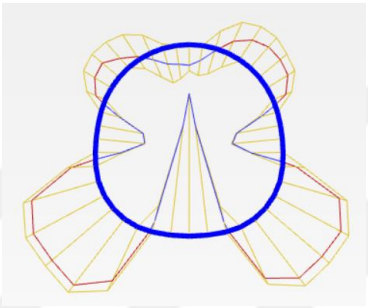	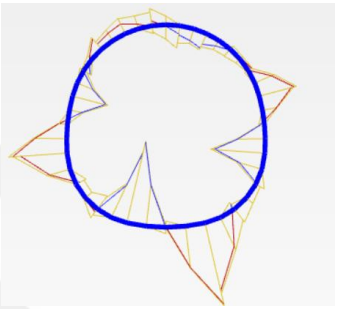
Box	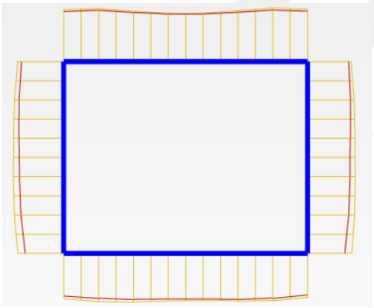	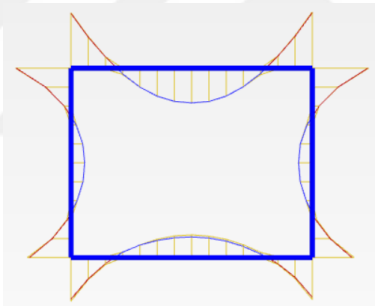	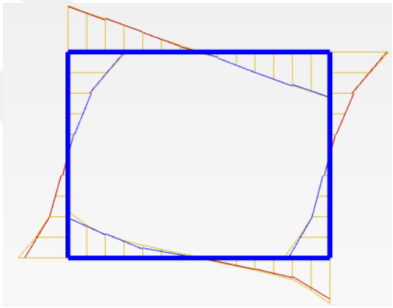

4.1.1 Static Cases

In this section, only the static state comparison of the rock parameters increasing with depth was conducted.

4.1.1.1 Site Class Comparison for Forces

In the static case, first of all, the maximum lining forces in site class B are lower than the lining forces in site class C for values where the depth is the same, as seen in Table 4.3 and Figure 4.1.

Table 4.3. Analysis results of rock properties increasing with depth for the static case

TUNNEL TYPES	STATIC CONDITION											
	SITE CLASS C						SITE CLASS B					
	2D			6D			2D			6D		
	MOMENT	SHEAR	AXIAL	MOMENT	SHEAR	AXIAL	MOMENT	SHEAR	AXIAL	MOMENT	SHEAR	AXIAL
CIRCULAR	58	39	1154	47	33	2793	15	11	986	19	12	2258
HORSE-SHOE	70	94	1142	125	183	2773	39	55	987	100	167	2316
BOX	676	826	874	1577	1826	1976	514	688	736	1590	2189	1852

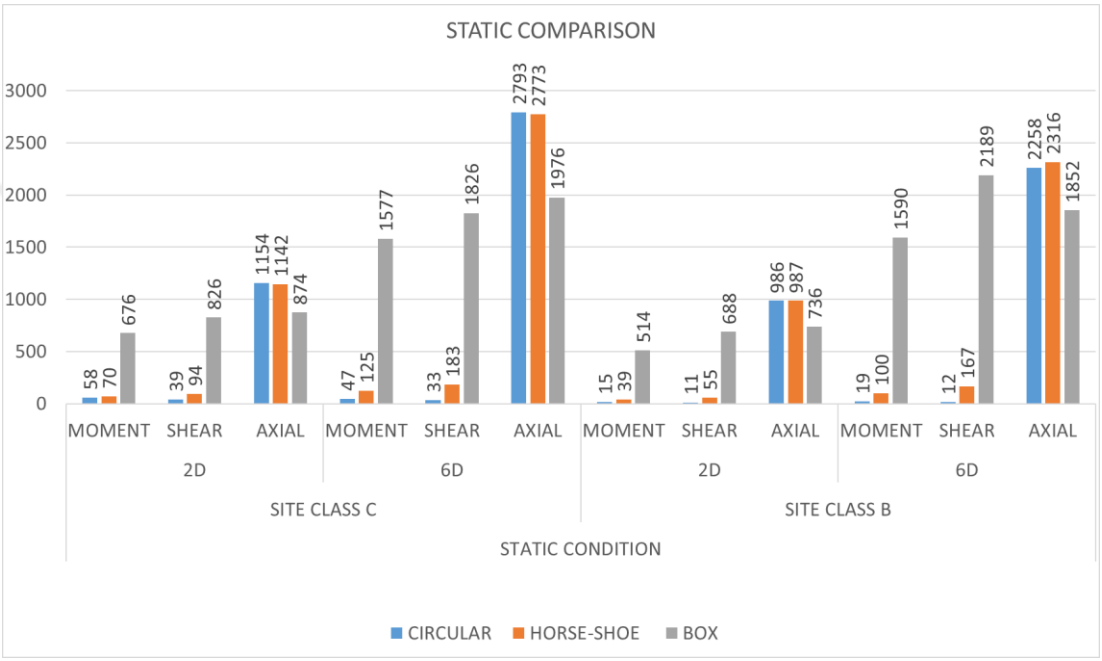

Figure 4.1. Comparison of analysis results for static condition of rock properties increasing with depth

4.1.1.2 Axial Force Comparison

It can be clearly seen from Table 4.4 and Figure 4.2 given below for axial force that as the cover depth on the tunnel increases, the maximum axial force on the lining tends to increase. The maximum axial force increases as the tunnel shape changes from box to circular.

Table 4.4. Analysis results of rock properties increasing with depth for the static case (axial force)

TUNNEL TYPES	STATIC CONDITION			
	SITE CLASS C		SITE CLASS B	
	2D	6D	2D	6D
	AXIAL	AXIAL	AXIAL	AXIAL
CIRCULAR	1154	2793	986	2258
HORSE-SHOE	1142	2773	987	2316
BOX	874	1976	736	1852

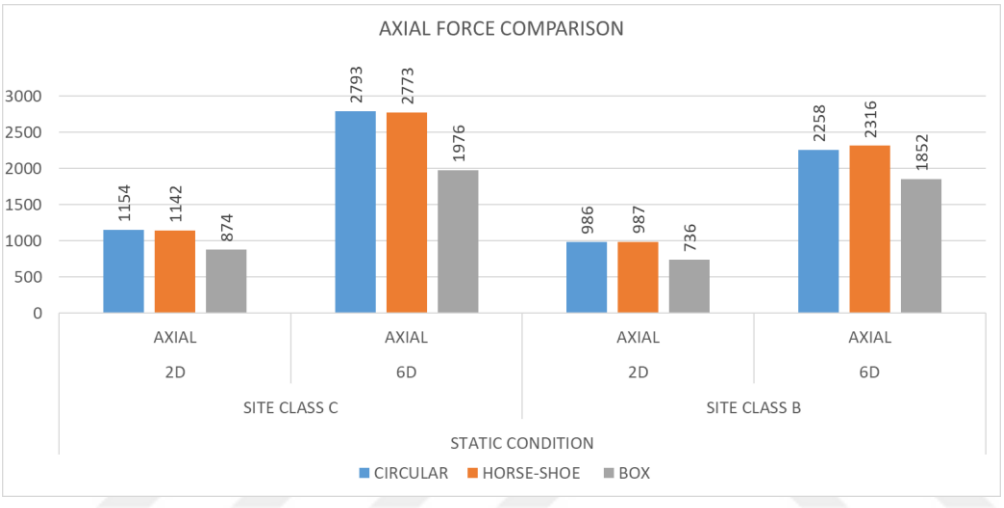

Figure 4.2. Comparison of analysis results for the static condition of rock properties increasing with depth (axial force)

4.1.1.3 Moment Comparison

It is understood from Table 4.5 and Figure 4.3 that the moment values increase with depth, except for one anomaly in the static case for circular tunnel. The maximum moment increases as the tunnel shape changes from circular to box.

Table 4.5. Analysis results of rock properties increasing with depth for the static case (moment)

TUNNEL TYPES	STATIC CONDITION			
	SITE CLASS C		SITE CLASS B	
	2D	6D	2D	6D
	MOMENT	MOMENT	MOMENT	MOMENT
CIRCULAR	58	47	15	19
HORSE-SHOE	70	125	39	100
BOX	676	1577	514	1590

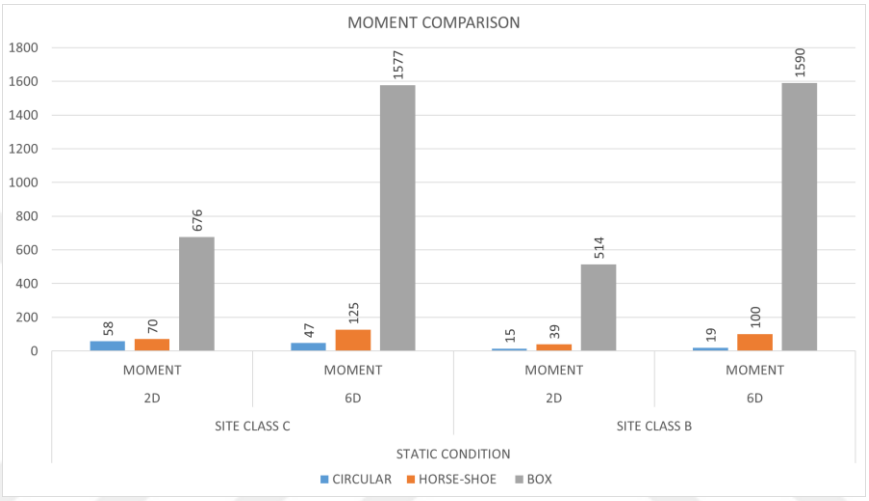

Figure 4.3. Comparison of analysis results for static condition of rock properties increasing with depth (moment)

4.1.1.4 Shear Force Comparison

It is understood from Table 4.6 and Figure 4.4 that the shear force values increase with depth, except for one anomaly in the static case for a circular tunnel. The maximum shear force increases as the tunnel shape changes from circular to box.

Table 4.6. Analysis results of rock properties increasing with depth for the static case (shear force)

TUNNEL TYPES	STATIC CONDITION			
	SITE CLASS C		SITE CLASS B	
	2D	6D	2D	6D
	SHEAR	SHEAR	SHEAR	SHEAR
CIRCULAR	39	33	11	12
HORSE-SHOE	94	183	55	167
BOX	826	1826	688	2189

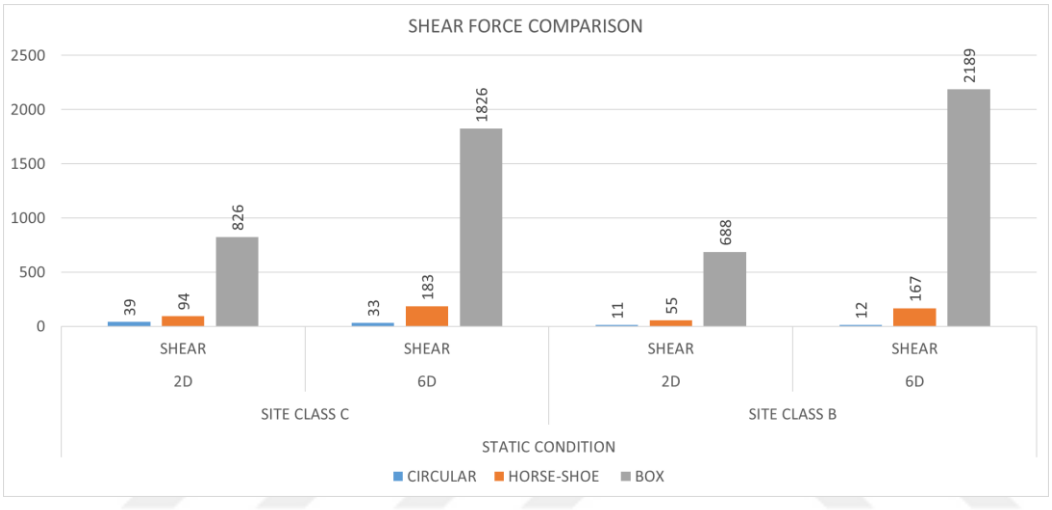

Figure 4.4. Comparison of analysis results for static condition of rock properties increasing with depth (shear force)

4.1.2 Dynamic Cases

In this section, the comparison of the sum of static and dynamic load is made for the case where increasing rock parameters with depth are conducted.

4.1.2.1 Site Class Comparison for Forces

In the earthquake case, the lining forces in site class B are lower than those in site class C for values where the depth is the same, as seen in Table 4.7 and Figure 4.5.

Table 4.7. Analysis results of rock properties increasing with depth for earthquake case

TUNNEL TYPES	EARTHQUAKE CONDITION											
	SITE CLASS C						SITE CLASS B					
	2D			6D			2D			6D		
	MOMENT	SHEAR	AXIAL	MOMENT	SHEAR	AXIAL	MOMENT	SHEAR	AXIAL	MOMENT	SHEAR	AXIAL
CIRCULAR	233	183	1565	97	105	3286	103	134	1733	90	137	3555
HORSE-SHOE	385	377	1602	260	364	3328	194	309	1781	176	303	3680
BOX	1330	1323	1313	2558	3002	2953	1182	1397	1622	2216	3155	3418

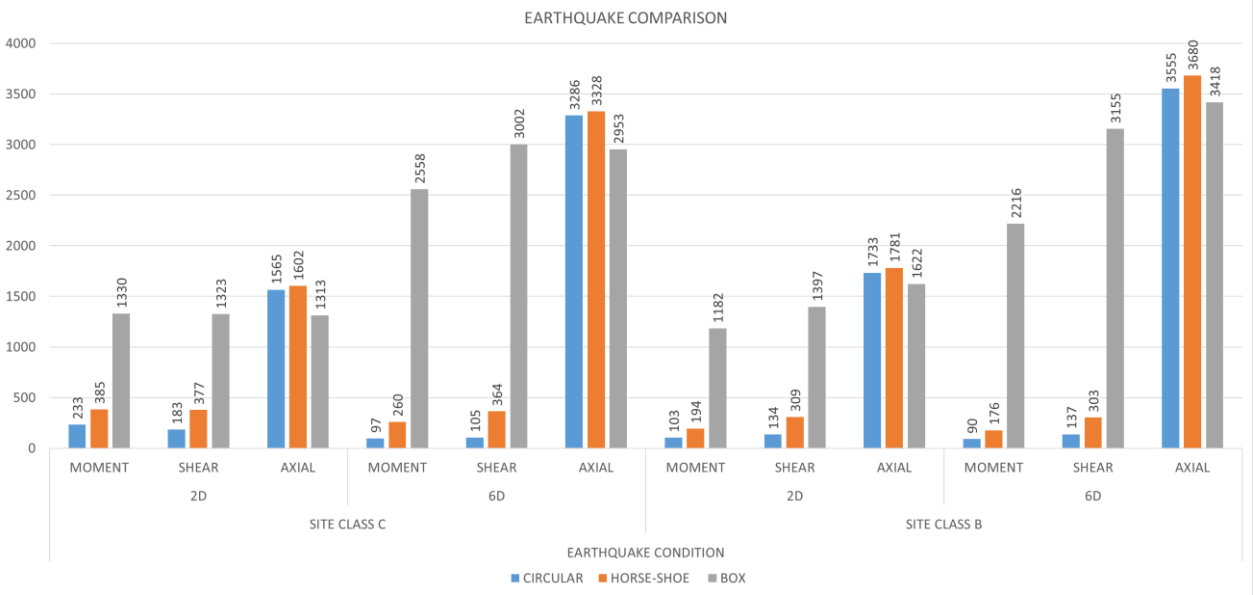

Figure 4.5. Comparison of analysis results for earthquake condition of rock properties increasing with depth

4.1.2.2 Axial Force Comparison

It can be clearly seen from Table 4.8 and Figure 4.6 given below for axial force that as the cover depth on the tunnel increases, the maximum axial force on the lining tends to increase. The maximum axial force increases as the tunnel shape changes from box to circular. The axial force for the horseshoe shape is the maximum. After that, a circular tunnel follows, and lastly, the box shape is the lowest axial force. The maximum axial force increases as the tunnel shape changes from box to circular.

Table 4.8. Analysis results of rock properties increasing with depth for earthquake case (axial force)

TUNNEL TYPES	EARTHQUAKE CONDITION			
	SITE CLASS C		SITE CLASS B	
	2D	6D	2D	6D
	AXIAL	AXIAL	AXIAL	AXIAL
CIRCULAR	1565	3286	1733	3555
HORSE-SHOE	1602	3328	1781	3680
BOX	1313	2953	1622	3418

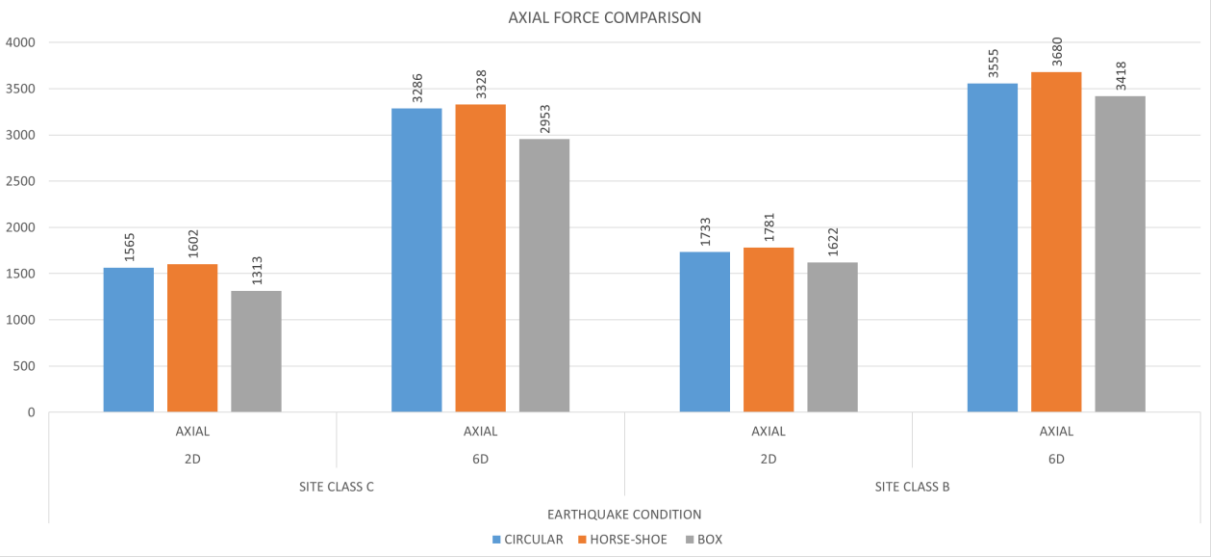

Figure 4.6. Comparison of analysis results for earthquake condition of rock properties increasing with depth (axial force)

4.1.2.3 Moment Comparison

It is understood from Table 4.9 and Figure 4.7 that the maximum moment values decrease with depth for circular and horseshoe shape tunnels for both site classes however, it increases for box shape tunnels. The maximum moment increases as the tunnel shape changes from circular to box.

Table 4.9. Analysis results of rock properties increasing with depth for earthquake case (moment)

TUNNEL TYPES	EARTHQUAKE CONDITION			
	SITE CLASS C		SITE CLASS B	
	2D	6D	2D	6D
	MOMENT	MOMENT	MOMENT	MOMENT
CIRCULAR	233	97	103	90
HORSE-SHOE	385	260	194	176
BOX	1330	2558	1182	2216

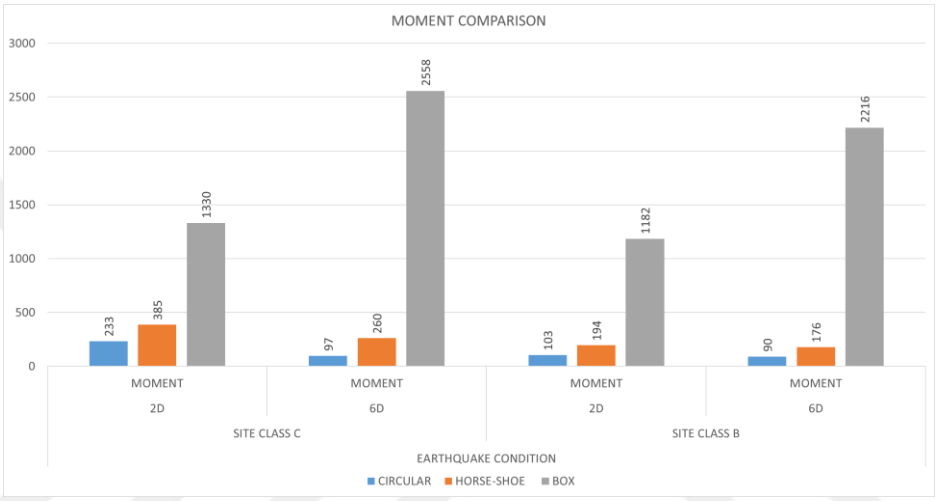

Figure 4.7. Comparison of analysis results for earthquake condition of rock properties increasing with depth (moment)

4.1.2.4 Shear Force Comparison

It is understood from Table 4.10 and Figure 4.8 that the maximum shear force values decreased with increasing depth in site class C for circular tunnel and remained approximately the same in site class B. Horseshoe tunnels remained approximately the same, with increasing depth in site classes C and B. For the box-shaped tunnel, it is clearly seen that the maximum shear forces increase with depth. The maximum shear force increases as the tunnel shape changes from circular to box.

Table 4.10. Analysis results of rock properties increasing with depth for earthquake case (shear force)

TUNNEL TYPES	EARTHQUAKE CONDITION			
	SITE CLASS C		SITE CLASS B	
	2D	6D	2D	6D
	SHEAR	SHEAR	SHEAR	SHEAR
CIRCULAR	183	105	134	137
HORSE-SHOE	377	364	309	303
BOX	1323	3002	1397	3155

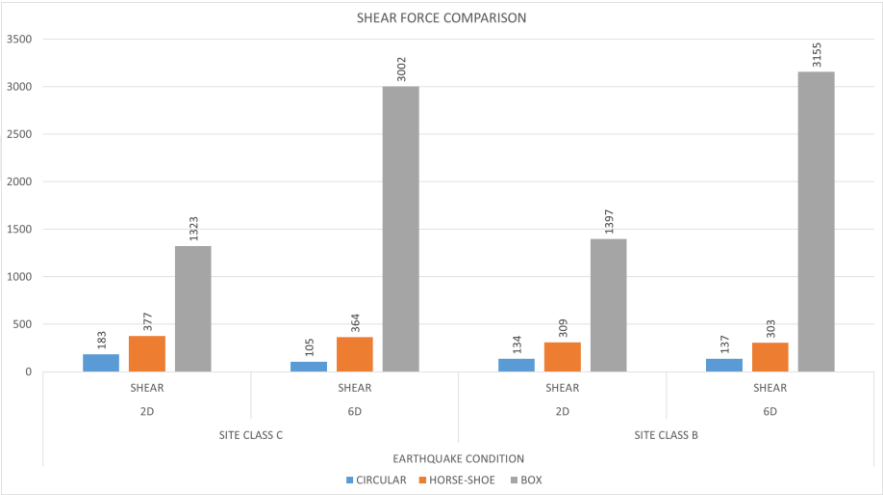

Figure 4.8. Comparison of analysis results for earthquake condition of rock properties increasing with depth (shear force)

4.1.3 Comparison of Earthquake Effects (Dynamic Induced Stress)

From section 4.1.1-4.1.4, only static forces are compared. In Sections 4.1.5~4.1.8, the comparison is made by looking at the sum of the earthquake effects in addition to the static forces. In this section, earthquake effects will be evaluated by subtracting the static forces in order to analyze only the earthquake forces.

4.1.3.1 Comparison of Earthquake Effects for C Site Class (Dynamic Induced Stress)

In Table 4.11 and Figure 4.9, only the forces for earthquakes are given for the C site class. As can be seen from the table and graph, maximum shear force and maximum moment values decrease with increasing depth for circular and horseshoe tunnels. On the contrary, the values increase for box shape. As expected, the maximum axial force increases with

the cover load on the tunnels, regardless of the tunnel shape. In general, as the tunnel shape changes from circular to box, the forces on the lining increase.

Table 4.11. Analysis results of rock properties increasing with depth for comparison of earthquake effects in C site class (dynamic induced stress)

TUNNEL TYPES	AVERAGE DYNAMIC-STATIC					
	SITE CLASS C					
	MOMENT		SHEAR		AXIAL	
	2D	6D	2D	6D	2D	6D
CIRCULAR	230	73	181	103	540	695
HORSE-SHOE	335	134	283	236	534	745
BOX	667	1089	521	1293	541	1415

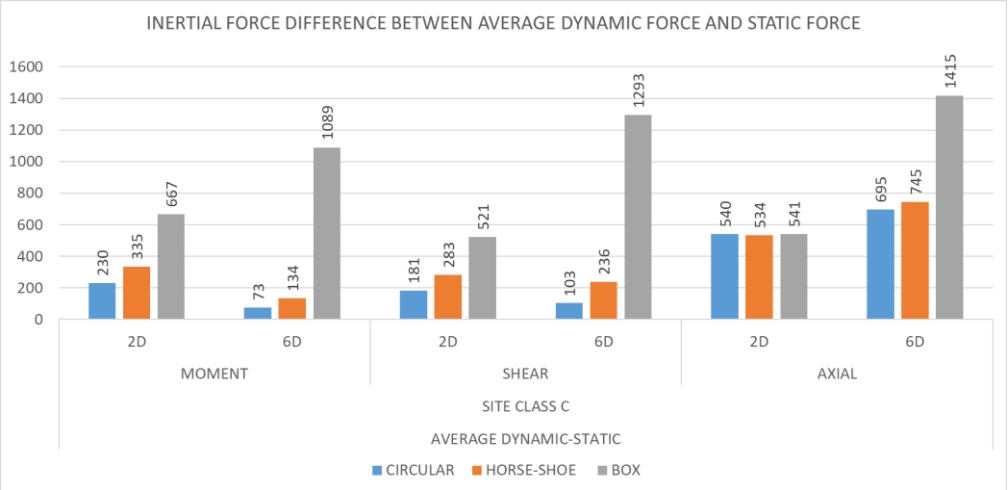

Figure 4.9. Analysis results of rock properties increasing with depth for comparison of earthquake effects in C site class (dynamic induced stress)

4.1.3.2 Comparison of Earthquake Effects for B Site Class (Dynamic Induced Stress)

In Table 4.12 and Figure 4.10 only the forces for earthquake are given for B site class. As can be seen from the table and graph, maximum shear force and maximum moment values decrease with increasing depth for circular and horseshoe tunnels (except for an anomaly for shear force of circular shape). On the contrary, the values increase for box shape. Maximum axial force increases with the cover load on the tunnels as expected regardless of the tunnel shape. In general, as the tunnel shape changes from circular to box, the forces on the lining increase.

Table 4.12. Analysis results of rock properties increasing with depth for comparison of earthquake effects in B site class (dynamic induced stress)

TUNNEL TYPES	AVERAGE DYNAMIC-STATIC					
	SITE CLASS B					
	MOMENT		SHEAR		AXIAL	
	2D	6D	2D	6D	2D	6D
CIRCULAR	91	88	134	137	971	1691
HORSE-SHOE	179	88	266	150	1019	1726
BOX	735	765	873	1261	1088	1743

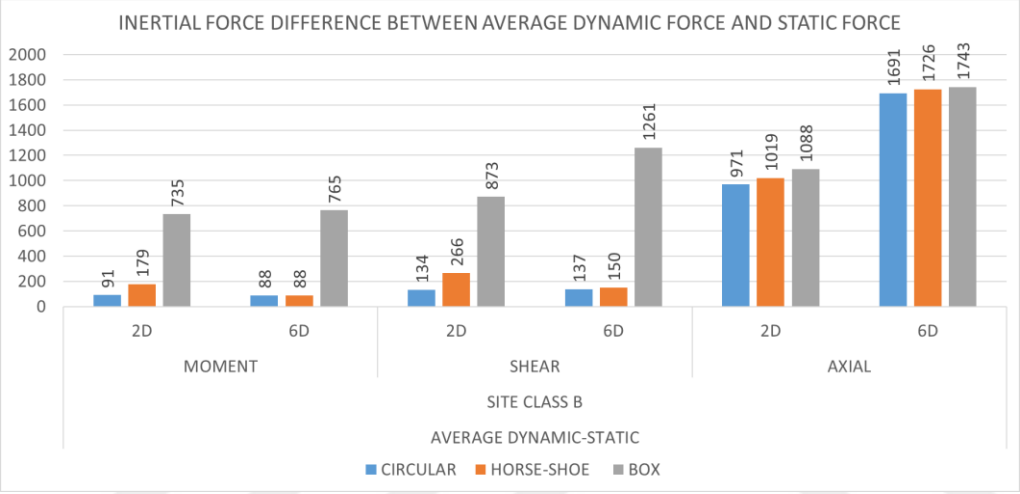

Figure 4.10. Analysis results of rock properties increasing with depth for comparison of earthquake effects in B site class (dynamic induced stress)

4.2. Analysis of Rock Properties Constant with Depth for Plaxis

The table of the results of the analysis performed with the assumption that the rock parameters constant with increasing depth are presented below.

Table 4.13. Analysis results of rock properties constant with depth

LOADING CONDITIONS	CIRCULAR											
	SITE CLASS C						SITE CLASS B					
	2D			6D			2D			6D		
	MOMENT	SHEAR	AXIAL	MOMENT	SHEAR	AXIAL	MOMENT	SHEAR	AXIAL	MOMENT	SHEAR	AXIAL
STATIC	33	25	1202	50	34	2942	11	10	970	20	13	2352
RSN_1111	80	72	1488	82	88	3524	46	53	1456	46	82	3587
RSN_285	104	99	1500	110	110	3786	47	57	1399	63	85	3665
RSN_1165	82	74	1474	71	81	3507	53	65	1501	50	76	3613

	HORSE-SHOE											
	SITE CLASS C						SITE CLASS B					
	2D			6D			2D			6D		
	MOMENT	SHEAR	AXIAL	MOMENT	SHEAR	AXIAL	MOMENT	SHEAR	AXIAL	MOMENT	SHEAR	AXIAL
STATIC	69	76	1175	127	190	2919	40	58	974	96	161	2403
RSN_1111	182	252	1555	311	413	3637	115	183	1588	197	337	3800
RSN_285	198	294	1536	319	458	3905	111	181	1472	186	346	3784
RSN_1165	191	272	1558	316	429	3611	116	182	1565	199	332	3850

	BOX											
	SITE CLASS C						SITE CLASS B					
	2D			6D			2D			6D		
	MOMENT	SHEAR	AXIAL	MOMENT	SHEAR	AXIAL	MOMENT	SHEAR	AXIAL	MOMENT	SHEAR	AXIAL
STATIC	562	628	859	1591	1878	2027	517	718	727	1590	2198	1889
RSN_1111	1081	1501	1538	2487	3083	3190	799	1262	1282	1947	2976	3472
RSN_285	1033	1343	1355	2399	2998	3206	736	1157	1171	1941	3076	3203
RSN_1165	1069	1487	1505	2655	3202	3251	1237	1237	1379	1960	2938	3584

This table will be evaluated in detail, starting from the static case. Afterward, comparisons will be made for the earthquake case using the average values obtained as a result of the 3 earthquake records used. The details of the internal forces of different shapes of tunnels are described in section 4.1.

4.2.1 Static Cases

In this section, only the static state comparison of the rock parameters constant with depth was conducted.

4.2.1.1 Site Class Comparison for Forces

In the static case, first of all, the lining forces in site class B are lower than the lining forces in site class C for values where the depth is the same as seen in Table 4.14 and Figure 4.11.

Table 4.14. Analysis results of rock properties constant with depth for the static case

TUNNEL TYPES	STATIC CONDITION											
	SITE CLASS C						SITE CLASS B					
	2D			6D			2D			6D		
	MOMENT	SHEAR	AXIAL	MOMENT	SHEAR	AXIAL	MOMENT	SHEAR	AXIAL	MOMENT	SHEAR	AXIAL
CIRCULAR	33	25	1202	50	34	2942	11	10	970	20	13	2352
HORSE-SHOE	69	76	1175	127	190	2919	40	58	974	96	161	2403
BOX	562	628	859	1591	1878	2027	517	718	727	1590	2198	1889

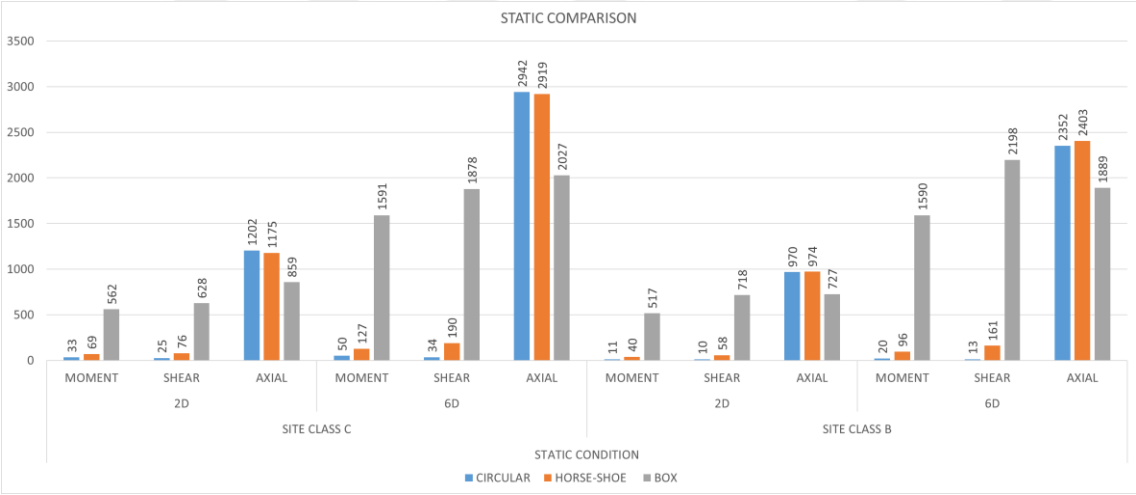

Figure 4.11. Comparison of analysis results for static condition of rock properties constant with depth

4.2.1.2 Axial Force Comparison

It can be clearly seen from the Table 4.15 and Figure 4.12 given below for axial force that as the cover depth on the tunnel increases, the maximum axial force on the lining tends to increase. The axial force increase as the tunnel shape changes from box to circular.

Table 4.15. Analysis results of rock properties constant with depth for static case (axial force)

TUNNEL TYPES	STATIC CONDITION			
	SITE CLASS C		SITE CLASS B	
	2D	6D	2D	6D
	AXIAL	AXIAL	AXIAL	AXIAL
CIRCULAR	1202	2942	970	2352
HORSE-SHOE	1175	2919	974	2403
BOX	859	2027	727	1889

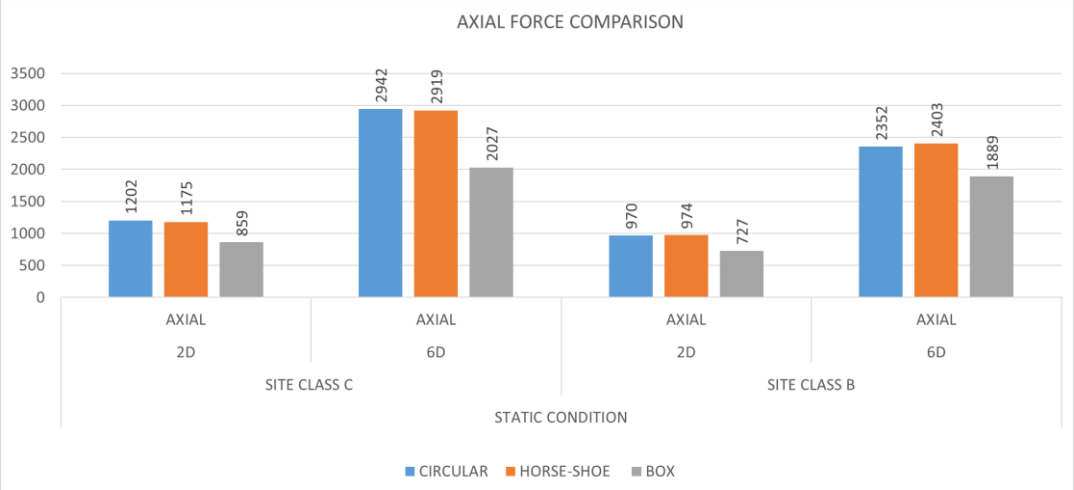

Figure 4.12. Comparison of analysis results for static condition of rock properties constant with depth (axial force)

4.2.1.3 Moment Comparison

It is understood from Table 4.16 and Figure 4.13 that the moment values increase with depth. The maximum moment increase as the tunnel shape changes from circular to box.

Table 4.16. Analysis results of rock properties constant with depth for static case (moment)

TUNNEL TYPES	STATIC CONDITION			
	SITE CLASS C		SITE CLASS B	
	2D	6D	2D	6D
	MOMENT	MOMENT	MOMENT	MOMENT
CIRCULAR	33	50	11	20
HORSE-SHOE	69	127	40	96
BOX	562	1591	517	1590

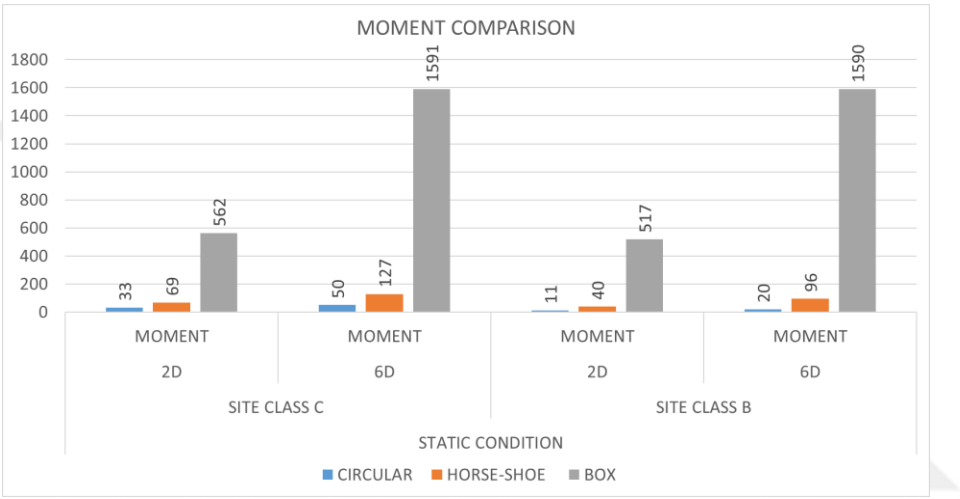

Figure 4.13. Comparison of analysis results for static condition of rock properties constant with depth (moment)

4.2.1.4 Shear Force Comparison

It is understood from Table 4.17 and Figure 4.14 that the shear force values increase with depth. The maximum shear force increase as the tunnel shape changes from circular to box.

Table 4.17. Analysis results of rock properties constant with depth for static case (shear force)

TUNNEL TYPES	STATIC CONDITION			
	SITE CLASS C		SITE CLASS B	
	2D	6D	2D	6D
	SHEAR	SHEAR	SHEAR	SHEAR
CIRCULAR	25	34	10	13
HORSE-SHOE	76	190	58	161
BOX	628	1878	718	2198

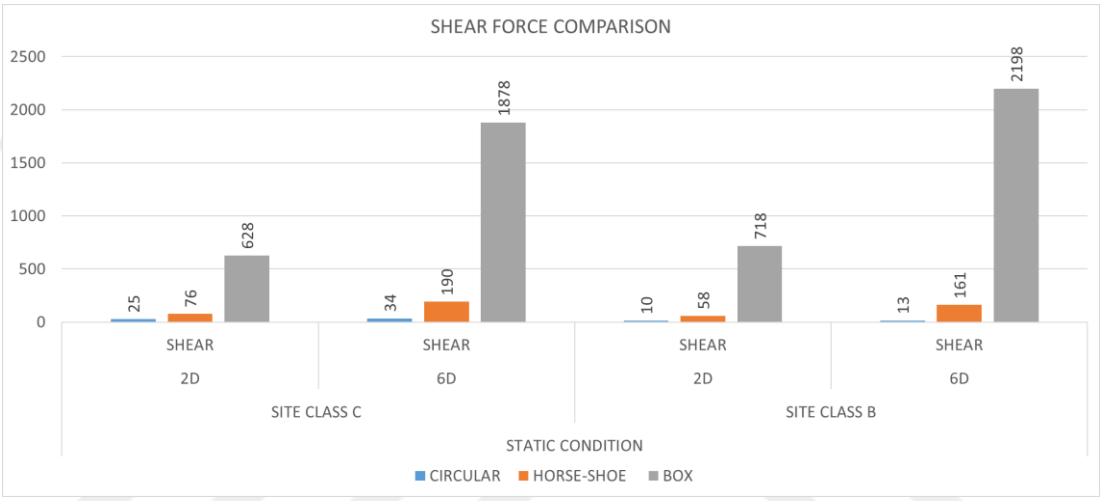

Figure 4.14. Comparison of analysis results for static condition of rock properties constant with depth (shear force)

4.2.2 Dynamic Cases

In this section, a comparison of the sum of static and dynamic load is made for the case where the rock parameters are constant with depth.

4.2.2.1 Site Class Comparison for Forces

In the earthquake case, the lining forces in site class B are lower than those in site class C for values where the depth is the same, as seen in Table 4.18 and Figure 4.15.

Table 4.18. Analysis results of rock properties constant with depth for earthquake case

TUNNEL TYPES	EARTHQUAKE CONDITION											
	SITE CLASS C						SITE CLASS B					
	2D			6D			2D			6D		
	MOMENT	SHEAR	AXIAL	MOMENT	SHEAR	AXIAL	MOMENT	SHEAR	AXIAL	MOMENT	SHEAR	AXIAL
CIRCULAR	89	82	1487	88	93	3606	49	58	1452	53	81	3622
HORSE-SHOE	191	273	1550	315	433	3718	114	182	1542	194	338	3811
BOX	1061	1444	1466	2514	3094	3216	924	1219	1277	1949	2997	3420

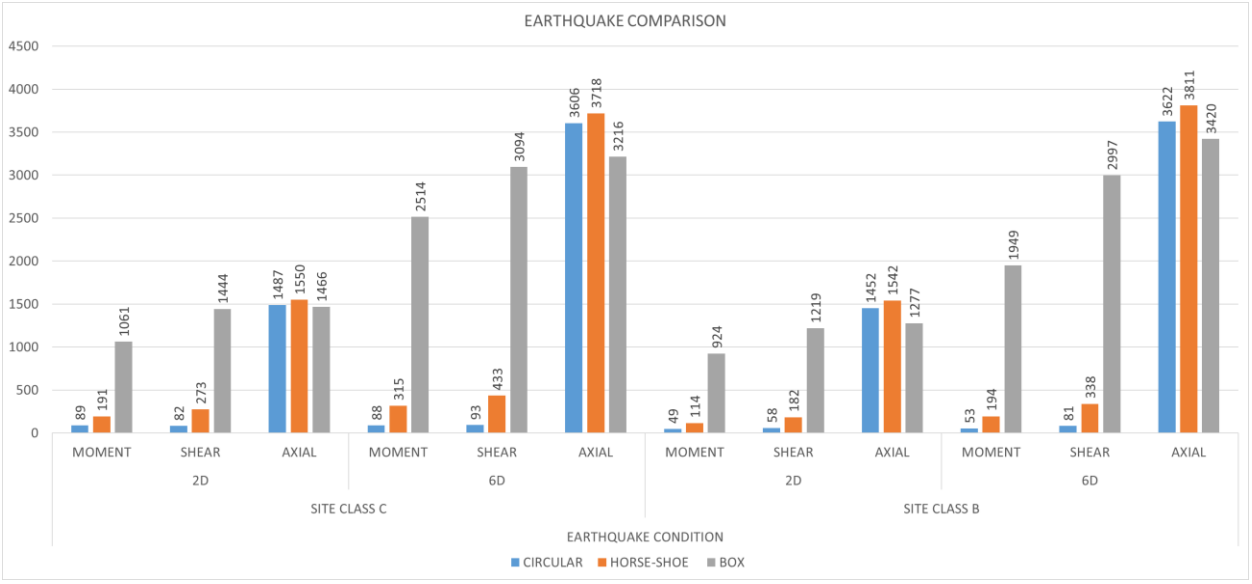

Figure 4.15. Comparison of analysis results for earthquake condition of rock properties constant with depth

4.2.2.2 Axial Force Comparison

It can be clearly seen from the Table 4.19 and Figure 4.16 given below for axial force that as the cover depth on the tunnel increases, the maximum axial force on the lining tends to increase. The axial force for the horseshoe shape is the maximum, after that circular tunnel follows and lastly the box shape is the lowest axial force. The axial force increase as the tunnel shape changes from box to circular.

Table 4.19. Analysis results of rock properties constant with depth for earthquake case (axial force)

TUNNEL TYPES	EARTHQUAKE CONDITION			
	SITE CLASS C		SITE CLASS B	
	2D	6D	2D	6D
	AXIAL	AXIAL	AXIAL	AXIAL
CIRCULAR	1487	3606	1452	3622
HORSE-SHOE	1550	3718	1542	3811
BOX	1466	3216	1277	3420

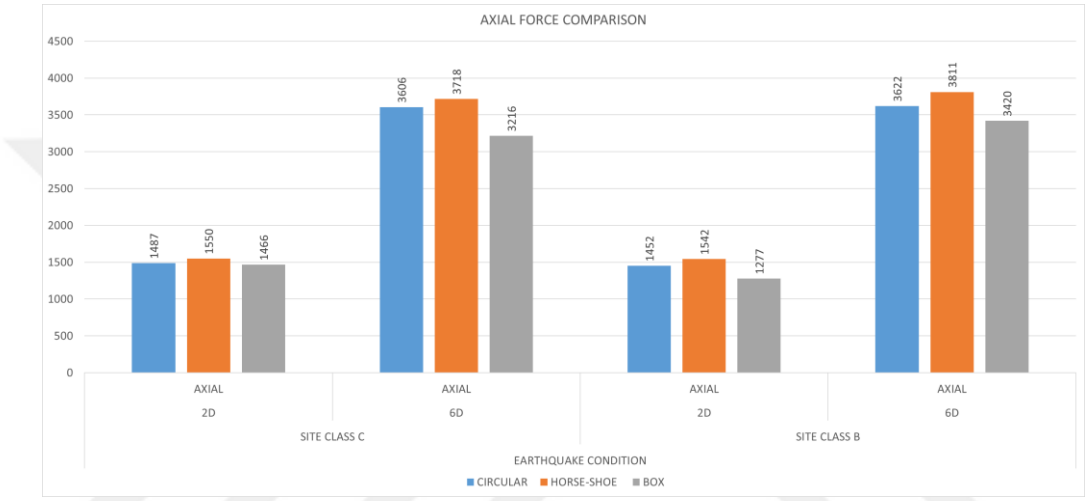

Figure 4.16. Comparison of analysis results for earthquake condition of rock properties constant with depth (axial force)

4.2.2.3 Moment Comparison

It is understood from Table 4.20 and Figure 4.17 that the maximum moment values increase with depth for all shapes of tunnels except an anomaly for circular shape of site class C. The maximum moment increase as the tunnel shape changes from circular to box.

Table 4.20. Analysis results of rock properties constant with depth for earthquake case (moment)

TUNNEL TYPES	EARTHQUAKE CONDITION			
	SITE CLASS C		SITE CLASS B	
	2D	6D	2D	6D
	MOMENT	MOMENT	MOMENT	MOMENT
CIRCULAR	89	88	49	53
HORSE-SHOE	191	315	114	194
BOX	1061	2514	924	1949

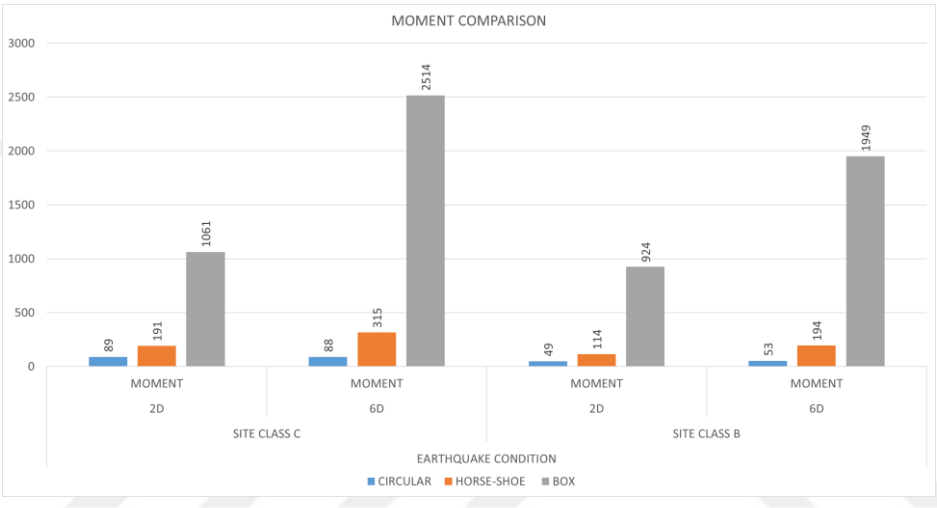

Figure 4.17. Comparison of analysis results for earthquake condition of rock properties constant with depth (moment)

4.2.2.4 Shear Force Comparison for Dynamic Case

It is understood from Table 4.21 and Figure 4.18 that the maximum shear force values increased for all shapes of tunnels without an exception. The maximum shear force increase as the tunnel shape changes from circular to box.

Table 4.21. Analysis results of rock properties constant with depth for earthquake case (shear force)

TUNNEL TYPES	EARTHQUAKE CONDITION			
	SITE CLASS C		SITE CLASS B	
	2D	6D	2D	6D
	SHEAR	SHEAR	SHEAR	SHEAR
CIRCULAR	82	93	58	81
HORSE-SHOE	273	433	182	338
BOX	1444	3094	1219	2997

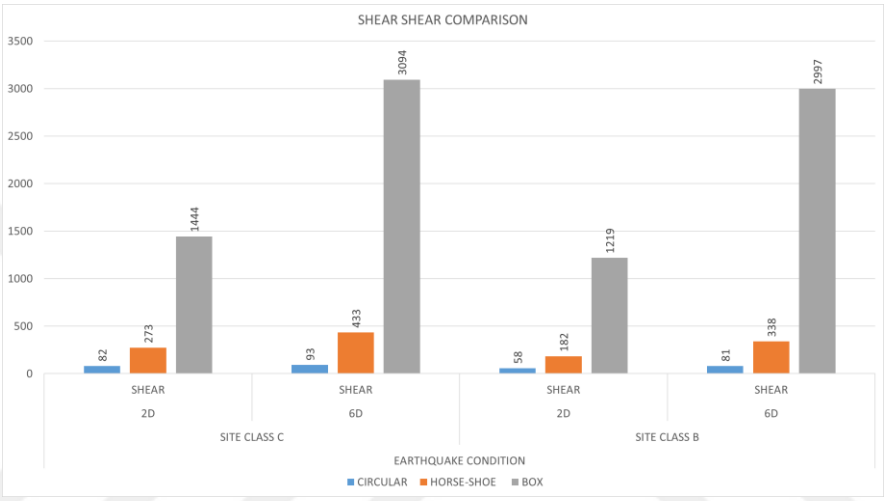

Figure 4.18. Comparison of analysis results for earthquake condition of rock properties constant with depth (shear force)

4.2.3 Comparison of Earthquake Effects (Dynamic Induced Stress)

From section 4.2.1~4.2.4 only static forces are compared. In Sections 4.2.5~4.2.8, the comparison is made by looking at the sum of the earthquake effects in addition to the static forces. In this section, earthquake effects will be evaluated by subtracting the static forces in order to analyze only the earthquake forces.

4.2.3.1 Comparison of Dynamic Effects for C Site Class (Dynamic Induced Stress)

In Table 4.22 and Figure 4.19, only the forces for an earthquake are given for C site class. As seen from the table and graph, forces and moment values increase with increasing depth for all shapes of tunnels except an anomaly for circular shapes. In general, as the tunnel shape changes from circular to box, the forces on the lining increase.

Table 4.22. Analysis results of rock properties constant with depth for comparison of earthquake effects in C site class (dynamic induced stress)

TUNNEL TYPES	AVERAGE DYNAMIC-STATIC					
	SITE CLASS C					
	MOMENT		SHEAR		AXIAL	
	2D	6D	2D	6D	2D	6D
CIRCULAR	66	63	73	84	549	969
HORSE-SHOE	127	189	202	304	587	1073
BOX	511	1029	820	1340	972	1604

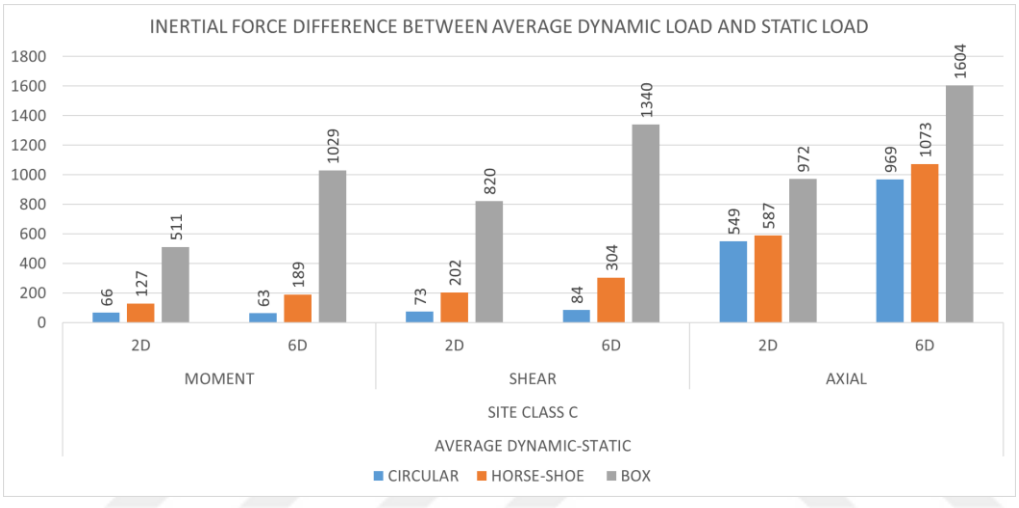

Figure 4.19. Analysis results of rock properties constant with depth for comparison of earthquake effects in C site class (dynamic induced stress)

4.2.3.2 Comparison of Dynamic Effects for B Site Class (Dynamic Induced Stress)

In Table 4.23 and Figure 4.20 only the forces for earthquake are given for B site class. As can be seen from the table and graph, forces and moment values increase with increasing depth for all shapes of tunnels except two anomalies for circular and box shape. In general, as the tunnel shape changes from circular to box, the forces on the lining increase.

Table 4.23. Analysis results of rock properties constant with depth for comparison of earthquake effects in B site class (dynamic induced stress)

TUNNEL TYPES	AVERAGE DYNAMIC-STATIC					
	SITE CLASS B					
	MOMENT		SHEAR		AXIAL	
	2D	6D	2D	6D	2D	6D
CIRCULAR	45	51	58	80	727	1736
HORSE-SHOE	72	102	123	181	804	1827
BOX	269	432	637	1155	786	1725

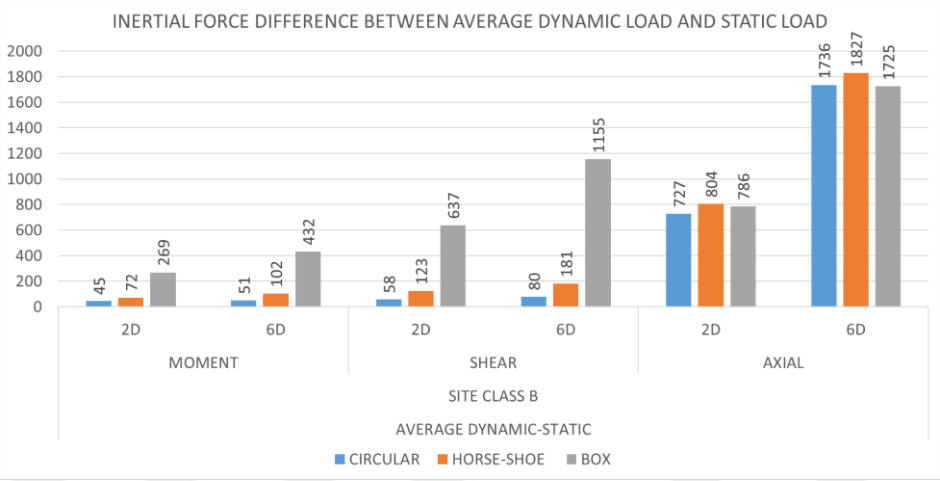

Figure 4.20. Analysis results of rock properties constant with depth for comparison of earthquake effects in B site class (dynamic induced stress)

4.3. Validation of Plaxis Results Using Analytical Methods

In this section, the verification of the results found with Plaxis 2D will be done with the help of the analytical equations presented in Section 2 by Wang in 1993. In this context, the model parameters with shear wave velocity that does not change with depth presented in Section 3 will be used as the equations are proposed assuming homogeneous medium. In addition, tunnels with burial depths of 6 and 60 meters, as well as depths of 14 and 42 meters, were included in the analyses in order to expand the sample space. Another important point is that the equations presented in Chapter 2 are presented only for circular shaped tunnels and the checks are performed accordingly. In this context, spreadsheets were written in order to automate the equation sets. In the following, only the solution for the RSN_1111 record at 2D depth for site class C is presented. The remaining calculations will not be presented, and a summary table is given for them.

OVALING CALCULATIONS (RSN_1111 RECORD-2D DEPTH-SITE CLASS C)

OVALING

Without Considering Soil-Tunnel Interaction

$\mathbf{a_{max}}$ =	0,82471	g	a_{max} : Peak ground particle acceleration
$\mathbf{a_{td}}$ =	0,74224	g	a_{td} : ground particle acceleration for tunnel depth
$\mathbf{V_s/a_{td}}$ =	32		V_s/a_{td}:Ratio of peak ground velocity to peak ground acceleration
$\mathbf{V_s}$ =	0,2	m/s	V_s : peak particle velocity for tunnel depth
$\boldsymbol{\gamma_t}$ =	21	kN/m^3	γ_t : unit weight of the tunnel medium
$\boldsymbol{\rho}$ =	2,14	ton/m^3	ρ : mass density of the tunnel medium
ν_m =	0,2		ν_m : the Poisson's Ratio of the medium
$\mathbf{C_s}$ =	600	m/s	C_s : shear wave propagation velocity for tunnel depth
$\mathbf{C_s'}$ =	480	m/s	$C_{s'}$: effective shear wave propagation velocity for tunnel depth
$\boldsymbol{\gamma_{max}}$ =	$\mathbf{V_s/C_s'}$		γ_{max}: maximum free-field shear strain
$\boldsymbol{\gamma_{max}}$ =	0,00050		
$\mathbf{G_m'}$ =	$\boldsymbol{\rho x (C_s')^2}$		G_m': effective shear modulus of the tunnel medium
$\mathbf{G_m'}$ =	493379	kPa	

For non-perforated groun (Free-field shear distortion)

$$\frac{\Delta D}{D} = \pm \frac{\gamma_{max}}{2}$$

ΔD/D = 0,00025 **Lining ΔD = 0,17 cm**

For perforated ground (Perforated ground shear distortion)

$$\frac{\Delta D}{D} = \pm 2\gamma_{max}(1-\nu_m)$$

ΔD/D = 0,00079 **Lining ΔD = 0,55 cm**

Since the lining is assumed to be absent in both of these calculations, tunnel-ground interactions is disregarded. The perforated ground would produce a significantly higher distortion in the free-field than the non-perforated, often by a factor of two or three (Hashash, 2001).

OVALING CALCULATIONS (RSN_1111 RECORD-2D DEPTH-SITE CLASS C)

With Considering Soil-Tunnel Interaction

Lining Stiffness

$\mathbf{E_m}$	=	1184111	kPa	E_m : Effective modulus of elasticity of the medium
$\mathbf{E_l}$	=	34000000	kPa	E_l : Elasticiy modulus of the tunnel lining
$\mathbf{\nu_l}$	=	0,20		ν_l : Poisson's Ratio
R	=	3,50	m	R : Radius
t	=	0,300	m	t : Thickness
I	=	0,00225	m^4/m	I : Moment of inertia

Compressibility Ratio

$$C = \frac{E_m(1-{v_l}^2)R}{E_l t(1+v_m)(1-2v_m)}$$

C= 0,5417

Flexibility Ratio

$$F = \frac{E_m(1-{v_l}^2)R^3}{6E_l I(1+v_m)}$$

F= 88,4858

The rigidity of a tunnel according to the surrounding medium is clarified by the compressibility and flexibility ratios (C and F), which are benchmark of the extensional stiffness and flexural stiffness (resistance to ovaling), respectively, of the ground between lining (Merritt et al., 1985).

OVALING CALCULATIONS (RSN_1111 RECORD-2D DEPTH-SITE CLASS C)

Tunnel Evaluation According to Wang (1993)

Full-Slip Conditions

$$K_1 = \frac{12(1-v_m)}{2F+5-6v_m}$$

K_1:lining response coefficient

K_1 = 0,05311

$$\frac{\Delta D}{D} = \pm\frac{1}{3}K_1 F\gamma_{max}$$

ΔD/D = 0,00078

Lining ΔD = 0,54 cm

Racking Ratio = 3,13

$$T_{max} = \pm\frac{1}{6}K_1\frac{E_m}{(1+v_m)}R\gamma_{max}$$

T_{max} = 15,13 kN

T_{max}: maximum thrust

$$M_{max} = \pm\frac{1}{6}K_1\frac{E_m}{(1+v_m)}R^2\gamma_{max}$$

M_{max} = 52,96 kN.m

M_{max}: maximum bending moment

No-Slip Conditions

$$K_2 = 1 + \frac{F[(1-2v_m)-(1-2v_m)C] - \frac{1}{2}(1-2v_m)^2 + 2}{F[(3-2v_m)+(1-2v_m)C] + C\left[\frac{5}{2} - 8v_m + 6{v_m}^2\right] + 6 - 8v_m}$$

K_2 = 1,09911

K_2: the lining thrust response coefficient

$$T_{max} = \pm K_2\tau_{max}R = \pm K_2\frac{E_m}{2(1+v_m)}R\gamma_{max}$$

T_{max} = 939,59 kN

T_{max}: maximum thrust

Wang did not propose an equation for the shear force. He proposed moment and thrust force equations for full-slip case and proposed thrust force equation for no slip case. Researchers suggested that the evaluations for full slip and no slip situations must be examined and the highest results should be used.It should be noted that the equations only calculate the forces for earthquake loads and do not include static forces.

The sample analysis presented above was calculated for all remaining cases and the summary table is presented below for the analytical approach. In order to make a comparison, the summary table of the loads obtained for the same cases in finite element analysis (Plaxis 2D) only for the earthquake conditions is given below, together with the analytical solution.

Table 4.24. Comparison of FE (Plaxis 2D) analysis and analytical (Wang, 1993) results for moment

TUNNEL SHAPE	CIRCULAR							
SITE CLASS	SITE CLASS C				SITE CLASS B			
DEPTH	6 m	14 m	42 m	60 m	6 m	14 m	42 m	60 m
PLAXIS 2D								
EARTHQUAKES	MOMENT	MOMENT	MOMENT	MOMENT	MOMENT	MOMENT	MOMENT	MOMENT
RSN_1111	35	59	55	60	16	43	44	63
RSN_285	40	81	85	91	16	43	60	81
RSN_1165	39	59	49	56	20	50	48	63
WANG, 1993								
EARTHQUAKES	MOMENT	MOMENT	MOMENT	MOMENT	MOMENT	MOMENT	MOMENT	MOMENT
RSN_1111	59	53	41	41	32	29	22	22
RSN_285	81	81	63	63	49	44	34	34
RSN_1165	71	71	55	55	38	42	30	30

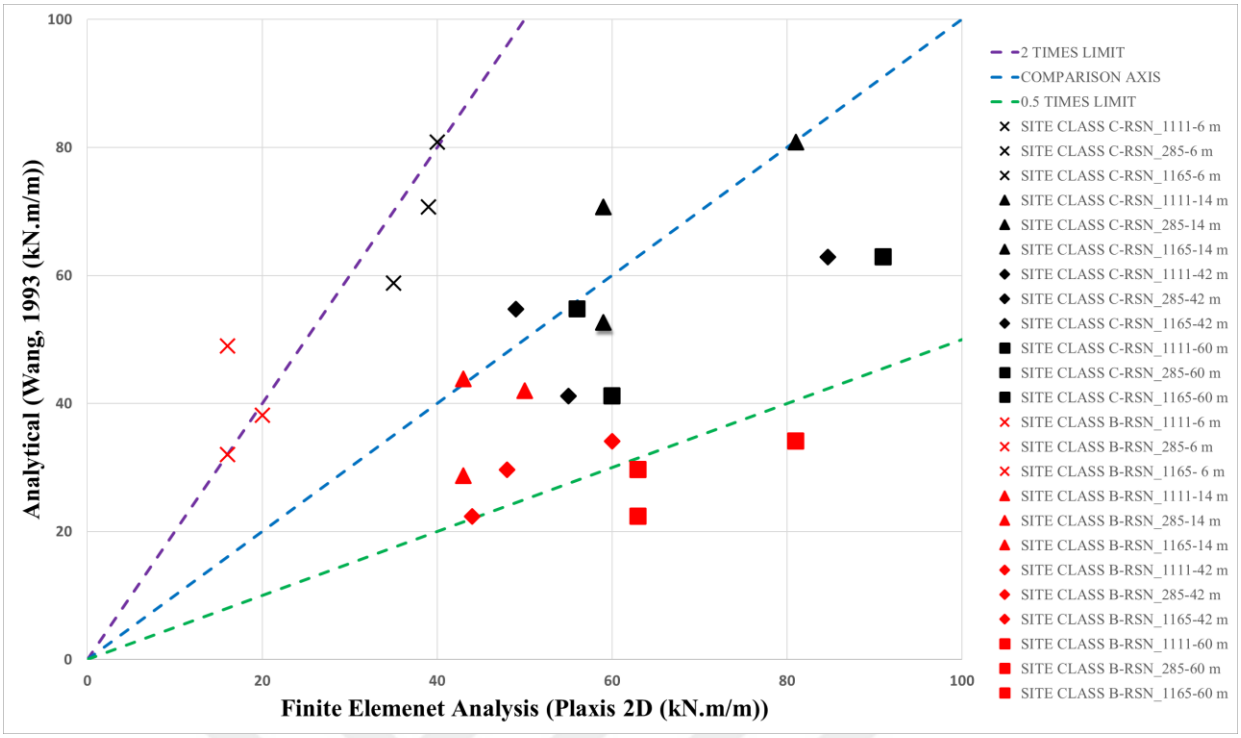

Figure 4.21. Moment values comparison between Plaxis 2D and Wang, 1993

Table 4.25. Comparison of FE (Plaxis 2D) analysis and analytical (Wang, 1993) results for axial force

TUNNEL SHAPE	CIRCULAR							
SITE CLASS	SITE CLASS C				SITE CLASS B			
DEPTH	6 m	14 m	42 m	60 m	6 m	14 m	42 m	60 m
PLAXIS 2D								
EARTHQUAKES	AXIAL	AXIAL	AXIAL	AXIAL	AXIAL	AXIAL	AXIAL	AXIAL
RSN_1111	320	576	890	942	416	750	1235	1987
RSN_285	297	527	1162	1302	419	672	1809	2565
RSN_1165	300	543	856	972	458	760	1709	1979
WANG, 1993								
EARTHQUAKES	AXIAL	AXIAL	AXIAL	AXIAL	AXIAL	AXIAL	AXIAL	AXIAL
RSN_1111	1043	940	731	731	1625	1462	1137	1137
RSN_285	1435	1435	1116	1116	2481	2233	1737	1737
RSN_1165	1249	1249	971	971	1944	2160	1512	1512

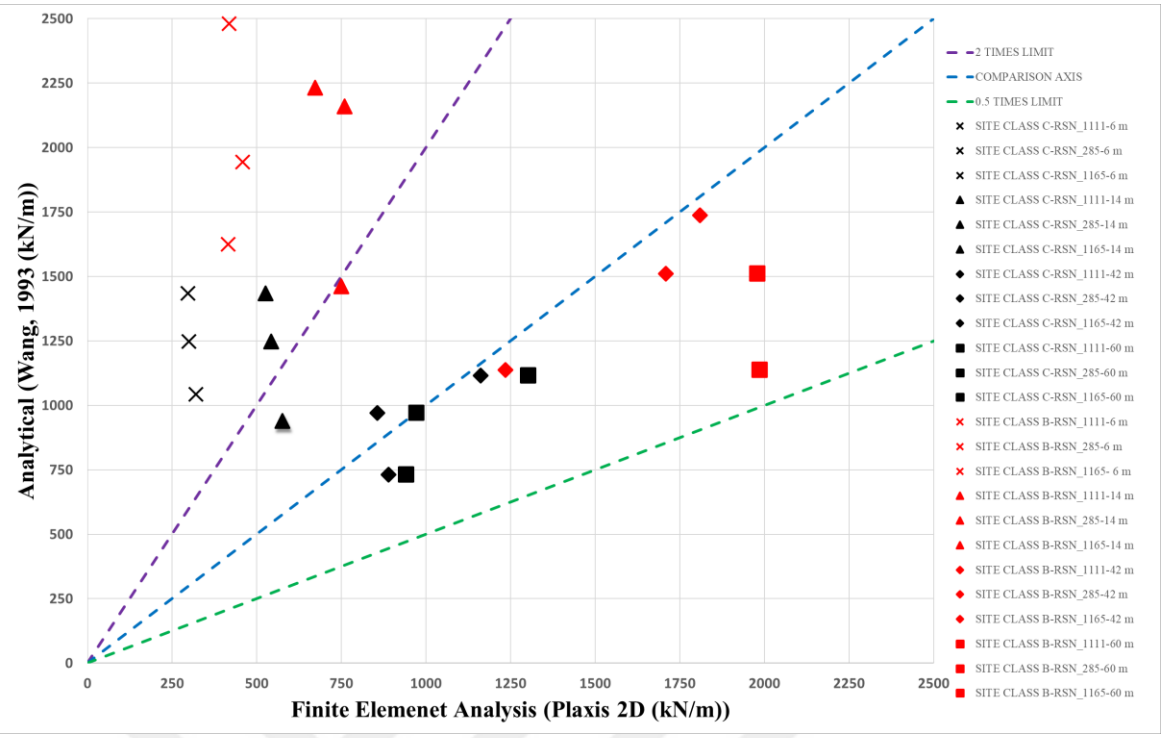

Figure 4.22. Axial force values comparison between Plaxis 2D and Wang, 1993

When the moment result graph is examined, it is observed that the analysis result ratios are close to each other. It is understood that the analytical approach generally gives higher results by staying on the safe side for Site Class C (black markers in Figure 4.21), however for Site Class B, although the results are very close to each other, the analytical results are lower than the finite element results. However, despite this, analytical approaches can change according to the designer's judgment and the result ranges may cover a wider area. In addition, it can be concluded that the analytical and finite element results agree for deeper tunnels. For shallow tunnels, i.e., tunnel depth is 6 m, the values are not within the range 1:2.

The normal force diagram was made considering only no-slip values from the analytical results because we already know that the full-slip condition underestimates the thrust results. Accordingly, when compared with Plaxis 2D results, it is understood that the values are generally higher especially for shallow tunnels. This reminds us that for the analytical approach, the tunnel condition is between no-slip and full-slip conditions as stated by Wang (1993). For this reason, the differences in normal force values are accepted as normal. However, a closer examination of the table shows that the consistency of the analytical approach with the numerical approach increases with depth. As a result,

it is understood that the full-slip condition dominates at shallow depths while the depths increase, converging to no-slip conditions.

5. SUMMARY, CONCLUSION AND FUTURE WORK

5.1. Summary

This study investigates the behavior of tunnels with different geometries under dynamic loading conditions. It also investigates how tunnels' burial depth affects tunnel lining behavior under dynamic loading conditions.

This was done by taking into account many different parameters in order to understand the behavior in detail such as:

- Tunnel shapes
- Tunnel depths
- Site classes
- Rock strength properties
- Earthquake records

The analyses were performed using Plaxis 2D software. In addition, analytical calculations were performed for models with homogeneous soil properties and circular tunnel shape as a validation. The results of the solutions of different tunnel shapes with the above-mentioned parameters are presented.

5.2. Conclusion

The outcomes and conclusions of this study are listed as follows:

- First of all, if the tunnel is located in a site class with higher shear wave velocity, (for the subject of this thesis, when changing from site class C to site class B), forces on the tunnel lining are decreased for the same loading conditions. In fact, this should be the expected result according to the equation given in 2.20. As the effective shear wave propagation velocity increases, the maximum strain in the ground environment will decrease. The effect of decreasing maximum strain on the lining is expected to decrease.
- Secondly, the most noticeable thing is that the axial force on the lining increases as the depth increases for the burial depths given in the thesis (14-42 m) regardless of the tunnel shape for both static and dynamic cases. It should be noted that the selected depths are not very deep relatively. Bursting problems are known to occur in extremely deep tunnels (1-2 km). However, since it is not within the scope of this thesis, it will not be discussed in more detail.

- It is seen that the earthquake-induced shear force and moment values for circular and horseshoe tunnel shapes decrease for the case where the rock properties are increasing with depth. However, for the box shaped tunnels, the values increase with depth except some anomalies.
- It is observed that the moment and shear force values increase with depth for tunnel shapes generally in the case where the parameter remains constant. At this point, the importance of sampling from an adequate number of points at required depths while creating a geological or shear wave velocity profile becomes clearer. The results can change completely according to the assumptions adopted.
- In conclusion, the axial force increases as the tunnel shape changes from box to circular. However, the shear force and the moment of the lining increase as the tunnel shape changes from circular to box.
- In order to verify the finite element analyses made within the scope of the thesis study, calculations were made using the analytical approaches presented in the literature. In this context, when the two studies are compared, it can be said that the moment values show high compliance. However, the normal force values are calculated higher for the no-slip situation in the analytical approach according to the numerical approach. This reminds that for the analytical approach, the tunnel condition is between no-slip and full-slip conditions.

5.3. Future Work

Future research could follow the following recommendations to understand the differences in earthquake behavior of different tunnel shapes:

- Monitoring tunnels of different shapes already located in a high earthquake hazard zone
- Scale model simulations and full-scale field tests represent appropriate approaches for research
- Tunnel performance can be determined by conducting a 3D finite element analysis

6. REFERENCES

- American Society of Civil Engineers, Minimum design loads and associated criteria for buildings and other structures, ASCE/SEI 7-16, **2017**
- Bilotta, E., Silvestri, F., A predictive exercise on the behavior of tunnels under seismic actions, **2012**
- Carranza-Torres C., Fairhurst C., Application of the Convergence-Confinement Method of Tunnel Design to Rock Masses That Satisfy the Hoek-Brown Failure Criterion, Tunneling and Underground Space Technology 15, **2000** p. 187-213
- Choundary, D., Patil, M., Ranjith, P.G., Zhao, J., Dynamic tunnel-soil interaction in soft soils considering site-specific seismic ground response, Indian Geotechnical Conference, Indian Institute of Science, Bengaluru, 13-15 December **2018**
- Einstein, H.H., Schwartz, C.W., Simplified analysis of tunnel supports, Journal of Geotechnical Engineering Division 105, **1979** p. 499-518
- Franke, K., Office Hours, CEEN 545 Introduction to Geotechnical Earthquake Engineering, https://www.youtube.com/@officehours4028, (Date of Access **10.08.2024**)
- Gao, F., Sun, C.-X., Tan X.-K., Zhu, Y., Li, H., Shaking table tests for seismic response of tunnels with different depths, Rock and Soil Mechanics Vol 36, No 9, **2015**
- Hardin, B.O., Drnevich, V.P., Shear modulus and damping in soils: Design equations and curves, Proc. ASCE: Journal of the Soil Mechanics and Foundations Division, 98(SM7), **1972,** p667–692
- Hashash, Y.M.A., Hook, J.J., Schmidt, B., Yao, J.I.-C., Seismic Design and Analysis of Underground Structures, Tunneling and Underground Space Technology 16 (**2001**) p. 247-293
- Hashash, Y.M.A., Park, D., Yao, J.I.-C., Ovaling deformations of circular tunnels under seismic loading, an update on seismic design and analysis of underground structures, Tunneling and Underground Space Technology 20, **2005** p. 435-441
- Hoek, E., Carranza-Torres C., Corkum B., Hoek-Brown Failure Criterion, **2002**
- Hoek, E., Diederichs M.S., Empirical Estimation of Rock Mass Modulus, **2006**
- Hung, C.J., Monsees, J., Munfah, N., Wisniewski, J., Technical Manual for Design and Construction of Road Tunnels-Civil Elements, FHWA-NHI-10-034,

December **2009**

- International Energy Agency, The Future of Rail, Opportunities for energy and the environment, January **2019**
- Kampas, G., Knappett, J.A., Brown, M.J., Anastasopoulos, I., Nikitas, N., Fuentes, R., The effect of tunnel lining modelling approaches on the seismic response of sprayed concrete tunnels in coarse-grained soils, Soil Dynamics and Earthquake Engineering 117, **2019** p. 122-137
- Lu, C.-C., Hwang, J.-H., Damage Analysis of the new Sanyi railway tunnel in the 1999 Chi-Chi earthquake: Necessity of second lining reinforcement, Tunneling and Underground Space Technology 73, **2018** p. 48-59
- Lu, Q., Chen, S., Chang, Y., He, C., Comparison between Numerical and Analytical Analysis on the Dynamic Behavior of Circular Tunnels, Earth Science Resource Journal, Vol 22, No 2, June **2018**, p. 119-128
- Möller, S., Tunnel induced settlements and structural forces in linings, Doctoral Thesis, Universität Stuttgart, Institut für Geotechnik, Stuttgart, **2006**.
- Jaky, J., The coefficient of earth pressure at rest, In Hungarian (A nyugalmi nyomas tenyezoje), Journal of the Society of Hungarian Architects and Engineering, **1944,** p 355–358.
- Owen, G.N., Scholl, R.E., Earthquake Engineering of Large Underground Structures, FHWA/RD-80/195, January **1981**
- Penzien, J., Seismically induced racking of tunnel linings, Earthquake Engineering and Structural Dynamics 29, **2000,** p. 683-691
- Penzien, J., Reitherman, R., and Scott, S., Interviewers, The EERI Oral History Series, **2004**
- Plaxis 2D, Material Models Manual 2D, version 2023.2, Plaxis-Bentley Systems, **2023**
- Power, M., Fishman, K., Richards, R., Makdisi, F., Musser S., Youd, T.L., Seismic Retrofitting Manual for Highway Structures: Part 2 – Retaining Structures, Slopes, Tunnels, Culverts and Roadways
- Roy, N., Sarkar, R., A Review of Seismic Damage of Mountain Tunnels and Probable Failure Mechanisms, Geotech Geol Eng 35, p. 1-28, **2017**
- Santos, J.A., Correia, A.G., Reference threshold shear strain of soil, its application to obtain a unique strain-dependent shear modulus curve for soil, In Proceedings 15th International Conference on Soil Mechanics and Geotechnical Engineering,

Istanbul, Turkey, Volume 1, **2001,** p. 267–270

- Sheory, P.R., A theory for in situ stresses in isotropic and transversely isotropic rock, **1994**
- St. John, C.M., Zahrah, T.F., Aseismic Design of Underground Structures, Tunneling and Underground Space Technology, Vol 2, No 2, (1987) p. 165-197
- Széchy, K., The Art of Tunneling, **1966**
- Terzi, V.G., Manolis, G.D., Basic numerical modelling issues in dynamic soil-tunnel interaction, Soil Dynamics and Earthquake Engineering 172, **2023**
- Tsinidis, G., de Silva, F., Anastasopoulos, I., Bilotta, E., Bobet, A., Hashash, Y.M.A., He, C., Kampas, G., Knappett, J., Madabhushi, G., Nikitas, N., Pitilakis, K., Silvestri, F., Viggiani, G., Fuentes, R., Seismic behavior of tunnels: From experiments to analysis, Tunneling and Underground Space Technology 99, **2020**
- Turkish Earthquake Building Code, **2018**
- Vlachopoulos, N., Diederichs, M.S., Improved Longitudinal Displacement Profiles for Convergence Confinement Analysis of Deep Tunnels, Rock Mechanics and Rock Engineering 42, **2009**, p. 131-146
- Wahlstrom, E.E., Developments in Geotechnical Engineering Book Series, Tunneling in Rock, Vol 3, **1973**
- Wang, J.N., Seismic Design of Tunnels: A State-of-the-Art Approach, Parsons, Brinckerhoff, Quade and Douglas Inc, New York, June **1993**
- Wang, T.-T., Kwok, O.-L.A., Jeng, F.-S., Seismic response of tunnels revealed in two decades following the 1999 Chi-Chi earthquake (Mw 7.6) in Taiwan: A review, Engineering Geology 287, **2021**
- Wang, W.L., Wang, T.T., Su, J.J., Lin, C.H., Seng, C.R., Huang, T.H., Assessment of damage in mountain tunnels due to the Taiwan Chi-Chi Earthquake, Tunneling and Underground Space Technology 16, **2001** p. 133-150